GRAMMAR FORMALISM FOR MEDICAL DATA ANALYSIS

Its Application in ECG, Scintigraphy and Tomography

Salah Hamdi

Asma Ben Abdallah

Mohamed Hedi Bedoui

Grammar Formalism for Medical Data Analysis

Grammar Formalism for Medical Data Analysis:

Its Application in ECG, Scintigraphy and Tomography

By

Salah Hamdi, Asma Ben Abdallah
and Mohamed Hedi Bedoui

Cambridge
Scholars
Publishing

Grammar Formalism for Medical Data Analysis: Its Application in ECG, Scintigraphy and Tomography

By Salah Hamdi, Asma Ben Abdallah and Mohamed Hedi Bedoui

This book first published 2022

Cambridge Scholars Publishing

Lady Stephenson Library, Newcastle upon Tyne, NE6 2PA, UK

British Library Cataloguing in Publication Data
A catalogue record for this book is available from the British Library

ISBN (10): 1-5275-8429-1
ISBN (13): 978-1-5275-8429-7

CONTENTS

CHAPTER 1

INTRODUCTION

The heart is the essential representative of the cardiovascular system and it can be prone to many diseases. According to annual statistics from the World Health Organization (WHO), cardiovascular pathologies are the most common cause of death in the world. As a result, the diagnosis of cardiac pathologies appears and imposes itself as a vital task. Doctors have powerful tools at their disposal to observe the functioning of the heart muscle and thus make their diagnosis based on the continuous development of resources and techniques. Among the possible techniques: electrocardiography, scintigraphy and tomography.

The most common test done is electrocardiography because it is quick to perform, inexpensive, and non-invasive. With the help of the electrocardiogram (ECG), important indicators can be determined. In general, the shapes and durations of the different peaks and waves are examined as signs of true heart abnormalities.

Cardiac scintigraphy, one component of nuclear imaging, is an additional test used by nuclear physicians to assess heart function. Scintigraphy is a technique that carries useful information to affirm or deny chest pain by recognizing the state of perfusion of the myocardium. The technique is performed following a stress test to achieve maximum heart rate for a satisfactory time or to stop the test due to pain or exhaustion.

In addition to taking a medical history of symptoms and risk factors, the doctor may perform certain tests to judge the quality of the carotid arteries using the technique called angiography. In the case of medical imaging, tomography is a technique that reconstructs the volume of an object in the human body from a series of sections obtained from the exterior of the object in question. The result is a reconstruction of the real properties of the interior of the object. In this examination, an iodinated contrast medium is used to increase the density of the blood in the arteries and thus enhance the vascular bed in the images. These images are obtained from different angles, which allow 3D reconstruction.

Several usual approaches to processing 1D and 2D medical data have been proposed. However, few works have been based on grammar. Grammar and language theory began in 1950. To this day, grammar involves analyzing programming languages, describing natural languages, and modeling logical circuits. However, grammatical rigor can be extended to cover other areas of application such as signaling and medical imaging. The main advantage of these methods concerns the representation that it can make available. Syntactic approaches can powerfully represent object structures and therefore make it easy to retrieve information. The input data appears to be a structured scene having a hierarchical order because grammars can clearly represent hierarchical structures using non-terminal and terminal nodes. In addition, syntactic approaches are able to describe a large set of complex objects using small sets of simple primitives and grammatical rules. Compared to statistical methods, the use of grammars offers more flexibility in applications.

It is in this context that our thesis topic arises and finds its interest. We offer 1D and 2D medical data processing techniques based on grammatical formalism. The idea is inspired by language theory and word recognition. Grammatical formalization can represent semantic patterns and patterns found in the signal or in the image. Indeed, we used syntactic methods to interpret the ECG signals from the MIT-BIH standard base and measure the associated parameters (R peaks, RR distances, QRS durations and QTc corrected intervals). Also, we will show how the idea of grammar is applied to medical 2D images such as scintigraphic image and tomographic image. The proposed method makes it possible to detect the contours of the epicardium and endocardium. In addition, quantitative information can be deduced such as the area and radius of each organ as well as the thickness of the epicardial muscle. Indeed, this type of work will certainly help physicians during a medical examination and during a decision-making process.

This report is mainly composed of four chapters.

The first chapter briefly introduces the basics of cardiology and the functioning of the cardiovascular system. It helps to understand in particular the origin of the electrical signals recorded by the ECG signal. Then, the first chapter presents cardiac scintigraphy and explains different types of scintigraphic images held in states of exertion and rest. Also, a part will be devoted to present tomography and more precisely of the carotid arteries using tomography angiography. As the second part of the chapter, we briefly report basic notions of grammatical formalism and the

different types of grammar. It makes it possible in particular to focus on the first two types which are regular grammar and grammar out of context. We focus more precisely on the basics in terms of languages, automata, vocabularies, rules, lexical analysis and syntactic analysis.

The second chapter details the state of the art of different ECG signal processing methods. It presents several techniques reported from the literature for the analysis and processing of ECG and the extraction of certain characteristic elements of the signal such as QRS complexes, P and T waves, R peaks, etc.

The third chapter presents the method we have developed for the detection of QRS complexes and cardiac cycles and illustrates the results obtained on several types of real ECG signals from the MIT-BIH standard database and those obtained from our exploration partner service in Sahloul University Hospital in Tunisia. The algorithm quantifies various indicators of the ECG signal such as RR distance, QRS duration and the corrected QTc interval. In addition, we added two parameters: the standard deviation of the RR distances denoted σRR and the standard deviation of the QRS durations denoted σQRS. These standard deviation parameters reflect the regularity of RR distances and QRS durations.

The fourth chapter details the state of the art of the different grammar-based image segmentation methods. It presents several techniques cited in the literature that are based on grammatical formalism to do image processing in general. This fourth chapter presents the method we have developed for the segmentation of medical images. An application on scintigraphic images and tomographic images has been established. For a scintigraphic image, the algorithm can detect the contours of the epicardium and endocardium. In addition, quantitative information can be deduced such as the area and radius of each organ as well as the thickness of the heart muscle. For a tomographic image, a region of interest (ROI) segmentation technique is proposed. A large series of segmented regions of interest allowed us to do the 3D reconstruction of the objects. The image base comes from our second partner service, the Nuclear Medicine Service of the Sahloul University Hospital in Tunisia. The manuscript ends with a general conclusion.

CHAPTER 2

BASICS OF CARDIOLOGY AND GRAMMATICAL FORMALISM

I. Introduction

Through this chapter two aspects will be exposed:

- An overview of the cardiovascular system is given, followed by a general description of physiological cardiac activity. This presentation is particularly limited to the various parameters describing the Electrocardiogram (ECG) signal, the scintigraphic images and the tomographic ones for a better understanding of the work presented in this thesis. The chapter ends with a general description of cardiac pathologies. Readers interested in more in-depth approaches will be able to consult the numerous available medical books [Deb'97, Fis'02].
- A presentation of grammatical formalism basics will shed light on the theory that will be adopted later for the processing of medical data resulting from the techniques that have been described in this chapter.

II. Cardiovascular system

The cardiovascular system ensures the continuous circulation of blood in the organism. The circulatory system therefore supplies oxygen to cellular tissues and transports wastes to the kidneys and carbon dioxide to the lungs. The cardiovascular system is made up mainly of the heart and a network of continuous and closed conduits that allow the transport of blood to the arteries and veins.

II.1 Heart

The heart is a concave and muscular organ equivalent to a pump which allows the circulation of blood to the arteries and veins. The shape of the

heart is comparable to an inverted cone. The heart is placed in the mediastinum which represents the middle part of the rib cage bounded by the following organs: the two lungs, the breastbone and the spine. The heart is located to the left of the center of the thorax and is able to pump four to five liters of blood, at relaxation, per minute. The heart is subdivided into four chambers: two atria and two ventricles [Obr'68] (Figure 2.1), allowing blood to be pumped to the cells of the human body. The two atria and the two left and right ventricles constitute the left heart and the right heart respectively.

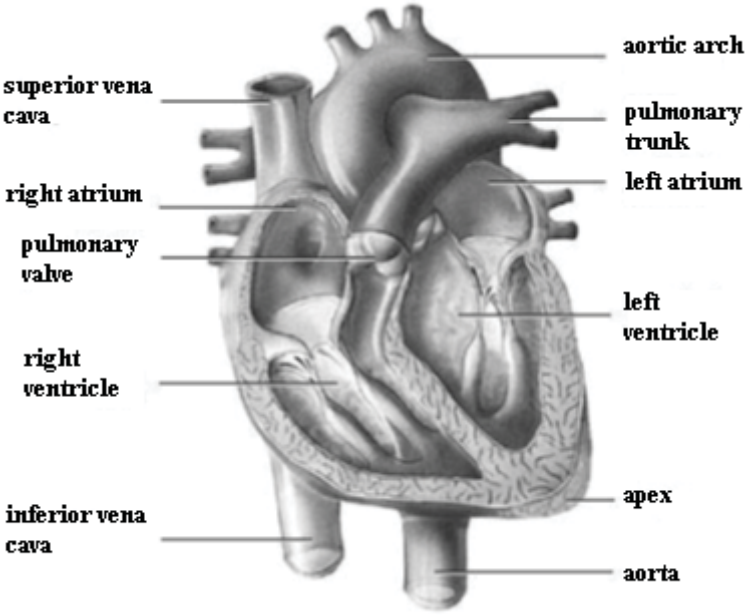

Figure 2.1: General diagram of heart [Fis'02]

II.2 Blood circulation

The right atrium picks up oxygen-poor blood from the upper and lower vena cava and throws it to the right ventricle after a phase of contraction. This phase is called systole. The systole is followed by another phase of diastole, making it possible to propel, through the pulmonary arteries, the blood in the lungs. Carbon dioxide carried by the blood will be cleaned by the lungs out of the body. Then the blood will be recharged with oxygen

and returns to the heart through the left atrium. After that, it circulates in the left ventricle and then to all the organs in the network of arteries through the aorta (Figure 2.1) [Fis'02].

III. Cardiac electrophysiology

The heart is an organ which automatically possesses all the tools for its functioning. This automatism is connected to the crucial tissue, and the heart contracts following a stimulus which originates from the posterior wall of the right atrium. This excitation passes through both atria and then passes to both ventricles. Consequently, the heart admits an intrinsic network of conductive cells which shape and retransmit electrical impulses vis-à-vis the cells that respond to impulses by phases of contractions. To better understand the origin of mechanical and electrical events in the heart, the electro-physiological properties of cardiac cells will be described first.

III.1 Electro-physiological properties of cardiac cells

The cells of the human heart are surrounded by a membrane which allows the passage of ions of different types, which produces differences in concentration on either side. Sodium is ten times less concentrated inside than outside the membrane, so the intracellular concentration of potassium is thirty times greater than outside. The concentration of calcium is much more concentrated on the outside than on the inside. Indeed, these differences in concentrations electrically generate potential differences between the outside and inside of the membrane [Deb'97, Fis'02].

Upon relaxation, the interior of the membrane is negatively charged with a -90mV potential difference, also called the resting potential. When the cell membrane is stimulated by chemical, mechanical or electrical excitation, momentary changes in the cell membrane will result in a cruel influx of sodium and calcium and an outflow of potassium. The potential level thus progresses from -90mV to +20mV, which is called the action potential. During the contraction of the cell membrane, exchanges of ions are transferred and thus induce an action potential, as described in Figure 2.2. The five resulting phases are represented as follows:

Rapid depolarization, or phase 0: After an electrical stimulus beyond the activation threshold, a rapid flow of sodium ions enters the cell and suddenly changes the polarity of the cell.

Early repolarization, or phase 1: It is characterized by short and rapid repolarization, due to the flow leaving the potassium ions and sodium inactivation.

Plateau, or phase 2: It represents slow repolarization. The phase is due to the slow entry of calcium ions into the membrane, which reduces the influence of potassium and consequently slows down the repolarization phase.

Repolarization, or phase 3: This phase corresponds to the final repolarization, and it is characterized by the closure of ion channels hence bringing the cell to a resting potential. Along this phase, potassium ions are continuously exiting, while the potential of the cell membrane tends towards a relaxation threshold.

Phase 4: This last phase describes the resting potential, in which the cell is no longer excitable.

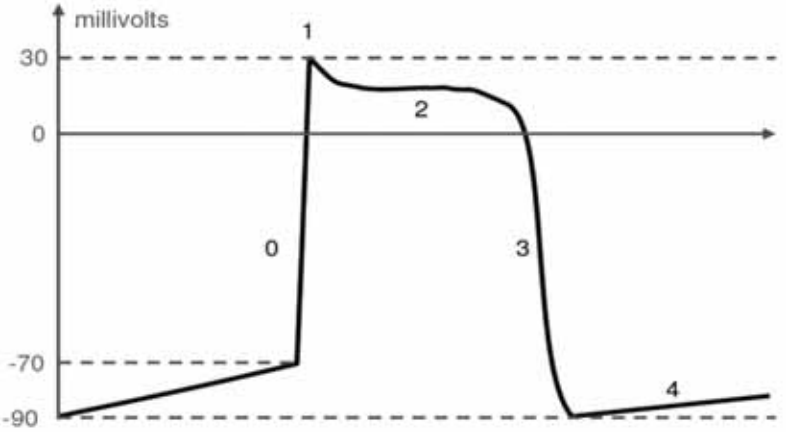

Figure 2.2: Five phases describing the action potential of cell membrane: phase 0 of depolarization, phase 1 of onset of repolarization, phase 2 of slow repolarization, phase 3 of rapid repolarization, and phase 4 of rest.

III.2 Electrical functioning of heart

The heart has an electrical system that keeps beating automatically. The heart muscle contracts and is governed by an electrical impulse in the

sinus node located in the superior vena cava, as shown in Figure 2.1, in the right atrium. The sinus node is formed by a set of automatically excitable cells which generate an electrical current of depolarization 60 to 100 times per minute.

Electrical self-excitation is transmitted to both atria causing atrial systole and occurs at the Atrioventricular (AV) node. The latter is the only point of passage between the ventricles and the atria located in the interventricular septum. At this stage, the self-excitation induces a short pause and consequently induces the phase of ventricular systole.

This pause is largely cruel to cause delayed stimulation relative to the atria and thus allows both ventricles to be fully filled during the atrial contraction phase. Consequently, the electrical system develops the conformity of the heart rhythms and so allows the coordination of the phases of the AV contractions.

IV. Electrocardiography

IV.1 History

In 1842: Carlo Matteucci was an Italian physicist who discovered that an electric current would follow every heartbeat.

In 1887: John Burden was an English physiologist who published the first ECG of a human being.

In 1897: Clément Ader was an engineer in electronics who adapted the galvanometer, which was an amplification system for telegraphic communications under marine.

In 1903: Einthoven managed to collect the electric currents by using an assembly called the Wheatstone bridge.

In 1924: Einthoven won the Nobel Prize for his activities on electrocardiography.

In 1932: Chest leads were used for medical diagnosis.

In 1942: Unipolar leads were used for medical diagnosis.

IV.2 Presentation

Electrocardiography is a slightly expensive technique, following a simple and non-invasive examination, controls the good functioning and progress of the cardiovascular pump.

This method was created in 1887 for the first time following the work of Waller [Wal'87]. Then it was reinforced by the invention in 1901 of the string galvanometer [Ein'88] vis-à-vis the medical community. In 1924, Dr. Wilhem Einthoven was awarded the Nobel Prize in Medicine. Since then, electrocardiography has been transformed into a primordial, essential and indispensable technique in cardiology.

The human body is observed as an electrical conductor. Therefore, the values of potentials generated at the levels of heart cells during mechanical activity can be recovered using metal electrodes arranged on the skin. The graphic recording obtained following the electrical activity of the human heart is always called “the ECG”.

The electrodes used are positioned for recording the ECG signal and they are known by electrocardiographic leads. The standard ECG signal is obtained on 12 leads (six precordial and six peripheral leads).

IV.3 System of electrocardiographic derivations

An electrocardiographic bypass is defined by two points of hearing from which the electrical activity of the heart is measured and the difference in the electrical potential is calculated. Often, EKG machines can record many potential differences simultaneously depending on the number of electrodes distributed and their locations on the body. Each value of these measured potentials is suitable for a lead of the ECG. The electrodes are located to better explore the full range of cardiac electrical fields produced by the contraction of the heart muscle and myocardium.

IV.4 Peripheral derivations

The peripheral leads provide the study of the electrical activities of the human heart on the frontal plane. Peripheral leads are obtained using four electrodes placed on the left arm, the right arm and the left leg. In order to eliminate the parasites, a neutral electrode is placed on the right leg. This arrangement was determined in 1912 by Dr. Wilhem Einthoven under the name “bipolar peripheral derivations” and subsequently completed in 1942

by Dr. Goldberger under the name “unipolar peripheral derivations” [Deb'97, Fis'02].

IV.4.1 Bipolar peripheral leads

Bipolar leads were decided by Einthoven in 1912, and they have also remained in use up to now (Figure 2.3). In fact, the leads are based on three electrodes distributed over the body. These electrodes are installed on the left and right arms and on the left leg in order to establish the Einthoven triangle. They are called bipolar derivations because we calculate the potential difference between each two electrodes. Any side of Einthoven's triangle symbolizes a lead by using two separate electrodes for each lead. The set of three derivations is:

- DI with DI = VL - VR
- DII with DII = VF - VR
- DIII with DIII = VF - VL

where V L is the potential value on the left arm, VR is the potential value on the right arm, and VF is the potential value on the left leg.

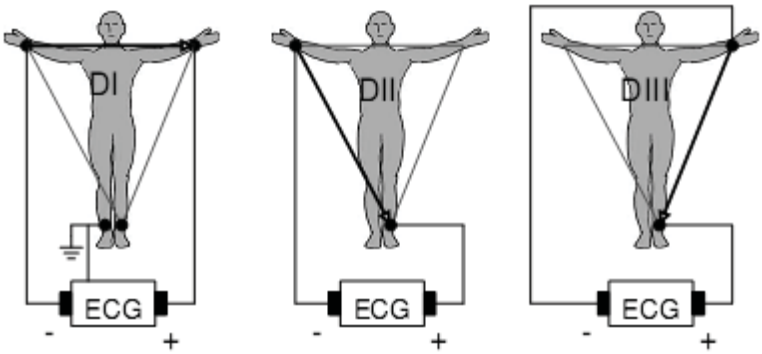

Figure 2.3: Einthoven triangle setup for recovery of bipolar leads.

IV.4.2 Unipolar peripheral leads

The unipolar leads were determined by Wilson (Figure 2. 4). In this type of lead, the values are measured between an exploratory electrode installed at the crest of the Einthoven triangle and a second central terminal. The latter is a neutral electrode whose potential value is equal to the average of the potentials of the three peaks of the triangle. This determines the

unipolar leads known by VL, VR and VF. Goldberg [Gol'42] changed the installation of Wilson's unipolar leads to extract three other unipolar leads called the augmented unipolar derivations aVL, aVR and aVF, as shown in Figure 2.4. The word augmented indicates that the Goldberg leads amplify the potential values of the old Wilson leads by a coefficient of 1.5.

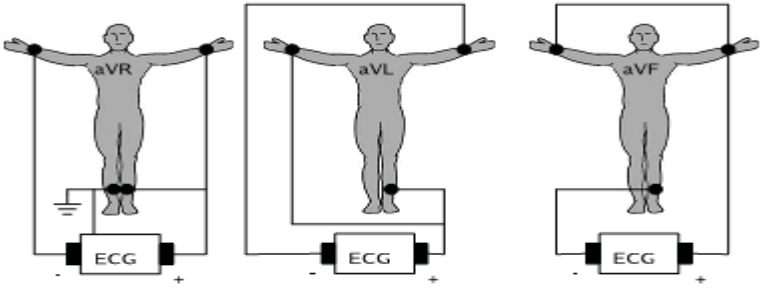

Figure 2.4: Goldberg system for recording unipolar leads

IV.4.3 Precordial derivations

To measure variations in potentials near the heart, Wilson proposed six new derivations of the horizontal plane V1, V2, V3, V4, V5, and V6 located on the left side of the thorax. The variations are measured from a positive pole in the form of an exploratory electrode located on the thorax and a negative pole in the form of a reference electrode connected to the central Wilson terminal. These leads are connected since the position of the exploration electrode is close to the left and right ventricles [Fis'02].

IV.5 ECG signal

As we have quoted before, an EKG is obtained from a machine called an EKG machine, which transforms the mechanical activity of the heart into a form of an electrical signal. The electro-physiological signal is obtained using metal electrodes located on the skin. The morphology of the ECG signal is presented in the form of a series of electrical waves which repeat with each cardiac cycle with particular shapes. In fact, the waveforms explain different phenomena relating to the levels of the action potentials of cardiac excitation and whose stages are illustrated in Figure 2.5 in successive ways. Figure 2.5 depicts the morphology of the normal single cardiac cycle ECG signal.

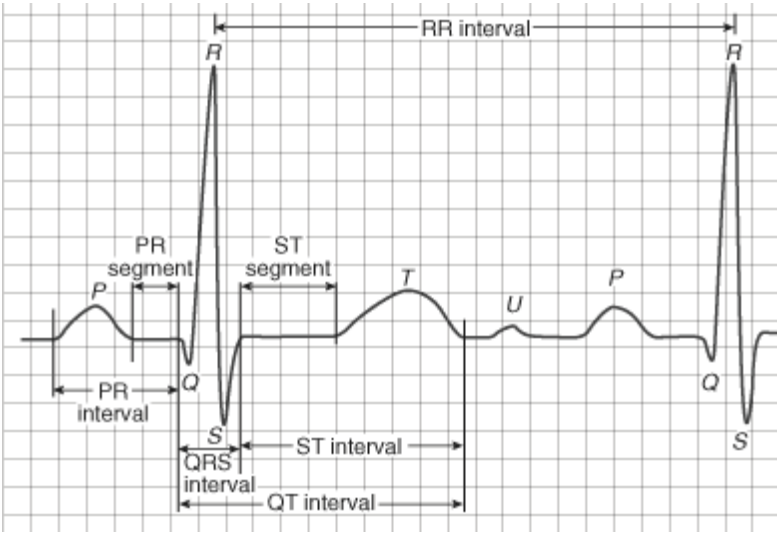

Figure 2.5: Morphology of normal ECG signal in single cardiac cycle

IV.5.1 Morphology of ECG signal

In an ECG signal, we notice that the phenomenon of the contraction and relaxation of the myocardium is exhibited in the form of a sequence of negative and positive deflections superimposed on a baseline of a zero potential which is suitable for the absence of cardiac events, as depicted in Figure 2.5. The letters P, Q, R, S, T and U are successively assigned to the waves of the ECG signal.

P wave: This is the first-order detectable wave. It appears when the electrical impulse is distributed through the sinus node in order to depolarize the atria. Muscle mass is partially light and results in a potential value of less than 0.25 mv. In the atria, the propagation of the depolarization wave is much lower than in the ventricles. Indeed, the place of the atria around the sinus node is depolarized very quickly compared to distant places. In addition, the repolarization front holds the same direction as the depolarization front and the result vector is directed towards the sinus node. Consequently, this phenomenon produces a repolarization wave in reverse of the depolarization P wave. Then, the repolarization phase of the atria explains the QRS complex. When this pulse is much stronger than the first, the repolarization wave will be hidden.

QRS complex: It is the set of negative and positive deflections which are suitable for the contractions of the two ventricles. For a normal case, the QRS complex has an amplitude between 5 and 20 mV and it lasts less than 0.12 seconds.

The QRS complex is often made up of three waves:

¬ L ' Q-wave: the first negative deflection.
¬ L ' R-wave: the first positive deflection.
¬ L ' S-wave: the second negative defection following peak A.

The shape of the QRS complex is variable depending on the positions of the electrodes as well as the leads used.

T wave: It comes after the QRS complex following a return to the basic power line. This wave is suitable for ventricular repolarization. Practically, it has a slight amplitude and does not confirm any mechanical phenomenon.

U wave: It is rarely observed. This wave is denoted U and can be observed after the T wave. It is a low amplitude wave and it is appreciable in some leads, especially in athletes. This wave is frequently associated with the phases of delayed ventricular repolarization.

Accordingly, a study of a normal EKG is shown in Fig.2.5. The characteristics of an ECG signal relate to the morphology of the P and T waves and of the QRS complex, the durations, the amplitudes, and other temporal indicators which are the PR, RR and QT intervals as well as the ST and PR segments.

IV.5.2 ECG intervals and segments

In addition to the different waves mentioned above which are the basic elements that characterize the ECG, there are other segments and intervals which support very essential information on the speed of the conduction of the impulse in the different organs of the body heart [Lim'09].

The most used segments and intervals are:

RR interval: This interval is very important and it corresponds to the time between two successive depolarizations of the ventricles. The RR interval is used to calculate the heart rate (1 / RR).

PR segment: This segment represents the time between the end of depolarization of both atria and the start of depolarization of both

ventricles. This is the time period in which the depolarization wave is surrounded at the AV node.

PR Interval: This PR interval represents the delay in the propagation of the depolarization wave from the sinus node to the ventricular cells.

QT interval: The QT interval corresponds to the duration of the ventricular systole, which begins at the onset of the excitation of the ventricles and stops at the end of their relaxation.

ST segment: This segment describes a phase during which all ventricular cells are depolarized; the segment has become isoelectric.

A detailed description of these characteristics of the normal ECG signal, physiological interpretation and numerous methods [Bro'98] for the calculation of the electrical axis of the QRS complex are available.

IV.5.3 Cardiac arrhythmias

In a state of rest, the heart is between 60 and 100 heartbeats per minute, often called beating heart. Acceleration in the number of beats is called tachycardia. A slowdown in the number of beats is called bradycardia. An irregular change in the heart beat is called an irregular rhythm. All these forms are the basic forms of arrhythmia [Joh'15].

Arrhythmia occurs when an electrical excitement manifests itself elsewhere than in the sinus node. In other words, the electrical impulse is registered in the AV node or in the ventricles, or the electrical excitation no longer propagates in normal paths.

Arrhythmia is sometimes accompanied by palpitations of beats. These palpitations cause you to feel the heartbeat and do not necessarily symbolize a heart rhythm disorder. This most often occurs when the pulse is beating faster or irregularly. On the other hand, a patient can have arrhythmia without necessarily feeling palpitations. There are different forms of arrhythmia. The main forms are as follows:

a) Extrasystole

It is very common arrhythmia. Extrasystole is an advanced heartbeat or excess that is perceived as an irregular or missing beat. A lot of people have this type of arrhythmia and do not even feel it. In most cases, this arrhythmia is not accompanied by other symptoms. This abnormality is mild and can even occur in a healthy heart. Sometimes extrasystole is

accompanied by little dizziness, but this case is not serious. The following figure describes the atrial extrasystole where the second and sixth complex occur in advance [Joh'15].

Figure 2. 6: Example of atrial extrasystoles

b) Atrial flutter

In this type of arrhythmia, abnormal depolarization propagates into the right atrium in a looping path and endlessly (Figure 2.7). The frequency of rotation is in the order of 300 beats / min. Depolarization occurs 300 times per minute at the entrance to the AV node and will cross the junction to the two ventricles only once in two or once in three. Indeed, the frequency of the ventricles will be a sub-multiple of 300 beats / min [Joh'15].

Figure 2. 7: Example of atrial flutter

Note that, in this type of abnormality, there is a major danger to the health of the patient due to disorders in the blood flow to the atria and the possibility of embolism occurring.

c) Atrial fibrillation

It is an atrial arrhythmia also called atrial fibrillation. The depolarization is divided into a set of fronts of different amplitudes and directions, ensuring a completely disordered electrical activity at the level of the atria. Often, this anomaly does not allow the atrial myocardium any phase of rest. Atrial fibrillation results in the absence of atrial waves in favor of a continuous irregular sinusoidal wave activity. The frequency of depolarization within the atria is often very high. Numerous depolarization fronts are consequently exposed at the AV node which acts as a filter by

allowing only a few fronts to pass at random. Generally, the rate of the ventricles is entirely irregular, between 90 and 140 beats / min depending on the state of the excitability of the node [Joh'15].

Figure 2. 8: Example of atrial fibrillation

However, the absence of atrial systoles results in a significant decrease in cardiac efficiency at two levels: first because the heart does not benefit from the atrial systole, which allows the ventricles to be filled with blood, and second because the average rate is often above 100 beats / min and can reach 200 beats / min. This arrhythmia is not serious, but the primary risk associated with this anomaly is flutter which is the possible transmission of emboli created in the atria. This major risk is probably low when atrial fibrillation is permanent, whereas it is immediately reinforced by episodes on a sinus background, especially during the change from one rhythm to another [Dal'07].

d) Supra-ventricular tachycardia

This atrial arrhythmia may have as its source a stimulation loop, an ectopic focus, or a pathway that closes the AV pathway, called the accessory pathway, with reentry by the AV node.

An ectopic focus is a case in which a group of cells placed in the atria depolarize naturally and as quickly as the sinus, thus taking its position. The depolarization of the atria is not of a sinus origin, the diffusion of the nerve impulse is different from that originating from the sinus, and a P wave of an exceptional shape is observed. The specific frequency characterizing this type of focus is between 120 and 200 beats / min and the ventricles operate at the same rate in the absence of conduction problems [Dal'07].

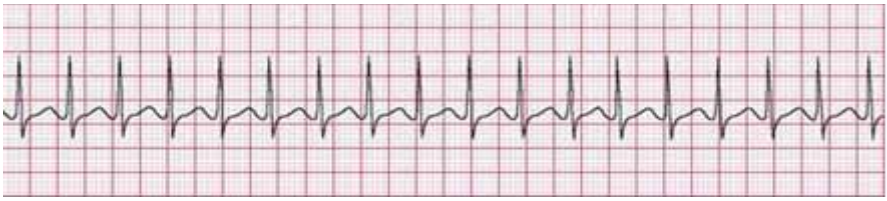

Figure 2. 9: Example of supra-ventricular tachycardia

In the event that the number of beats can reach 250 beats / min, periodic discharge from an ectopic focus located in the AV node can still be the cause of tachycardia, known as junctional or nodal tachycardia. Unlike atrial tachycardia, a P wave that precedes QRS complexes is never found, because there is no atrial activity that precedes the beat [Dal'07].

This type of pathology has a main risk which is the lack of efficiency of the ventricles; either forced to contract frequently, or because the ventricles do not have enough time to fill with blood properly. Thus, the body's supply of oxygen can be corrupted.

e) Ventricular fibrillation

Arrhythmia is equivalent to atrial fibrillation, but it affects the ventricles. The latter are therefore discharged in a completely desynchronized manner, and there is still no cardiac systole. The ECG signal records a disordered, irregular, rapid and oscillatory ventricular activity [Dal'07].

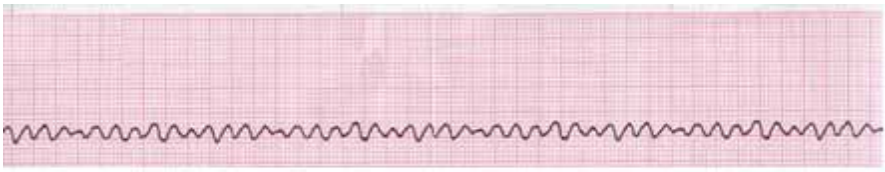

Figure 2.10: Example of ventricular fibrillation

Usually, ventricular fibrillation constitutes a serious arrhythmia, since it is a warning of sudden death. This is because the heart no longer functions at all its usual pumping activity and the blood no longer circulates, which causes the asphyxiation of all the tissues of the body. Without immediate defibrillation intervention, the depolarization of all myocardial cells are resynchronized and the cardiac movement restarts, hence ensuing death. A defibrillator allows people at risk of ventricular fibrillation to benefit from

its implantation. The defibrillator is located at the level of the thorax and it is accompanied by a probe capable of detecting the rhythmic abnormality and causing the device to give a strong electric shock [Dal'07].

f) Ventricular tachycardia

This type of arrhythmia has as source one or more ventricular ectopic foci which may in turn depolarize. Heartbeats take the form of tightly connected ventricular extrasystoles. If it is not treated by using a defibrillator, this pathology is dangerous because of its possible transformation into ventricular fibrillation, which can lead to the death of the patient within minutes of its appearance [Dal'07].

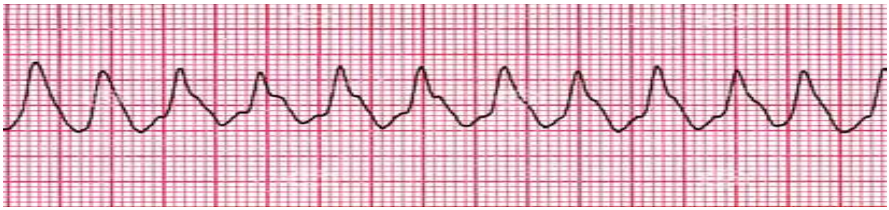

Figure 2.11: Example of ventricular tachycardia

V. Heart scintigraphy

V.1 Presentation

Scintigraphy is a non-invasive imaging technique. The images obtained from cardiac scintigraphy provide functional information. Scintigraphy is useful for studying myocardial perfusion. In this case, it is called cardiac or myocardial scintigraphy. This technique is still used at the level of the brain and the bone. Around the object in question, the acquisition heads are in rotation [Mar '00], and projections are successively acquired so dozens of images are obtained, each from a different angle. This way of acquisition ensures the distribution of the tracer in space and in 3D. Due to the tomographic reconstruction, a 3D representation of the left ventricle is made. Atherosclerosis is an anomaly characterized by a gradual obstruction of the arteries by a covering composed mainly of calcium and lipids, which generates a narrowing of one or certain coronary arteries. This is because the formation of thickening of the arterial wall and plaques causes stenosis. When this disorder affects the coronary arteries, then it irrigates less heart muscles, which become ischemic or necrotic. In this case, the technique of myocardial scintigraphy is useful to check the viability of the

myocardial tissue and to specify the ischemic territory. The patient is put on an activity and two groups of myocardial perfusion images are obtained by scintigraphy. A group is taken in the state of rest and another group in the condition of effort. The comparison between the art series of images allows having a distribution of zones in the myocardium in light of three degrees of intensity [Mar'00]:

- If the intensity value is normal in both images, then the area is normal.
- If the value of intensity is normal in the image rest and low in the image effort, then the area is reached by the ischemia effort.
- If a value of intensity is lower in both images, then it comes to a narrow stenosis of the coronary artery or there is a necrosis [Com'05].

Myocard scintigraphy is based on the muscle ability to accumulate different radioactive tracers. In fact, there are two types of cardiac tracers which are technetium products and thallium. Figure 2.12 shows the general principle of the technique of scintigraphy:

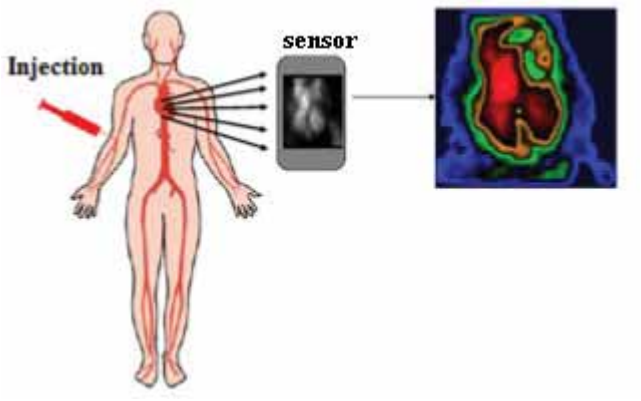

Figure 2.12: Principle of scintigraphy.

Myocardial perfusion provides series of 2D images that provide functional information and assess the irrigation of the heart muscle. The patient receives the molecules and sends out the radiation once they are received by the organ to be explored. In practice, the gamma-camera machine detects the radiation emitted by the body. Finally, the resulting image is

reconstructed. The inner wall is called endocardium and the outer wall is called epicardium.

In a single sequence, the E numbers are 2D images which vary according to the value of the inter–cross-section used. The more reduced the value of inter-cross-section the bigger the number of images (Figure 2.13) and the better the 3D reconstruction.

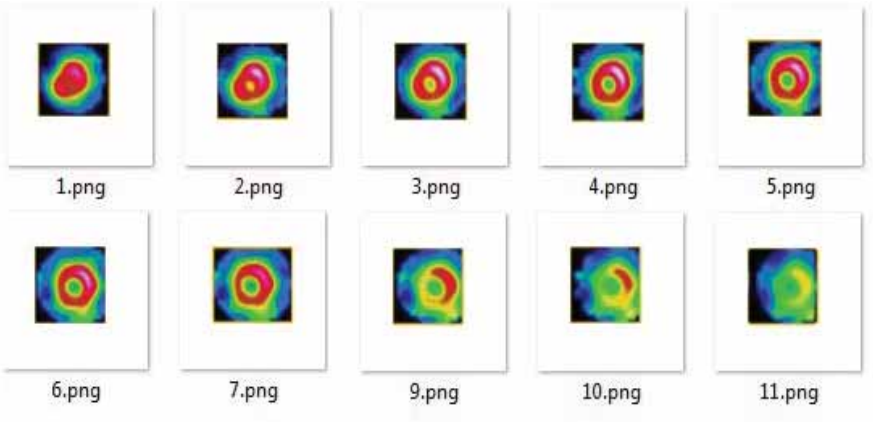

Figure 2.13: 2D scintigraphic cross-sections.

V.2 Ejection fraction

On echocardiography, the Ejection Fraction (EF) of the left ventricle can be calculated. The EF can also be measured by data provided by cardiac MRI, scintigraphy or coronary angiography. It indicates the degree and order of emptying of the ventricle. The EF is a useful indicator for efficiently estimating the contraction capacity of the heart. The normal EF is of the order of 60% in an individual. In the case of a contractility abnormality, the EF decreases. In case of a major dysfunction, the EF value may decrease by up to 20%. In case of heart failure, the EF level can distinguish between diastolic and systolic heart failure.

The formula for calculating the EF is defined by the ratio between the ejected volume (Vtd - Vts) and the telediastolic volume Vtd:

$$EF = \frac{Vtd - Vts}{Vtd} * 100 \quad (2.1)$$

Normally, the FE value is between 55 % and 75 %. The average value is of the order of 67%. If the value is more than 75%, then the efficiency of the cardiac system decreases. In this case, there will be an increase in the mechanical energy so that the myocardium is compressed to a systolic volume. The gain of the ejected volume is minimal, since the ventricular cavity becomes short tele-systole. The phase of diastole ensures a fair ventricular filling.

VI. Tomography

VI.1 Presentation

Tomography is technical imaging using contrast dye to highlight the carotid arteries in the captured image. The dye used is introduced into the blood vessel. When it goes to the carotid arteries, computed tomography forms radiographic images of the brain or the neck under many angles of observation.

3D tomography is based on techniques which make it possible to obtain the image of a volume at a given time by using a suitable acquisition system, with the possibility of. providing information on any volume in the shortest moment. Thus, the principle of computed tomography, also called computer-assisted voludensitometry, is used for the reconstruction of cross-sections and the reconstruction of the object volume in question.

Generally, the X tomography system permits the real 3D acquisition using a source of X-rays that rotates around the object. The reconstruction of the 3D image translates to each position, and the source acquires an X-ray radiography of the object which has a 2D projection (1.14). By rotating the detector-source system, it gathers a set of radiographs representing the entire set of projections under the different viewing angles, through which 3D reconstruction must be performed (Figure 2.15). Extensions have been proposed for other imaging modalities such as the MRI and the ultrasound. In a certain extent of formalism concerning tomography, X can be retaken [Com'05].

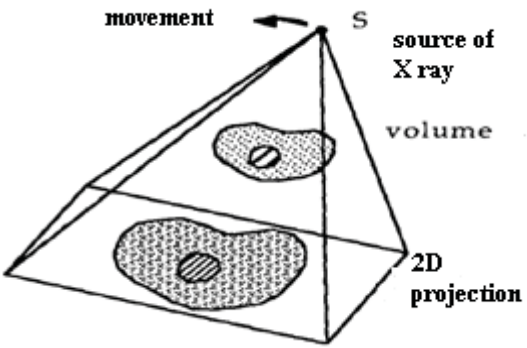

Figure 2.14: Principle of real 3D acquisition from conical sources of X-rays.

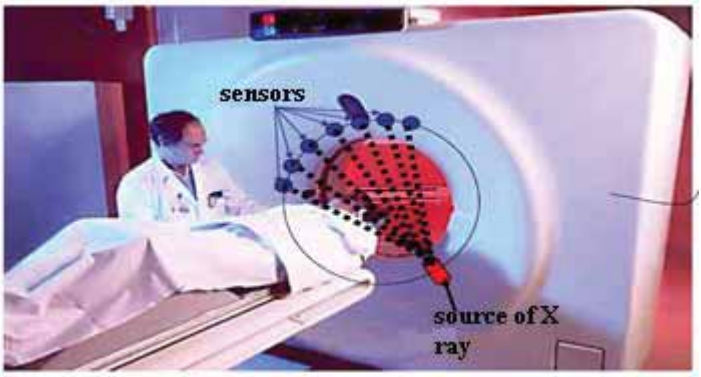

Figure 2.15: Emission scanner of X-rays

The Positron Emission Tomography (PET) technique is a method recognized in noninvasive functional nuclear medicine which ensures a clinic diagnostic of human cells by measuring the metabolic activity. It calculates the 3D distribution of a molecule pointed by a positron emitter. This method is experiencing a constant evolution as regards the used detector and the algorithms. A modern generation of PET scanners provides additional information that can rectify mitigation, delineate lesions and correct therapeutic procedures [Com'05].

PET acquisition can be done either in a 2D mode or in a 3D one. A PET camera is equipped with a system that has the appearance of a scanner but

works otherwise. In fact, the radioactive atom is decomposed by emitting a positron after a short course of one millimeter. This annihilation provides two gamma photons which emerge in the same direction but inversely, which makes the tomographic processing of the data easy. The photon sensors are located around the patient and detect the annihilation photons occurring at the same time, which makes it possible to know the line on which the photons are emitted. Then, a computer system reconstitutes, in the form of a 2D image or of a 3D object, the images resulting from the distribution of the tracer at the level of a part or of the whole body [Ber'08].

However, the problem of reconstructing 3D images from measurements corresponds to integrals of the volume on lines in space. This problem generalizes that of the reconstruction of 2D images from 1D projections. This leads us to recall the basic principles s of 2D tomography. The reconstruction problem was first dealt with in different ways, based on the general methodologies of the inverse problems of image restoration or the theory of the Radon transform.

Generally, the Radon transform is associated with function f (x) of n variables, and its integrals over hyperplanes of R^n. If f (x) is a function of R^n, then its Radon transform can be determined as a function of a real variable r and a unit vector θ as follows:

$$Rf(r,\theta) = \int_{\theta} f(r\theta + s)\, ds \qquad (2.2)$$

For n = 2, the Radon transform r means taking the integral of function f (x) on the straight lines of the plane.

For n = 3, the Radon transform integrates f (x) on the space planes. It can also be expressed by using the distribution of Dirac on R^n, denoted δ, as follows:

$$Rf(r,\theta) = \int_{\theta} f(x)\, \delta(x\theta - r)\, dx \qquad (2.3)$$

VI.2 2D computer-assisted tomography

In computer-aided tomography, 2D acquisition photons allow obtaining a series of 1D projections, which we state a usual parametrization. Let f (x, y) be the continuous function, infinitely differentiable, and to be reconstructed on a bounded support. The projection of an angle θ denoted

p θ (u) is equal to the integrals of function f (x, y) along a straight parallel in the same direction, and limited by the angle θ defined as follows:

$$p_\theta(u) = \int_{R^2} f(x,y)\,\delta(x\,cos\theta + y\,sin\theta - u)dx\,dy \qquad (2.4)$$

Figure 2.16 illustrates an example of a 2D section of an angiographic tomographic image of the carotid artery. The word carotid can refer to a carotid artery, but there is the primary carotid artery and the common carotid artery whose two branches form the internal carotid artery and the external carotid artery.

The internal carotid artery is an artery derived from the common carotid artery and the vascularis is a part the greater the brain, the eye and the inner ear. One of the two side branches of the common carotid artery is the external carotid artery. The latter ensures the vascularization of a good part of the face and the upper part of the neck.

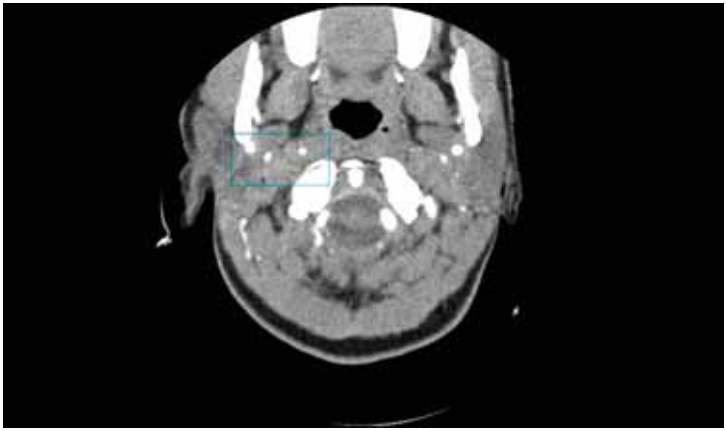

Figure 2.16: Example of 2D cross section of hagiographical tomographic image of carotid artery.

VI.3 Computer-assisted 3D tomography

3D computer-assisted tomography consists in determining variate function f (x, y, z) from its bivariate projections. However, there are two types of projections: divergent and parallel.

The following figure illustrates an example of a 3D image of a 3D computer-assisted angiographic tomographic image of the carotid artery.

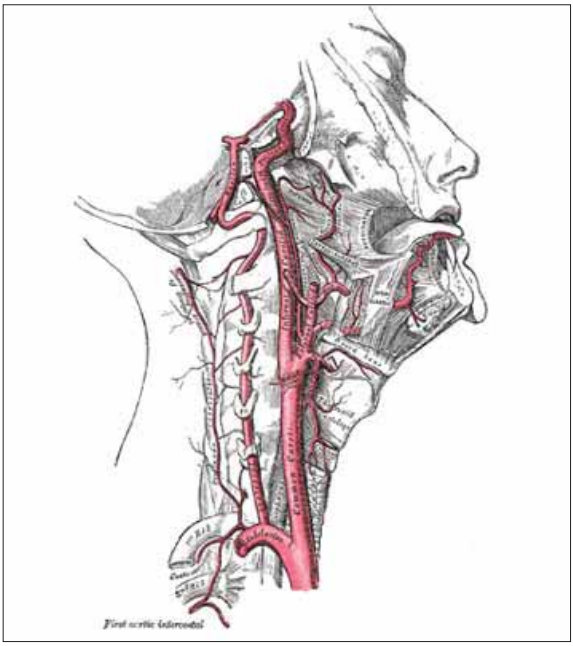

Figure 2.17: Example of picture 3 D of carotid artery.

In the previous sections, we have presented the main modalities of acquisition of cardiac signals and images used for the diagnosis of cardiac abnormalities. We were particularly interested in electrocardiography, scintigraphy and tomography. The study carried out in this first chapter on the anatomy of the heart as well as the electro-physiological properties of the cell membrane has made it possible to better understand the origin and nature of the ECG signal, scintigraphic images and tomographic images.

In the next section, we will first present the basic notions of grammatical formalism. This will allow us to shed light on the theory that will be adopted later for the processing of medical data resulting from the techniques that have been described in this chapter.

Grammar is a formalism allowing to describe a language and to recognize all the learned words [Her'05]. Thus, to start with grammar, several assumptions must be taken into account beforehand in terms of vocabulary, empty words, regular expressions and production rules. We seek to exploit this rigor in the field of 1D and 2D medical data processing

and more particularly in the field of segmentation. Significant data are assimilated to words recognized by automata which take a word as input and accept or reject them. We will show how this idea is applied to the ECG signal and the segmentation of real 2D medical images. This type of task is requested, enough at some point, in applications intended for doctors, explorers and pathologists.

VII. Basics of grammatical formalism

VII.1 Alphabet

We call alphabet (also called vocabulary) a finite non-empty set of symbols. An alphabet is often denoted by $\sum$, A or V, for example $\sum$ = { a, b, c }.

VII.2 Word

We call a word any finite sequence of elements of an alphabet by concatenations.

The concatenation of two given words u and v results in a new word uv constituted by the juxtaposition of the symbols of u and the symbols of v.

Examples of words on $\sum$: a, ab, bac, ca,…

ε: empty word

VII.3 Language

We call language on an alphabet $\sum$ any subset of $\sum$ *.

Example:

Let the alphabet be $\sum$ = { a, b, c }.

Let L 1 be the set of words in $\sum$ * having as many a as b. L 1 is the infinite language.

VII.4 Regular language

A regular language L over an alphabet $\sum$ is defined recursively as follows:

{ε} is a regular language over ∑.
If a is a letter of ∑, {a} is a regular language over ∑.
If R is a regular language over ∑, then R n and R * are regular languages over ∑.
If R 1 and R 2 are regular languages over ∑, then R1∪R2 and R 1 R 2 are regular languages.

A language is represented by regular expressions. All finite languages are regular.

VII.5 Regular expression

Regular languages are very easily described by a regular expression. A Regular Expression (RE) is a sequence of characters which describes a set of possible character strings according to a precise syntax.

ε is an RE which describes language {ε}.
If a ∈ ∑, then a is an RE which describes {a}.
If r is an ER that describes the R language, then (r) * is an ER that describes R *.
If r is an ER that describes the R language, then (r) + is an ER that describes R +.
If r and s are ERs which respectively describe languages R and S, then (r)|(s) is an ER describing R ∪S.
If r and s are ERs which respectively describe languages R and S, then (r) (s) is an ER denoting RS.

VIII. Lexical analysis

Lexical analysis is the first step in compilation. It consists in specifying the recognized words of the language from an input program. The recognized entities are called lexemes, which are a series of characters separated by blanks such as identifiers, keywords, constants, etc.

VIII.1 Automaton

An automaton is a model which takes a word as input and accepts or rejects it.

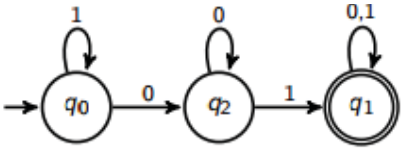

Figure 2.18: Example of PLC

There are two types of automaton: deterministic and non-deterministic.

VIII.2 Deterministic finite automaton

A language denoted by regular expressions is recognizable by a Deterministic Finite automaton (DFA).

A DFA is a quintuplet (Q, ∑, δ, q0, F) where:

∑ is an alphabet,
Q is a finite set of states,
δ : Q × ∑ →Q is the transition function,
q0 is the initial state,
F is a set of final states.

The initial state is marked with an incoming arrow and the final states are marked with a double circle.

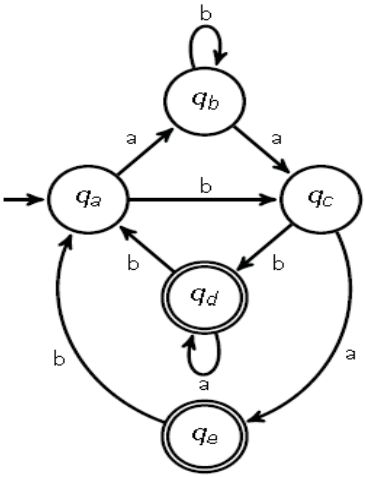

Figure 2.19: Example of DFA

$\sum = \{a, b\}$.
$Q = \{qa, qb, qc, qd, qe\}$.
$q0 = qa$
$F = \{qd, qe\}$
$\delta (qa, a) = qb$
$\delta (qa, b) = qc$
$\delta (qb, b) = qb$
$\delta (qb, a) = qc$
$\delta (qc, b) = qd$
$\delta (qc, a) = qe$
$\delta (qd, a) = qd$
$\delta (qd, b) = qa$
$\delta (qe, a) = qa$

Language L (A) is accepted by an A DFA:

$A = (Q, \sum, \delta, q0, F)$ is defined by $L (A) = \{m \mid \delta (q0, m) \in Q\}$.

Word m is said to be accepted if and only it belongs to L (A).

Kleene's theorem: Any language recognized by a DFA is regular, and vice versa.

In other words:

Any language accepted by a DFA is regular.

Any regular language is accepted by a DFA.

VIII.3 Non-deterministic finite automaton

A Non-deterministic Finite Automaton -(NFA) is a quintuplet $(Q, \sum, \delta, q0, F)$ where:

$\sum$ is an alphabet,

Q is a finite set of states,

q0 is the initial state,

F is a set of final states,

δ is a function from $Q \times \sum$ to the parts Q

δ associates with any state q ∈ Q, and symbol c ∈ ∑ a subset δ(q, c) of Q.

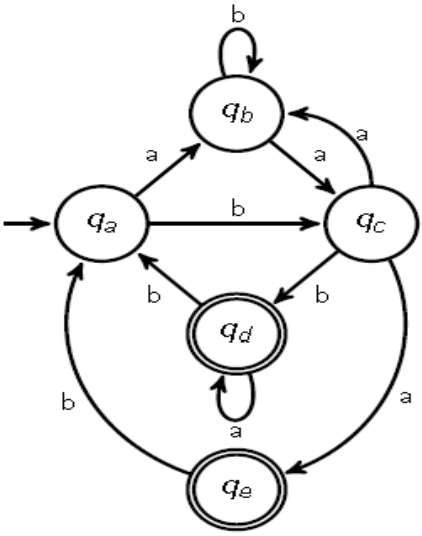

Figure 2.20: Example of NFA

Here, we allow several transitions with the same symbol. The terminology "non-deterministic" is because the current state and the read symbol does not "determine" the next state.

The set of transitions is:

δ (qc, a) = {qe, qb}
δ (qc, b) = {qd}
δ (qa, a) = {qb}
δ (qa, b) = {qc}
δ (qb, b) = {qb}
δ (qb, a) = {qc}
δ (qd, a) ={qd}
δ (qd, b) ={qa}
δ (qe, b) ={qa}

In Figure 2.20, state qc and symbol a do not determine the next state (qb or qe), so it is indeed an NFA.

VIII.4 Lexical analyzer

A lexical analyzer makes it possible to specify the recognized words of the language from an entered program. Table 2.1 defines the most used lexical analyzers, their languages and their operating systems.

Table 2.1: Examples of lexical analyzers

Lexical analyzer	Language	Operating system
Lex	C	Unix
Flex	C	Unix
JLex	Java	Unix
Ocamllex	OCaml	Unix

Generally, the analyzers mentioned above have compatible versions also under Windows. Otherwise, installing a Unix simulator on Windows, such as Cygwin, may resolve this compatibility issue.

Few errors are detectable at the lexical level alone and the errors occur when the analyzer is confronted with a series of symbols, which does not correspond to any of the lexical unit models. Thus, a syntactic analysis will be able to better detect errors.

IX. Parsing

The syntactic analysis structures the sequence of lexemes according to a grammar. The goal of parsing is to determine whether or not a word belongs to the language generated by a grammar.

IX.1 Notion of grammar

Regular languages are expressed using regular expressions, but most of the time languages are not regular and cannot be expressed as an RE. We therefore need a more powerful tool: grammars.

A grammar is a quadruplet G = (T, N, S, P) formed by:

- A set of terminal symbols T,
- A set of non-terminal symbols N where $T \cap N = \emptyset$,
- An axiom often notes S,

- A set of production rules P of type A →B.

IX.2 Types of grammars

There are four types of grammar. First, we have type 3-grammar, also called regular grammar.

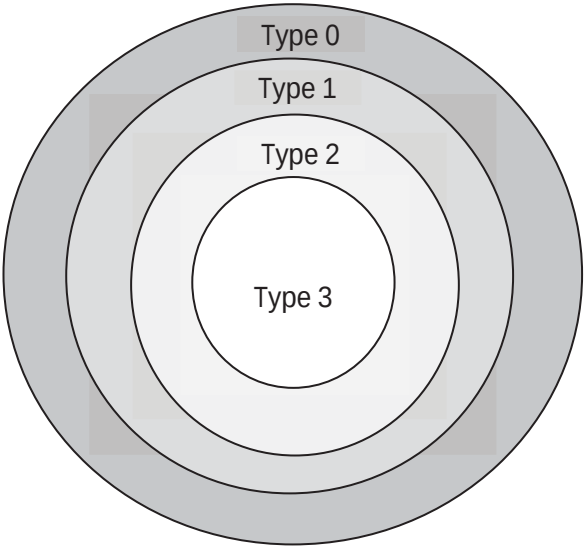

Figure 2.21: Types of grammars

We have the type 2-grammar, also called the context-free grammar. Then we find the type 1-grammar, also called contextual. Finally, we have the type 0-grammar which encompasses any type of grammar. The following figure illustrates these different types in the form of united sets.

IX.2.1 Regular grammar (type 3)

The production rules are of the form A →wB or A →Bw or A →B

where A, B ∈ N and w ∈ T.

IX.2.2 Grammar out of context (type 2)

The production rules are of the form A →B

where A ∈ N and B ∈ $(N \cup T)^*$.

IX.2.3 Contextual grammar (type 1)

The production rules are of the form A →B

where A ∈ $(N \cup T)^+$ and B ∈ $(N \cup T)^*$ et |A| ≤ |B|.

IX.2.4 Grammar type 0

The production rules are of the form A →B

where A ∈ $(N \cup T)^+$ and B ∈ $(N \cup T)^*$.

Type 0 grammars encompass Type 1 grammars which encompass Type 2 grammars that encompass Type 3 grammars.

IX.3 Bypass tree

We call a derivation tree or syntactic tree any tree such that:

The root is the axiom;

The leaves are lexical units or ε;

The nodes are non-terminal symbols;

The children of a node α are $\beta_0, \ldots, \beta_n$ if and only if $\alpha \rightarrow \beta_0, \ldots, \beta_n$ is a production.

Let the grammar have S for axiom and for production rules P:

$$P = \left\{ \begin{matrix} S \rightarrow aTb|c \\ T \rightarrow cSS|S \end{matrix} \right\}$$

A derivation tree for the word accacbb is:

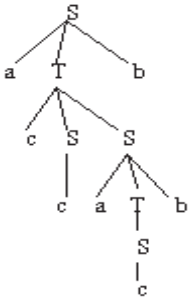

Figure 2.22: Example of derivation tree

For a given word of the language generated by a grammar, the derivation tree is not necessarily unique. The existence of several derivative trees for the same program generally means that there are several possible interpretations for it. They say the grammar is ambiguous.

IX.4 Battery operated automaton

Pushdown automata are re-connoisseurs of context-free languages.

A pushdown automaton is a quintuple (∑, e0, E, T, δ, Γ, τ) defined by:

- a finite set of state E
- an initial state e0
- a finite set of final states T an alphabet ∑ of symbols d 'input
- an alphabet Γ of stack symbols a bottom stack symbol τ
- a transition relation

This automaton (figure 2.23) is a pushdown automaton recognizing the $a^n b^n$ language. It starts by reading a series of a by stacking them, then pops an a for each b read.

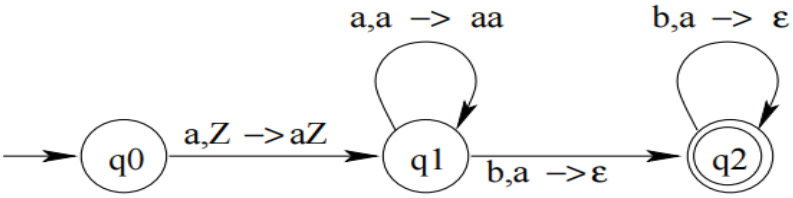

Figure 2.23: Battery-powered automaton for $a^n b^n$

A battery-powered automaton recognizing { $a^n b^n$ }:

E = {q0, q1, q2}
T = {q2}
e_0 = q0
∑ = {a, b}
Γ = {Z}
τ = ∅

The transitions are:

δ (q0, a, Z) = {(q1, aZ)}
δ (q1, a, a) = {(q1, aa)}
δ (q1, b, a) = {(q2, ε)}
δ (q2, b, a) = {(q2, ε)}

IX.5 parser

A parser takes a stream of tokens (tokens) and must say if this flow is syntactically correct, i.e. if it is a word of the language generated by the grammar it has or not. It must therefore try to construct the derivation tree of this flow. If it succeeds, then the word is syntactically correct, otherwise it is incorrect. Table 2.2 defines the most used parsers, their languages and their operating systems.

Table 2.2: Examples of parsers

Parser	Language	Operating system
Bison	C	Unix
Ocamlyacc	C	Unix
Yacc	C	Unix

Some fundamental properties of the source language to be translated cannot be described using context-free grammar because they depend on the context. The role of semantic analysis is therefore to verify these constraints.

X. Areas of application of grammar

In this part, we will briefly cite different fields of application of grammar. The latter is a key step that facilitates data compression, interpretation of video scenes, pattern recognition, ECG signal classification and 2D image segmentation.

X.1. Pattern recognition

In [Moj'00], the author had a set of rules production governing the use of the criteria similarity to judge the similarity between objects in an image. The objective was to design an intelligent perception system based on retrieving patterns from a database. The system should retrieve the closest match in terms of similarity to a request image entered by the user.

In [Fla'10], the author used the grammar for the syntactic recognition of forms. The main idea is to represent a model as a structure of chains, trees or graphs. Then a set of structures is considered as a formal language which can be analyzed with an automaton. The process recognition of syntactic forms consists of three the following main phases:

- Image preprocessing (filtering, improvement…).
- Generation of structural presentations.
- Analysis of structural representations (syntactic analysis).

X.2. Interpretation of video scenes

In [Chr'96], the author described a method which used grammars to direct a vision system for the interpretation of dynamic scenes. The system was implemented based on production rules for the interpretation of the scenario 'put a cup on a saucer on a table then'. Once a feature (fi) is detected and given the current state (qi), a production rule (Pi) is invoked, which results in a new state (qj). The transition from state (qi) to state (qj) indicates a stage in the interpretation of the scene. Each transition in (Pi) therefore has an associated semantic description which describes the observed phenomena.

This is an example of a scenario described by a grammar for putting a cup on a table:

Coffee break → *Putting the coffee cup, Drinking, Cleaning*
Put the coffee cup → *put the saucer, put the cup*

According to Petersohn et al. [Pet'09], because books had chapters, sections, paragraphs and sentences, videos too had an inherent hierarchical structure. The author focuses on recent research in the fields of scene extraction. The first step was the detection of shot transitions with separate detectors for difficult cuts. Then complex cuts were segmented into semantically significant units called sub-cuts. Finally, the results were used to extract the scenes. The author proposed to use the cinematic grammar according to the types of transition to improve the scene detection results. The suggested algorithms were robust to the distortions and artifacts found in the video.

X.3. Data compression

The grammar-based lossless coding theory was proposed in 1999 and 2000 respectively by Kieffer [Kie'99, Kie'00]. The encoding first transforms the original sequence of data to an irreducible grammar which is then compressed using arithmetic encoding. It has been shown that grammar-based encoding can specifically predict good performance on files that exhibit multimedia characteristics.

Let X be a sequence to compress. The transformed irreducible grammar starts from the grammar G composed of the sole production of rule s0 →X, where s0 is the first variable of G, and repeatedly applies the reduction rules in a certain order to reduce G into an irreducible grammar

G'. Therefore, the function of reduction rules is to ensure that an irreducible grammar G exists. The code-based grammar then uses a zero-order arithmetic code to compress the irreducible grammar G to achieve the high compression ratio.

Let x be a sequence to compress.

x = 100111000100011100011.
s0 → 100111.

Each time, add an element to the right then transform the grammar obtained into an irreducible grammar.

s0 → 1001110.
s0 → s1011s1
s1 → 10.

In conclusion, the compressed sequence will be described by the following final grammar G:

s0 → s1s3s2s3s4
s1 → 100
s2 → s10
s3 → s4s2
s4 → 11.

Once the final irreducible grammar G is obtained, it will be compressed using a zero-order arithmetic code of a dynamic alphabet. The decoder retrieves sequence x from grammar G, and then performs the parallel replacement of the overlay procedure as follows:

s0G → s1s3s2s3s4
s1s3s2s3s4G → 100s4s2s10s4s211
100s4s2s10s4s211G → 10011s10100011s1011
10011s10100011s1011G → 100111000100011100011.

XI. Synthesis and discussion

In the previous part, we have succinctly stated several fields of application of grammar. The latter was used for data compression, interpretation of video scenes and pattern recognition.

The use of the grammar for the processing of ECG signals and the extraction of elements of complex types QRS and P and T waves will be described in detail in the following chapter. Much will be devoted to the processing of the ECG signal based on grammar.

Also, later in chapter 4, we will detail image segmentation techniques based on grammatical formalism. Several types of images will be studied such as medical images, facades, cars, buildings, etc.

The following table summarizes some fields of application of grammatical formalism, the primitives and the results.

Table 2.3: Summary of application domains based on syntactic methods

Application areas	Primitives	Results
Data compression	The axiom is the sequence to be compressed; the terminal vocabulary = {0,1}; the non-terminal vocabulary = {subsequence ; transitions attempt to reduce the size of the sequence.	Grammar-based lossless coding. The encoding transforms the original sequence of data to an irreducible grammar.
Interpretation of video scenes	The transition from one state to another indicates a step in the scene.	An associated semantic description describes the observed phenomena.
Pattern recognition	Patterns from a database.	Using the criteria similarity to judge the similarity between objects in an image.

XII. Conclusion

In this chapter, we have presented the main methods of acquiring cardiac signals and images used for the diagnosis of cardiac abnormalities. We were particularly interested in electrocardiography, scintigraphy and tomography. The study carried out in this first chapter on the anatomy of the heart as well as the electro-physiological properties of the cell

membrane have made it possible to better understand the origin and the nature of the ECG signal, scintigraphic images as well as tomographic images.

Also in this chapter, we have presented the types of grammars and the basics of grammar in terms of languages, automata, vocabulary, rules, lexical analysis and semantic analysis. Then, a second part has been devoted to focus on the fields of application of grammatical formalism.

We seek to exploit this rigor in the field of 1D and 2D medical data processing. We will show how this idea is applied to the ECG signal and the segmentation of real 2D medical images. The growing need in this area and the diversity of issues encountered by users justify our investigations.

The following chapter is devoted to the presentation of the different approaches of the literature which apply to the ECG signal, which makes it possible to measure its various parameters.

CHAPTER 3

STATE OF THE ART OF ECG SIGNAL PROCESSING METHODS

I. Introduction

In most pattern recognition applications and for the automatic identification of cardiac impulses, the characterization step is essential. This characterization step is necessary for the rest of the work because it makes it possible to extract useful information from the ECG signal. It also makes it easy to use, both by doctors and by algorithms for automatic processing of information. These correspond to the parameters used by cardiologists to define the cardiac cycle, particularly the cardiac rhythm, the intervals and amplitudes of the peaks and the waves constituting the ECG signal. For a cardiologist, the extraction of information is performed each time a patient's ECG signal is analyzed. In addition, the automation of ECG analysis is very important given the large amount of data. Indeed, this will ensure a significant saving of time as well as a good capacity to carry out numerous analyses. In this chapter, the characterization of the ECG signal is explained by the detection of the QRS complex and the P and T waves of each heartbeat. Thus, the extraction of the fundamental significant parameters will make it subsequently possible to clearly distinguish between pathological beats and normal beats.

II. ECG signal preprocessing

The different noises that affect an ECG electrocardiogram are observed as undesirable and can attack more or less the clinical information. In addition, the complications of the detection of QRS complexes are explained, mainly, in the high variation in the shape of the signal and the presence of these unnecessary noises and of various origins. It is therefore important to know what types of noise can potentially alter an ECG signal.

II.1 Types of noise in ECG signal

During the recording phase of the ECG signal [Qin'03], undesirable events called artefacts may be created on the electrocardiographic tracing. The problem is usually stated during automatic signal analysis, where the presence of these artifacts can produce errors in the diagnosis. These artefacts are considered to be noises and they have been the focus of many studies in the literature [Che'06, Bor'05]. However, processing these noises to date remains difficult to perform automatically. Generally, the noises can be classified according to their origins into two large classes: noise of physical origin and noise of technical origin.

II.2 Technical noise

Noises of technical origin are noises which are generated by the equipment used during the acquisition and of which the most usual noises are:

II.2.1 Noise from the 50Hz network

The 50Hz noise, shown in Figure 3.1, comes from the power supply by the electrical distribution network. This noise affects the EKG signal with oscillations with an extreme harmonic of 50 Hz. Often, this type of noise is present in all acquisitions and it can be quite loud. However, the 50Hz noise is commonly eliminated with a selective filtering phase.

II.2.2 Noise due to electrode-skin contact

When the electrodes used for recording the ECG signal peel off or the gel used enters the electrode and the skin becomes dry, this can provide a noise which is presented by sudden changes in the signal amplitude (see Figure 3.1), besides low frequency baseline medications. In addition, poor conduction between the skin and the electrodes can have an undesirable effect on the EGC signal with a decrease in the amplitude and the appearance of peaks, which can be confused with the waves of the normal signal. This kind of noise is difficult to rule out because its energy is seen in the same frequency range of QRS complexes.

II.2.3 Other noises

Among the other technical noises that can alter an electrocardiogram, we can cite various artefacts due to:

- Movements / displacement of electric cables,

- Saturation of measuring instruments,
- Poor wiring capacity,
- Wearing synthetic clothes,
- RF waves emitted by electrosurgical devices.

II.3. Physical noise

These types of noises of physical origin are produced by movements during breathing or by electrical activities of the body such as muscle contraction.

II.3.1 Baseline fluctuations

The baseline of an EKG is the horizontal line held as a reference for analyzing the amplitudes and shapes of different heart waves. Often the fluctuation of this baseline results in low frequency deviations of the signal amplitude. This fluctuation is mainly linked to the movements of the patient during their breathing. This is because respiratory activity at a steady rate is able to oscillate from the baseline in an ECG recording. This type of noise is illustrated in Figure 3.1. Often, these fluctuations are not very troublesome for the study of the ECG signal and they can be filtered since their energies are in the low frequencies.

II.3.2 Noise due to EMG electromyogram signal

Although EKGs are intended to be particularly sensitive to contractions of the myocardium, an ECG signal can also acquire contractions of other skeletal muscles. Consequently, the noise due to the EMG signal results in the contraction of muscle tissue which is followed by depolarization of the cells. Indeed, this phenomenon gives an electromyogram signal superimposed on the ECG signal in the form of high frequency oscillations.

This type of noise is quite annoying, especially when the patient is moving or shaking. This can drown out P and T waves and sometimes avoid the detection of R peaks. Such a noise is shown in Figure 3.1.

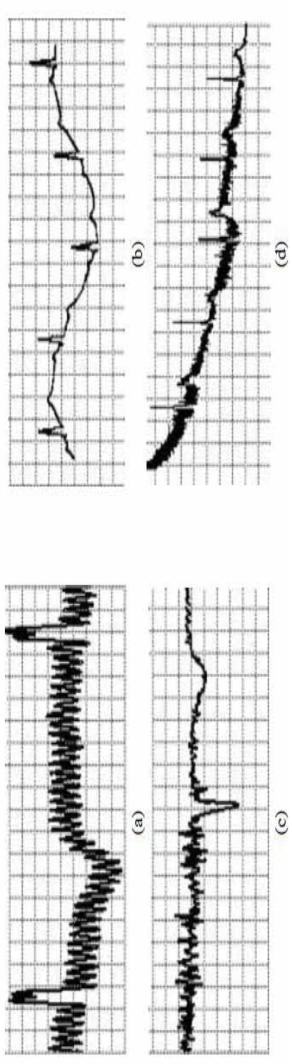

Figure 3.1: Types of noise in ECG signal: (a) Noise from the 50Hz sector; (b) Fluctuations in baseline; (c) EMG signal; and (d) Artifacts due to patient movement.

II.3.3 Other noises

The ECG signal can be too bothered by the diseases such as ischemia, hyperthyroidism and hypokalemia. In addition, the use of certain drugs can slow the heart rate, change the pace of the tracing, and identify AV conduction. This is because it can cause a decrease in the ST segment, an inversion of the T waves and a lowering of the QT interval.

III. State of the art for ECG signal filtering

The primary objective of the preprocessing step is to filter the signal from unwanted noise. For the ECG signal, the noises are well recognized, yet some of them have the specificity of overlapping with the same spectral signal band, which sometimes expresses the difficulty of filtering. In this part, we present some methods and techniques found in the literature as well as the pre-treatments cited to accomplish the characterization of cardiac impulses.

In the literature, several techniques have been proposed for the elimination of artifacts which alter the ECG signal [Ino'98, Nik'00, Nik'01]. Most work has been based on adaptive filters or Infinite Impulse Response (IR) filters by specifying a passband which corresponds to the target information [Sor'06, Lag'92, Bal'09]. Chouhan et al. [Cho'07] developed a filter averager for filtering the ECG signal. Beforehand, the average of the entire signal is subtracted from the ECG signal. Then, a polynomial of order five is applied to have an estimate of the baseline which will be subsequently subtracted from the signal. Shusterman et al. [Shu'00] applied an algorithm based on multi-rate filters. The proposed algorithm minimizes the computation time with respect to a single filter and makes it possible to prevent signal phase shifts.

The ECG is a non-stationary signal which has certain spectral components and it is often contaminated by noise correlated to the signal such as for example muscle artifacts. Consequently, multi-resolution analysis appears to be an adequate tool for preprocessing. For this reason, most recent work has tended to use filters based on the wavelet transform [Sor'06, Rod'07].

In the last decade, methods based on the wavelet transform have become very popular and more used to de-noise the ECG signal. Thus, wavelet-based techniques exploit the fact that the noises are indicated by the set of low-amplitude wavelet coefficients while the useful energy of the signal is focused on the high-amplitude coefficients. In fact, the noise suppression

can be achieved by setting the low coefficients to zero following a thresholding operation and the reconstruction of the signal is established by applying the inverse wavelet transform.

Donoho et al. [Don'95] proposed a de-noise algorithm based on the wavelet transform and carried out in three successive steps:

(1) Applying the wavelet transform to the ECG signal,
(2) The filtering of the coefficients according to a certain thresholding criterion,
(3) The calculation of the inverse wavelet transform, through the coefficients obtained in the previous step.

III.1 Electrical noise cancellation

The current power is originally the most frequent interference in the art recording ECG for the reason that the spectral bandwidth of the ECG signal is between 0 and 250 Hz. The interference results in power line carrier cords and its influence can be minimized by displacing the noise sources. Generally, the power line has a typical frequency of 50 to 60Hz. Therefore, the interference is often excluded by exploiting a filter with an exact stop band centered on the frequency of the power line. Usually, the frequency is 0.05-100Hz.

The powerline interference can be removed by exploiting a non-finite recursive IR. A notch filter for the line carrier can be applied by the guidelines given for ECG monitoring. Nevertheless, the noise powerline is not a pure sinusoid; yet it is deformed. In this case, the use of an adaptive filtering technique is more efficient. Furno et al. [Fur'83] and Sahakian et al. [Sah'83] developed a filter that would eliminate a 60 Hz sine wave from the ECG signal. An adaptive filtering technique can be applied to the termination of the power line and interference due to the EMG signal. In addition, [Ham'86] showed that adaptive filtering introduces less noise compared to a non-adaptive notch filter for ST segment measurement [Par'98, Par'01].

III.2 Reduction of the baseline

When acquiring ECG signals, low frequency noises can be expressed by breathing, by coughing, with a large movement of the chest when an arm or a leg is mobilized. Also, sweating of the patient under the electrodes or

poor contact with the electrodes can modify the electrode impedance. Indeed, artifacts at low frequencies can be provoked.

The fluctuation of the base line may occasionally be experimented by the variation of the temperature and the polarization in the art instrument's measurement and amplification. Thus, digital high pass filters can be used for baseline removal and to filter the ECG signal.

However, the termination of electrical noise can introduce distortions in the ST segment. The latter plays a fundamental role in the detection of heart disorders such as the abnormal coronary artery. Thus, the choice of an ideal cut-off frequency so that the filter can have a minimal distortion is problematic. Some sophisticated filtering approaches used digital filters based on the transformed short-time Fourier or on the wavelet transform [Zhe'95] for the determination of cutoff filters. One study comparing in detail the various techniques of the line cancellation of the basic ECG signal can be found in the literature.

III.3 EMG noise reduction

EMG noise is a motion artifact which translates into an overlap with the cardiac components in the same frequency domain. It is painful to remove this type of noise reliably and efficiently without altering the basic cardiac components in the ECG signal. Accordingly, a bandpass filtering is insufficient to cancel these artifacts. The normal adaptive filtering architectures designed for disappearance are the sounds of ECG signals, the types of noise, and the EMG or artifacts.

Recently, a nonlinear Bayesian filter has been presented for one filtered noisy channel of ECG recordings [Pol'95]. The technique is based on a modified nonlinear dynamics model used for generating a realistic synthetic ECG signal. A modified variety of this model is suggested for several Bayesian filters such as the Kalman filter, the extended filter Kalman, the smoother extended, and the filter odor of Kalman. Indeed, superior results are found for the elimination of non-stationary artifact s muscles, over conventional methods, like the die-sound effects such as bandpass filtering, adaptive filtering and wavelet.

IV. Detection of QRS complex

The detection of QRS complexes is a key step to perform automatic analysis of ECG signals [Li'95, Li'00, Li'01, Inc'09, Min'99]. Usually, the

detection of QRS complexes can be accomplished by simple signal thresholding since, in terms of amplitudes, R peaks are generally larger than other waves. But occasionally the amplitude of the T wave is similar to that of the R peak. Indeed, this can cause errors in the end result and the detection rate. In addition, the R peak can sometimes have a variable morphology and a low amplitude from one cardiac cycle to another. Consequently, very good detection of QRS complexes is essential. This task therefore requires very adequate processing of the signal, taking into account the difficulties encountered. The evolution of the robustness of computer tools for digital processing has ensured the design and implementation of different versions of algorithms intended for the automatic detection of QRS complexes. As a result, the detection of QRS complexes has been the objective of much of the work and continues to be a very active research axis [Dib'09, Dib'11, Wen'09, Wil'87].

Moreover, the variation in the heart rate may alter the duration of the PQ interval and the ST segment, so that the duration of the QRS complex, the P wave and the T wave may also remain a normal heart. In a complex QRS, the R peak is the component famous of the cardiac cycle which can be clearly recognized with a high amplitude and a sharp edge. Thus, it is absolutely significant to limit the ECG signal of the QRS complex to monitor the heart rate. Detecting complex QRS designs is based on the majority of analysis algorithms, which are ECG signals, especially those intended for monitoring arrhythmia, delimiting waves and measuring intervals. It is expressed by the importance of complex QRS in cardiac monitoring.

Several QRS complex search algorithms have been used extensively based on the proportionately high amount of QRS energy found in the 5-25Hz band [Khe'07]. Most algorithms are based on the network of neurons, the hidden Markov model, and the syntactic methods [Szu'92, Bar'98, Bor'96, Cao'90 Lin'01, Lin'03, Olm'97, Oso'01, Ros'98, Shu'12, Wei'10]. However, they are little used in applications with low computational costs. More details on technical detection of QRS complexes and comparison of their efficiencies and their computational complexities can be found in [Khe'07] in the presence of artifacts. Generally, the art QRS detection algorithms are based on one method of derived time, wavelets, filter banks and the mathematical morphology [Ben'09, Ben'10, Ben'12, Wie'99]. In the following sections, the methods of detection of QRS complexes, found in the literature, are discussed. These approaches are very efficient and effective and have a high accuracy rate that exceeds 99%.

Kohler et al. [Koh'02] established a detailed study which synthesized different techniques for the detection of QRS. The discussed methods were sorted by categories with a comparison of their performance.

Christov et al. [Chr'04] made a comparison between time-frequency descriptors and morphological descriptors for the recognition of heartbeats in an ECG signal. Other newer approaches have been based on the wavelet transform and they have proved their efficiency for the search for QRS ([Ruc'10, Din'02]). Thus, this area of research is still active and new techniques have been presented.

IV.1 Time derivative

The complex QRS exhibits high slopes. This feature inspires the use of time derivatives during detection. In the method derivatives, the ECG signal is first of all smoothed with n filters to cancel high-frequency noises outside the 5-25Hz band. Then, the smoothed signal is temporally differentiated to identify the high slopes and ignore the smooth waves and the base line. Globally, the results of these operations correspond to the spectral band of the QRS complex and cancel the low frequencies which correspond to the P and T waves. Then, the amplitude of the derivative signal is squared and allows raising much more derivatives of QRS complexes.

After that, a search algorithm of local maxima above a suitable threshold is performed. The search algorithm can be further optimized by eliminating points that lie within the duration of ventricular activity.

IV.2 Wavelet transform

The art approaches based on wavelets are based on the principle of detecting the feature compared to wavelet coefficients. The latter are analyzed at several scales in [Mal'89, Gra'00, Pal'10, Sax'02, Shy'04, Tik'99] to locate the positions which correspond to two consecutive scales and the local maxima. This technique is based on the assumption that the energy of the QRS complex and the time scales are spread on the spectral bands and the noises do not have this property in the signal ECG. Thus, by using this multiscale approach, the rate of false detection can be reduced.

The wavelet transform is a very powerful tool for a good detection of the R peak in a QRS complex of the ECG signal. Among the essential properties of the wavelet transform lies in the localization of the peak of a

wave [Kha'09, Duv'02, Har'96, Has'06, Lag'04, Lu'00, Sah'97a, Sah'97b, Sah'98].

The characteristic of the continuous wavelet transform is given by the equation which verifies this property:

$$\psi_{a,b}(t)dt = \frac{1}{\sqrt{a}}\psi(\frac{t-b}{a}) \quad (3.1)$$

where :

$a \in \mathbb{R}^+$ is a scale factor (expansion parameter),
$b \in \mathbb{R}$ is a translation parameter.

Morlet proposed to create function bases built on the following model [Mis'03]:

$$\psi_{j,k}(t)dt = a0^{-j/2}\,\psi(a0^{-j}t - kb0) \quad (3.2)$$

where:

a0> 1 and b0> 0 are fixed and j, k ∈ Z

This discretization assigns values on a logarithmic scale *a* with translation parameters *b* which are proportional to it:

$$a = a0^{j} \; et \; b = kb0a0^{j} \quad (3.3)$$

A commonly used range of scales is the dyadic range, i.e. a0 = 2 and b0 = 1.

We thus obtain families made up of functions of the form:

$$\psi_{j,k}(t)dt = 2^{-j/2}\,\psi(2^{-j}t - k) \quad (3.4)$$

The greatest energy of the QRS complex of the ECG signal (between 5 and 15Hz) is at scale 24 of the Dyadic Wavelet Transform (DyWT). Based on this property, we design a location algorithm of the QRS complex and then detect the R-wave of the complex.

The adopted method is based on the use of a technique applied to the detection and precise localization of the R wave of the QRS complex by dyadic decomposition using a Daubechies4 wavelet, which is characterized by its model that is close to the ECG signal, is described as follows:

i. Calculate the DyWT of the electrocardiogram signal by (3.4), and then we choose scale 24 of this transform:
ii. For window i, find the positive maxima and the negative minima of the DyWT, to locate the different waves of the ECG signal.

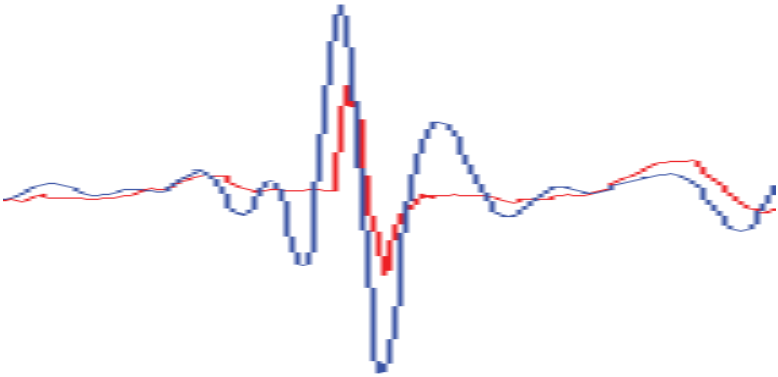

Figure 3.2: DyWT: (a) the cardiac cycle (red) and (b) the positive maximum and negative minimum of DyWT (blue).

In the previous figure we can notice that the DyWT QRS, we are trying to locate, has the largest amplitude in comparison with other wave characteristics of the ECG signal. This prompts us to use thresholds large enough so that only the DyWT waves of the QRS complex are detected.

These operations are performed as follows:

i. Choose a positive threshold Sp(k) and a negative threshold Sn(k), the first to determine the positive maximum Mp(k) and the second for the negative minimum Mn(k) of the wavelet transform of the QRS:
ii. Check if the DyWT, calculated by (3.4), exceeds the thresholds:

$$\text{If } C_{3,k} > S_p(k) \text{ then } M_p(k) = C_{3,k} \text{ is a probable positive maximum,}$$
$$\text{If } C_{3,k} < S_n(k) \text{ then } M_n(k) = C_{3,k} \text{ is a probable positive minimum,}$$

Then Mp(k) and Mn(k) are the maximum of Mp(k) and the minimum of Mn(k), respectively, for the same maximum positive-minimum negative torque.

iii. Remove redundant maxima and minima and isolated torques. The principle is to eliminate among two minima (or maxima) the minimum (or maximum) furthest from the maximum (or minimum) of the torque, so as to have at the end only the couples of the closest positive-negative minimums. and which are most likely to be the wavelet transform of the QRS complex.
iv. Since the peak of each complex or the R wave is located between a positive-negative maximum at zero crossing, we limit the search for R in this interval.
v. Find the R peaks of QRS complexes from different intervals limited by the max-min pairs while trying to have DyWT (i) = 0.

IV.3 Mathematical morphology

Mathematically, the length of a curve is determined by the sum of the Euclidean distances between the pairs of successive sampling points. In an ECG signal, l is the length of the curve as a function of the values of samples and the sampling time. In a uniform sampling in time we measure the increment of the value of the sample to calculate the length of the curve. Practically, the length of the waveform in an ECG signal is viewed in a window at a length that corresponds to the QRS complex. With a perfect alignment window with the start of the QRS complex, the local maximum is determined to delineate the QRS complex. In [Tao'1 0], an approach based on the length of the curve was used for the detection of the QRS complex. As a preprocessing step, the author used a low-pass filter with a frequency cutoff of 16Hz to cancel noises.

In the literature, numerous studies have been tested and confirmed on the basis of MIT-BIH. The methods are very varied and each of them is based on an appropriate technique. A comparative study is summarized in Table 3.1.

Table 3.1: Comparison of performance of QRS complex detection algorithms cited in the literature.

Reference	Method	Specificity (%)
[Pan'85]	Derivative approach based on slope analysis	99.30
[Ham'86]	Derivative approach based on an optimized decision rule process	99.46
[Szu'92]	Approach based on adaptive filtering and a neural network	99.50
[Sai'12]	Approach based on Euclidean distance and a K Nearest Neighbor (KNN) algorithm	99.81
[Cho'12]	A multi wavelet packet decomposition	99.14
[Had'10]	An empirical modal decomposition (EMD)	99.92
[Scream'04]	Method based on the use of adaptive thresholding	99.65
[Gha'08]	Mathematical model based on the continuous wavelet transform (TOC)	99.91
[Kyr'88]	Approach based on recursive temporal prediction	99.00
[Meh'08]	support vector machine-based approach	99.75
[Gri'98]	Transformation based on time and energy	99.26
[Ben'12]	Method based on discrete wavelet decomposition and energy calculation	99.39

In the next section, we will briefly cite popular methods for detecting QRS complexes found in the literature. We can cite the techniques based on:

a) Digital filters (Nagin et al. [Nag'01], Daskalov et al. [Das'99]).

b) Linear and non-linear transformations: (Gritzali, [Gri'98], Pan and Tompkins, [Pan'85]), the Hilbert transform (Benitez et al. [Ben'01]), the first derivative (Arzeno et al. [Arz'06]).
c) Statistical analyses (Silipo et al. [Sil'98], Watrous et al. [Wat'95]).
d) Time-frequency analyses (Afonso et al. [Afo'99], Li et al. [Li'95], Senhadji et al. [Sen'95], Kadambe et al. [Kad'99], Kyrkos et al. al. [Kyr'88]).
e) Evolutionary methods (Poli et al. [Pol'95]).
f) Neural-fuzzy approaches (Engin et al. [Eng'04]).
g) Hidden Markov models (Coast et al. [Coa'90]).
h) Mathematical morphology models (Trahanias et al. [Tra'93], Taouli et al. [Tao'10], Chu et al. [Chu'06]).

In practice, it is impossible to find a single technique that is both efficient and complete with a complete preprocessing for the reduction of the different types of noises and for the detection of QRS complexes [Cey'07, Tig'03]. A compromise can be established between the robustness and the false detection. This is based on the choice of filter bandwidth and the size of the window used.

V. P and T wave detection

In an ECG signal, the sequence of appearance of waves is P-QRS-T. This sequence represents a single cardiac cycle. In the preliminary part, we study the detection methods of QRS complexes found in the literature. However, the detection of the P and T waves is also essential as the P wave indicates the atrial activity and the T wave symbolizes the repolarization of the ventricles.

Nevertheless, the analysis of the P and T waves n is more obvious as they represent amplitudes and lower slopes. However, we can search for both P and T waves in appropriate time slots before and after the location of the QRS complex.

In a cardiac cycle, the T wave has the greatest level of energy. The location of this wave depends on the peak R and the duration time measured between two successive R peaks, referred to simply as distance RR. Thus, if the RR distance is greater than 700ms, the T wave search window is based on the position of the peak R, in the range of 140 to 500ms.

For the P wave, the search window is produced in the 240 to 400ms time interval preceding the R peak of the QRS complex. As soon as the search windows are determined before and after the localization of the QRS complex, an appropriate method is employed to improve the distinctive properties of the P and T waves and find its limits.

The methods of the detection waves P and T are based on the wavelet transform (WT) [Bul'02, Ben'03]. The latter describes the signal in the time domain and allows a representation of the temporal characteristics with different resolutions of a signal. Comparable with QRS detection, the wavelet transform has already shown interesting results for the delineation and detection of waves P and T.

Li et al. [Li‘95] presented a method for detecting the complex QRS based on the Discrete Wavelet Transform (DWT). Moreover, the author also applied in the same job the WT to delimit the P and T waves. Martinez et al. [Mar‘04] generalized this method of delimitation of the P and T waves to be applied to a wide range of morphologies.

In [Cab’08], Cabasson et al. considered the problem of the delimitation of the P and T waves identical to a problem of time delay estimation.

Other methods have been based on the DWT. Indeed, in the ECG signal, the local minima and maxima of the DWT define the local singular points. The sampling rate is graded the same and it is applied on all scales to preserve the temporal resolution and the time invariance.

During the last two decades, several approaches have been proposed to detect P and T waves in an ECG signal [Li'95, Mar’04, Cha'04, Chi'06a, Chi'06b, Chi'08, Gho‘09, Kir'09, Lag'00, Ube'05, Ube'08, Ube'09].

Furthermore, the other delineation strategies of P and T waves are applied such that the uniform thresholding, the transformation length, the theory of the function approximation, the characterization of the TU complex, the pattern recognition [Ste'02], the support vector machines [Kam'09, Meh'08, Mel'08] and the syntax methods. These latter types of syntactic methods will be detailed in the next section.

VI. Discussion of usual methods

The analysis of ECG signals, by the temporal and frequency methods presents major drawbacks in the diagnosis of certain very complex cases. These limits of these methods can make the observation of certain

pathologies difficult and this is due to the non-stationary nature of these signals. To overcome the weaknesses of one-dimensional techniques, the use of the time-frequency technique, which takes into account both the time parameter and the frequency parameter, on non- stationary ECG signals is inevitable.

In [Pan'85], the size of the integration window must be adapted to the average width of a QRS complex. If it is too large, the maximum is shifted in time with respect to the position of R (influence of the T wave); if, on the contrary, it is too small, we obtain several peaks for the same R wave. The size chosen by Pan & Tompkins empirically is 150ms, which corresponds to double the average width of a QRS complex. After signal integration, the available signal has an absolute maximum for each QRS complex; it also has other local maxima, generally of a lower amplitude; they correspond either to noises or to T waves. The algorithm presented by Pan & Tompkins presents a detection rate of QRS complexes of 99.3%. However, the weak point of the algorithm is the low detection rate at the level of some records such as 108 and 222 from the MIT-BIH database. In fact, for recording 108, the error rate is very high because the amplitude of the P waves is comparable to that of the QRS complexes. In record 222, the P-wave morphology is comparable to that of QRS complexes, which is a cause of error and will increase the rate of false positives.

The algorithm presented by Dubois et al. [Dub'04] has a detection rate of 98.90%.Detection errors appear for some particular pathologies such as ventricular tachycardia or the case of low amplitude extrasystoles. Indeed, for a ventricular tachycardia (record 207), the error rate is very high because the patient presents periods of ventricular tachycardia on several occasions. During these periods, the reference annotations are absent. On the other hand, the algorithm annotates the recording at the frequency of a tachycardia. Another weak point of the algorithm is the detection of low amplitude extrasystoles. These are assimilated to T waves because their amplitudes and speed of variations are of in the same order.

The algorithm of Ying et al. [Yin'92] is tested on some signals from the MIT-BIH database. Detection errors appear for a few recordings such as record 108 where the amplitude of P waves is comparable to that of QRS complexes; a very high error rate is thus reported because the P waves are considered to be R waves.

Different statistical methods of detecting QRS complexes of the ECG signal have been described and they are based on a temporal analysis of

the ECG signal. Their performance has been evaluated and their limits studied. These limitations are mainly related to the quality of the ECG signal. Indeed, a very noisy recording or even which presents other parameters, such as the ventricular extrasystoles of low amplitude, the P and T waves comparable to that of the R waves and the sharp decrease in the amplitude of the R wave, greatly affect the detection of QRS complexes and so decreases the robustness of each of the methods.

Moreover, the usual methods which are based on a temporal analysis of the signal mainly suffer from two limitations: their sensitivity to noise and to the choice of the threshold. For methods based on wavelets, the art work depends on the mother function used. The art methods have been based on neural networks, where the network must be fully connected, and they suffer some slow learning time.

However, the approach syntax does not have any very important features. Indeed, it advocates some points, as confirmed in the following section. These characteristics are: simplicity, brevity, clarity, comprehensibility and modification of the computer program which implements the syntactic approach.

In order to improve the detection rate of QRS complexes and to diversify the techniques for processing the ECG signal, grammar-based methods are proposed, described and evaluated in the following section.

VII. Syntax methods for processing ECG signal

Trahanias et al. [Tra'90] presented an application of a syntactic method for the recognition of the ECG signal and the measurement of its parameters. The work consists of two parts: peak extraction and peak grammar analysis.

VII.1 Extraction of peaks

Each peak is characterized by three points: the two left and right end points plus an energy value. A peak can be either linear or parabolic. The peaks and endpoints are extracted by traversing the signal interval by interval.

In [Tra'90], a method of recognizing erroneous peaks or false peaks in an ECG signal was presented. The erroneous peaks appeared under the shape of the adjacent peaks to satisfy a set of criteria. The direct methods

recognize all the peaks $\{P_1, P_2,\ldots, P_i\}$, and then reject the false peaks based on a set of criteria.

Each peak P_i is characterized by a time Px_i and an amplitude Py_i.

The criteria are applied to each five consecutive peaks $\{P_{i-3}, P_{i-2}, P_{i-1}, P_i, P_{i+1}\}$ as illustrated in Figure 3.3

The peak evaluation criteria are based on the amplitudes and durations of the five peaks:

$$Py_{i-3} <= Py_{i-1} \quad AND \; Py_{i-1} >= Py_{i-2} \tag{3.4}$$

$$| Py_{i-2} - Py_{i-1} | <= \text{threshold s1} \tag{3.5}$$

$$\Delta t_m <= \text{threshold s2} \tag{3.6}$$

$$\text{if } \Delta t_m <= \text{ threshold s3 then ignore} \tag{3.7}$$

$$\Delta t_m >= \Delta t_g \; AND \; \Delta t_m >= \Delta t_d \tag{3.8}$$

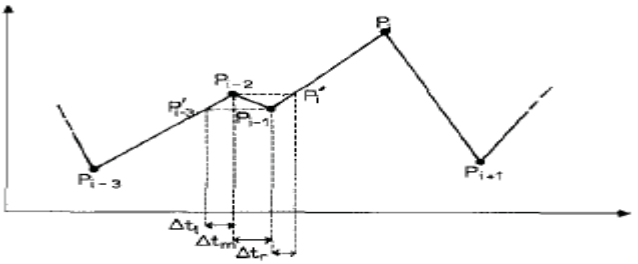

Figure 3.3: Method application of on each group of five peaks and detection of false peaks.

The peaks having amplitudes greater than a fixed threshold are not considered as false peaks.

The peaks having durations greater than a fixed threshold are not considered as false peaks.

The false peak detection algorithm applies to a group of five consecutive peaks:

Start

i ← 0
P0 ← the first peak of the signal
Step1: find the next peak
If there are no following peaks then
End
End if
Step 2 : i ← i + 1
If i <3 then
Go to step1
End if
Step3 : If the peer (P_{i-2}, P_{i-1}) is not noisy then
goto Step1
End if
P_{i-2} ← P_i
i ← i-2
If i <3 then
goto step1
End if
goto step3

End

A sequence of n peaks is considered a QRS complex if they have satisfied the following two conditions:

1) The sum of energies of the n peaks is greater than threshold s1:

$$\sum_{i=1}^{n} e_i >= s1$$

2) The angle between the two consecutive peaks (peak i and peak i + 1) is less than threshold s2:

Angle (peak i, peak i + 1) <= s2

The concept of angles makes it possible not to confuse the QRS complexes and the P and T waves. The recognition of the P and T waves is based on the measurement of the amplitude and the wave width compared to thresholds s3 and s4.

One or two consecutive peaks are recognized as being a P or T wave, by fixing their width and their amplitude according to the syntactic rule

evaluated. They are discriminated from other peaks by comparing their energies. Noisy peaks in a region between two QRS complexes must have less energy than the energy of the P and T complexes in that region. The alternative of the syntactic rule which corresponds to a P or T wave specifies its morphology. It is noted that the P and T waves that occur before the first and after the last QRS complex found are not recognized. It helps to make the grammar easier.

VII.2 Grammatical analysis of recognized peaks

In [Tra'90], the author used alphabet $\sum$ = {K +, K-, rest, wave} knowing that:

K + would describe a positive peak,
K- would describe a negative peak.

Indeed, an ECG signal was assimilated to a series of symbols of $\sum$. Each symbol was assigned corresponding values. Next, the author used a context-free grammar G = (VT, VN, S, P) to describe an ECG signal where VT represented the terminal vocabulary, VN represented the non-terminal vocabulary, S was the axiom, and P represented the production rules.

Grammar G = (VT, VN, S, P)
VT = {K +, K-, rest, wave}
VN = {ECG, Start, End, Cardiac_cycle, Cardiac_cycles, QRS, Peak, Segment, Rest, Non_QRS, Q, R, S, P, T, R ', S', R'', S'', SR, ST, TR, SP, PR, TP, A, B, C, D, E, F}
S = {ECG}

P represented the following rules where "." is a concatenation operator:

ECG → Start . Cardiac cycles . End
Start → ∈ | Segment . Start | Peak . Start
Segment → rest | wave
Peak → K + | K-
End → QRS . Rest
Rest → ∈ | Segment . Rest | Peak . Rest
Cardiac_cycles → Cardiac_cycle . Cardiac cycles
QRS → [Q]? . R . S . R' . S' . R''. [S"]? | [Q]? . R . S . R' . [S']? | [Q]? R . [S]? | Q . S

Non_QRS → SR | ST . T . TR | SP . P . PR | ST . T . A
A → B | C | D | E
B → ∈ | P . B
C → TP . P . PR . P . PR
D → TP . P . PR
E → ∈ | Peak . E | Segment . E
ST → F
TP → F
PR → F
TR → F
SP → F
PP → F
SR → Segment . F | Peak . F
F → ∈ | Segment . F | Peak . F
T → K + . K- | K- . K + | K + | K-
P → K + . K- | K- . K + | K + | K-
R → K +
R' → K +
R" → K +
Q → K-
QS → K-
S → K-
S' → K-
S" → K-

In [Tra'90], the classification of QRS complexes was performed by a KNN nearest neighborhood classification algorithm. The distance between a given QRS complex and a given class of QRS complexes was calculated as the average of the distances between the given QRS complex and each QRS complex in the given class of QRS complexes. Morphological (structural) and quantitative (statistical) characteristics were taken into account in the distance calculation. The normalized duration and the normalized amplitude were the statistical characteristics used. Morphological characteristics, in calculating the distance between two complexes, were taken into account by aligning the complexes so that they would match the best.

Kokai et al. [Kok'97] used grammar rules to recognize QRS complexes and distinguish between QRS and non-QRS data. A QRS complex had to meet the following three conditions:

The value of a peak had to be greater than threshold s1.

The angle between the right segment of peak i and the left segment of peak i + 1 had to be less than threshold s2.

The angle of each peak was less than threshold s3.

The author used grammar G = (VT, VN, S, P):

- VT = {K +, K-, line, parabola}

where K + described a positive peak and K- described a negative peak.

- VN={Cardiac_cycles, Cardiac_cycle, Peak, Peaks, QRS, Non_QRS, Segment, Interwave_segment, SR, T_or_P, P, T}
- S = ECG
- P represented the following rules:

  Cardiac cycles → Cardiac cycle . Cardiac cycles
  Cardiac cycles → ∈
  Cardiac cycle→ QRS . Non_QRS
  QRS →Peak . Peaks
  Peaks → Peak . Peaks
  Peaks → ∈
  Peak→ K+ | K-
  Non_QRS → SR | Interwave_segment . T . Interwave_segment | interwave_segment . P . interwave_segment | Interwave_segment . T . Interwave_segment . P . Interwave_segment
  SR → segment . Interwave_segment | Peak . Interwave_segment
  Interwave_segment → ∈ | Segment | Interwave_segment | Peak. Interwave_segment
  T → T_or_P
  P → T_or_P
  T _or_P→ K+ | K- | K+ . K- | K- . K+
  Segment → line | parabola

Hanieh et al. [Han'15] proposed a method to detect atrial arrhythmias. The suggested method modeled arrhythmias using regular expressions. In fact, the ECG signal was transformed into a series of symbols, each symbol of which represented an element of the wave or peak type signal.

VII.3 Discussion

Although the syntactic method appears to be suitable for the problem of recognizing ECG signals and measuring parameters, little progress has been made so far. In the reported attempts, only specific aspects of this problem have been addressed. A context-free grammar for the recognition of the peak in ECGs is described. Grammars have been proposed for the detection of QRS complexes. Grammars out of context have been used for the detection of some ventricular arrhythmias. An attempt at arrhythmia analysis using the finite state automaton model is described, and even filtering ECG waveforms by the syntactic method has also been investigated.

The application of the syntactic approach to the recognition of ECG signals and to the measurement of parameters, which has been described in this document, has given results inferior to those reported by some implementations using the non-syntactic approach. However, the non-syntactic approach is quite mature in this particular problem after considerable research work over many years. In the syntactic approach, there is a lot of room for improving the results by further refining the method. We have observed that the extractor primitive pattern does not always accurately define the limits of the peaks. This type of error spreads into the following steps and is responsible for many inaccurate results. Removing this deficiency will considerably improve the overall performance of the approach.

Hanieh et al. [Han'15] applied their method on the MIT-BIH basis of arrhythmias. However, the algorithm showed an average sensitivity rate that did not exceed 96.3%. In [Kok'97], no information was given on the database used and the sensitivity rate achieved. In addition, the methods mentioned above were very sensitive to noises. Due to noise, several morphologies could be found and thus interfere with the grammatical description of the signal and generate erroneous peaks. Indeed, grammar could classify several signal types as an ECG signals. On the other hand, the grammatical formalism was only used at level 3 (Figure 3.4) to make the spatial interpretation of the elements of the signal. In other words, the authors did not exploit the formalism of the grammar during the peak extraction phase at level 2 (Figure 3.4).

In addition, the syntactic methods cited above are sensitive to the choice of energy thresholds (amplitudes) and intra and inter peak thresholds. Indeed, our objective is to extend the level of use of the grammar and to utilize the grammar to make the extraction of forms (level 2) as well as their spatial

interpretation (level 3) while adding other standard deviation and duration criteria. We will use a type-3 grammar for the extraction of QRS complexes from an ECG signal and a type-2 grammar for the recognition of the ECG signal.

The following chapter presents the work carried out in the application of the syntactic method to the whole problem of recognizing ECG shapes and measuring parameters. Solutions to the subproblems of selecting primitive patterns, extracting primitive patterns, linguistic representation and formulating a pattern grammar will be described.

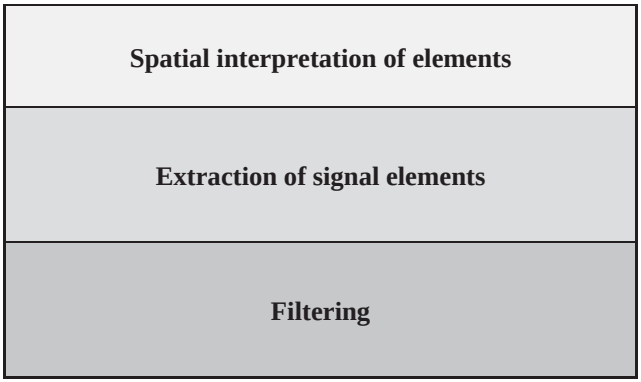

Figure 3.4: Three levels of signal processing.

VIII. Conclusion

In this chapter we have mentioned an overview of ECG signal preprocessing techniques as well as QRS complex detection approaches and P and T wave delineation methods. To improve the heartbeat detection rate, it is important to do a signal processing step. The characterization of ECG signals lies in the localization of QRS complexes and the recognition of P and T waves in each cardiac cycle. In fact, the parameters representative of these elements are necessary and make it possible to clearly distinguish between pathological beats and normal ones.

The usual and statistical methods of processing the ECG signal have been based on a temporal analysis of the signal. Their limitations are mainly related to the quality of the ECG signal. Indeed, a noisy recording or one which presents P and T waves comparable to that of R waves, or a sharp

decrease in the amplitude of the R wave, has a huge influence on the detection rate and thus reduces the robustness of the methods.

In order to improve the detection rate, we will present, in the next chapter, a method for detecting QRS complexes based on regular grammars as well as a second method for detecting whole cardiac cycles based on the same principle.

CHAPTER 4

QRS COMPLEX EXTRACTION AND GRAMMAR BASED HEART CYCLE RECOGNITION

I. Introduction

A grammar is the formalism for describing languages and recognizing all the words learned. However, few grammar-based approaches for ECG signal processing [Tra'90, Kok'97]. Kokai et al. [Kok'97] have presented a learning machine capable of learning both the syntax and the semantic rules of an ECG grammar. The QRS complex is considered a negative peak followed by a positive peak followed later by a negative peak. Trahanias et al. [Tra'90] applied a syntactic recognition method to measure the associated parameters of an ECG signal. In addition, Gao et al. [Gao'00] asserted that, compared to statistical methods, the use of grammars would offer more flexibility in applications.

The main advantage of these methods concerns the representation that it can make available. Syntactic approaches can powerfully represent object structures and thus make it easy to retrieve information. The input data appears to be a structured scene having a hierarchical order because grammars can clearly represent hierarchical structures using non-terminal and terminal nodes. Moreover, syntactic approaches are able to describe a large set of complex objects using small sets of simple primitives and grammatical rules [Ped'13].

In this context, our work is registered and we will describe an ECG signal as a sequence of waves and of peaks on the basis of a specific vocabulary and set of grammatical rules with constraints. First of all, the aim of our analyzers is to classify the input signal in the case of an ECG signal or not. Then, if it is retained as an ECG signal, our analyzers aim to determine the number of cardiac cycles and the various indicators such as the QRS complex duration, the RR distance, and the QT and PR intervals for each cycle.

Indeed, in the next section we will use the regular type-3 grammar for the recognition of QRS complexes in the first place and for the recognition of cardiac cycles in the second place.

II. Recognition of QRS complexes by regular grammar

In this part, we will show that the regular grammar and the deterministic automata are also useful for the extraction of QRS complexes and RR distances and the interpretation of ECG signals. The automata will be used to represent a normalized QRS complex as a sequence of positive and negative peaks based on the regular grammar. The method is applied to ECG signals from the MIT-BIH standard database. For an input ECG signal, several parameters are determined, such as QRS times, RR distances and amplitudes of recognized peaks.

Figure 4.1 summarizes all the steps of the proposed method. The amplitude of the input signal is filtered, centralized and normalized. Then, the lexical analysis step recognizes the lexemes corresponding to the rest phases, to the positive peaks and to the negative peaks. Based on the length and standard deviation of the lexical units, the analyzer differentiates between the rest, the peak and the wave. Taking into account the sampling frequency and the time, the analyzer then calculates the RR distances and the QRS times and generates a medical report.

II.1 Signal preprocessing

In fact, an ECG signal S [n] is too noisy and contains many artifacts, hence the need for preprocessing phases to reduce noise and facilitate lexical analysis afterwards. The band pass filter reduces the influence of muscle noise, the 60Hz interference and the T wave interference and promotes the baseline. The desirable bandwidth to maximize the energy QRS is about 5-15 Hz [Pan ’85].

The mathematical equations below describe the different stages of the preprocessing phase: bandpass filtering, centralization and normalization of the signal amplitude. An example is shown later in Figure 4.2 where an ECG signal representing tachycardia is filtered by a band pass filter, normalized and centered.

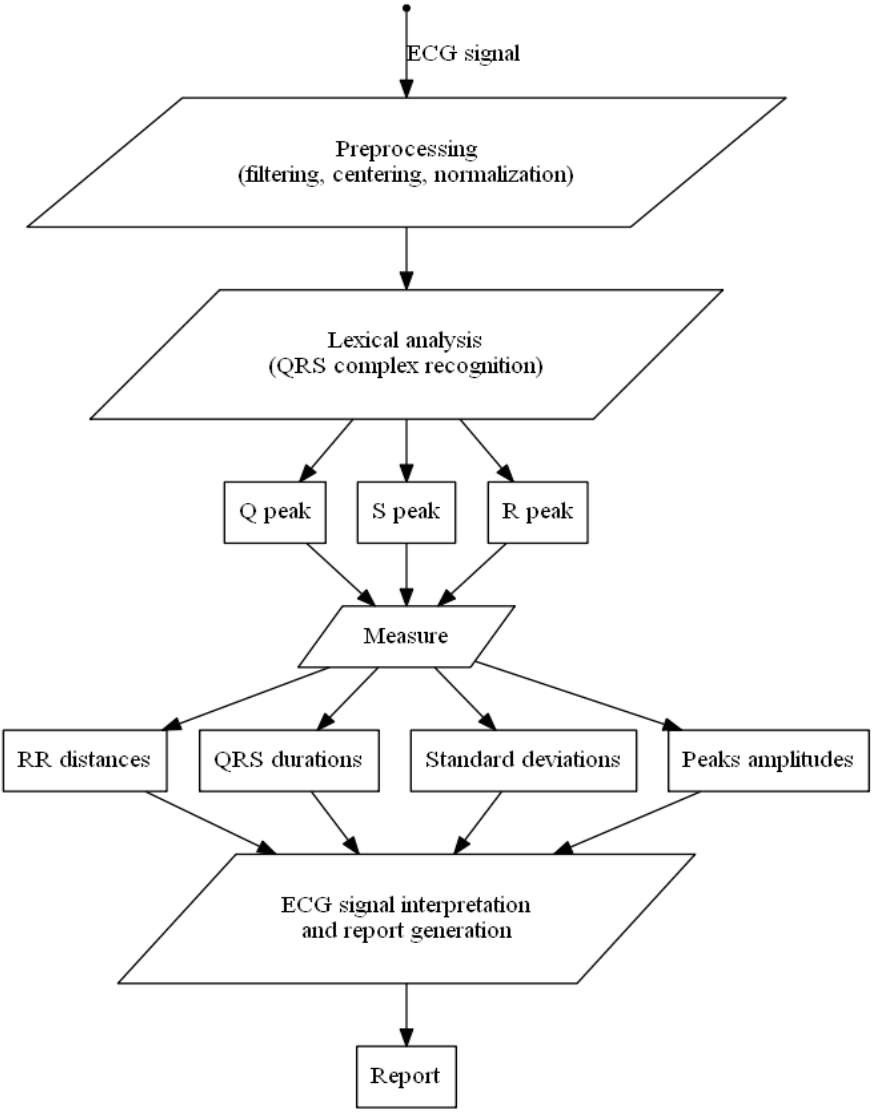

Figure 4.1: Diagram of the proposed method for QRS complexes extraction based on regular grammar.

Step 1: Bandpass filtering:

S[n] is the signal and H[n] is the bandpass filter where the cutoff frequency is 5-15 Hz.

$$S1[n] = S[n] * H[n] \quad (4.1)$$

Step 2: Centralization of the signal:

$$S2[n] = S1[n] - \frac{\sum_{n=1}^{m} S1[n]}{m} \quad (4.2)$$

Step 3: Standardization of the signal amplitude:

$$S3[n] = \frac{S2[n] - Mean(S2[n])}{Max(S2[n] - Mean(S2[n]))} \quad (4.3)$$

Figure 4.2 shows an example of an actual ECG signal before and after the filtering process. The input signal was from a patient who represents tachycardia. The preprocessing process eliminated the artifacts well and centralized the signal.

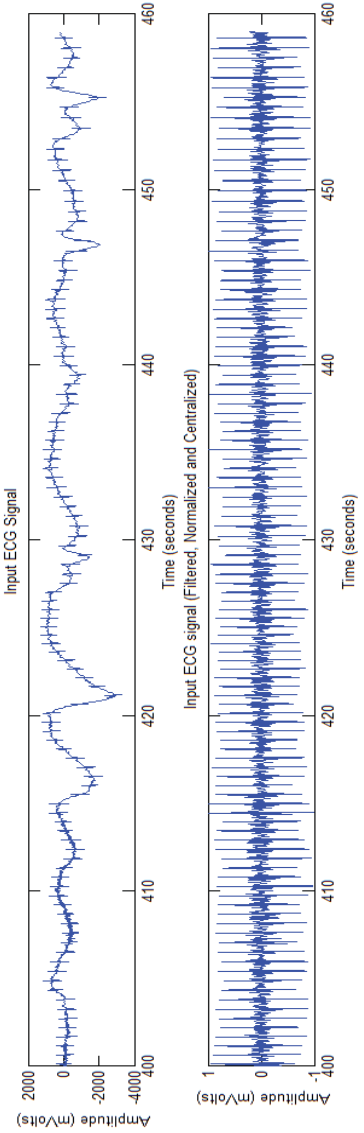

Figure 4.2: (a) Input ECG Signal representing tachycardia. (b) Centered signal and filtered by a bandpass filter.

II.2 Grammatical analysis of the signal

Here, the amplitude of the signal is treated as a sequence of values belonging to the bounded interval [-1, 1]. Normalized amplitude is described as a sequence of near zero, negative, and positive values. In other words, the signal is assimilated to a language where a QRS complex represents a sequence of words.

The amplitude of the output signal is processed as a sequence of values belonging to the bounded interval [-1, 1]. A normalized amplitude is described as a sequence of near zero, negative, and positive values. In other words, the signal is assimilated to a language where the QRS complex represents a sequence of words.

Alphabet $\sum$ = {0,1,2,3,4,5,6,7,8,9, -,.} contains all the symbols which can represent a normalized amplitude belonging to the bounded interval [-1, 1]. Then, regular expressions allow the lexical analysis of the signal. In fact, deterministic automata and regular expressions represent the rest phase, the positive peak and the negative peak. The latter form the QRS complex with an addition of standard deviation constraints.

Mathematically, a positive peak or a negative peak must have a very large standard deviation σ compared to that of a wave and greater than a predefined threshold σ1 for a very short duration Δ less than a predefined threshold Δ1.

Given the sampling frequency Fe, a peak (positive or negative), a wave or a rest phase, is formed by a series of n normalized amplitudes {a1, a2,…, an} having an average amplitude. The calculation of a gap type σ and term Δ is as follows:

$$\sigma = \sqrt{\sum_{i=1}^{n} \frac{(ai-\bar{a})^2}{n}} \tag{4.4}$$

$$\bar{a} = \sum_{i=1}^{n} \frac{ai}{n} \tag{4.5}$$

$$\Delta = \frac{n}{Fe} \tag{4.6}$$

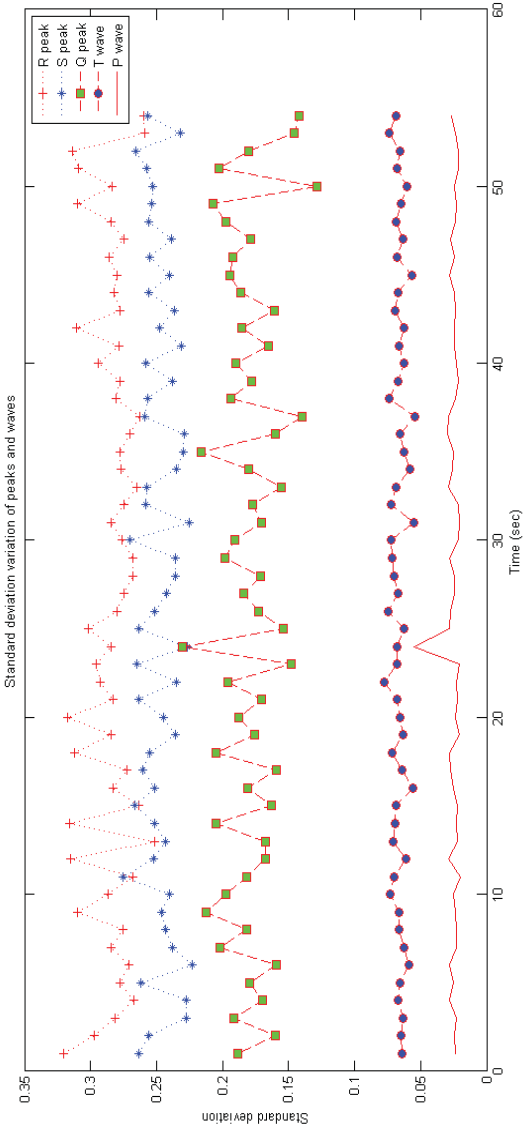

Figure 4.3: Standard deviations changes of peaks and waves

Figure 4.3 shows the values of the standard deviations of the numerous Q, R and S peaks and of the different P and T waves. The figure confirms that the two peaks R and S show very large standard deviations greater than 0.2. Peak Q has standard deviations greater than 0.1, while both P and T waves have very low values of standard deviations below 0.05.

According to Figure 4.3, we can designate $\sigma 1 = 0.1$. From this value, we can distinguish between peaks and waves. In fact, a QRS complex is thought of as a pair of adjacent peaks that meet criteria for standard deviations.

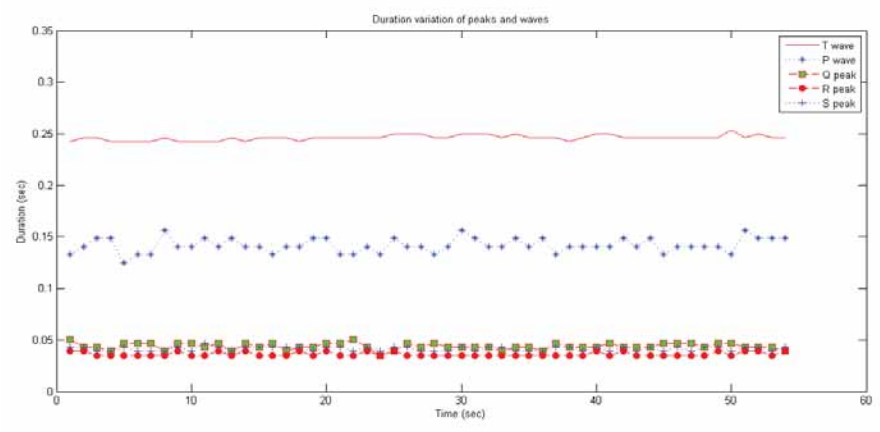

Figure 4.4: Variation of peak and wave durations

Figure 4.4 shows the values of the durations of the multiple Q, R and S peaks and of the various P and T waves. The figure confirms that the three Q, R and S peaks show very short durations of less than 0.1 sec. While the two P and T waves have very important values of durations which exceed 0.1 sec.

According to Figure 4.4, we can designate $\Delta 1 = 0.1$ sec. From this value, we can distinguish between peaks and waves. In fact, a QRS complex is thought of as a pair of adjacent peaks that meet criteria for standard deviations and durations.

In what follows, grammatically, the character "∈" is an empty word with zero length. The character '*' means "zero or more times", the character '+' means "one or more times", and '?' means "zero or once".

A deterministic finite automaton consists of a finite set of states (often denoted by Q), a finite set Σ of symbols (alphabet), a transition function which takes as argument a state and a symbol and returns a state (often denoted by δ), a starting state often denoted by q0 and a set of final states (often denoted by F). We have $q0 \in Q$ and $F \subseteq Q$.

Indeed, a deterministic finite automaton (DFA) is a quintuplet (Q, ∑, δ, q0, F) where:

Σ is an alphabet,
Q is a finite set of states,
$\delta: Q \times \Sigma \rightarrow Q$ is the transition function,
q0: is the initial state,
F: is a set of final states.

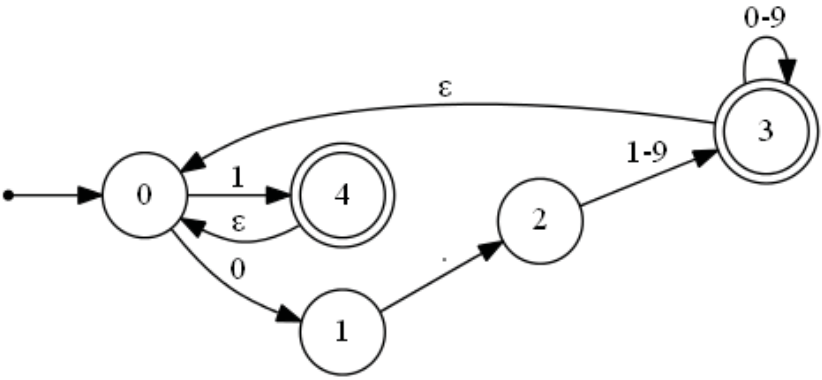

Figure 4.5: Deterministic automaton representing normalized positive peak (R)

Often, the initial state is marked with an incoming arrow, the states are symbolized by single circles, and the final states are marked with double circles.

The initial state q0 = {0}.
The finite set of states Q = {0, 1, 2, 3, 4}.
The set of finite states F = {3, 4}.
The finite set of symbols ∑ = {0,1,2,3,4,5,6,7,8,9, -,.}

The functions of the transitions are:
δ (0,0) = 1
δ (1,.) = 2
δ (2,1-9) = 3
δ (3,0-9) = 3
δ (3, ε) = 0
δ (0,1) = 4
δ (4, ε) = 0

The deterministic automaton above (Figure 4.5) and the regular expression describe a normalized positive peak of type R:

$$R = \{ 0.[1\text{-}9]\ [0\text{-}9]^*|1\}+ \tag{4.7}$$

$$\sigma R > \sigma 1 \tag{4.8}$$

$$\Delta R < \Delta 1 \tag{4.9}$$

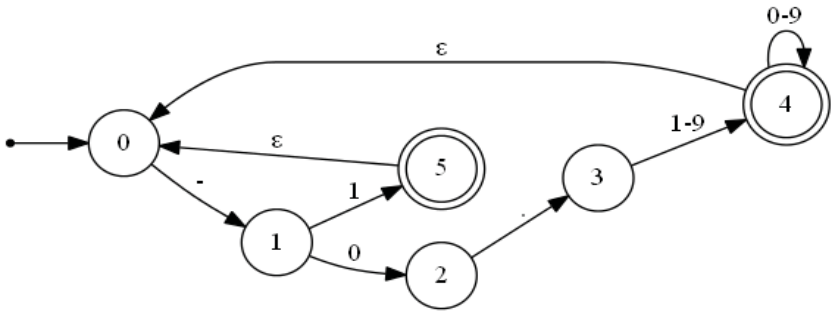

Figure 4.6: Deterministic automaton representing normalized negative peak (Q or S)

The following deterministic automaton (Figure 4.6) as well as the regular expression below describes a normalized negative peak:

$$Q = \{- 0.[1\text{-}9]\ [0\text{-}9]^* \mid -1\}+ \tag{4.10}$$

$$\sigma Q > \frac{\sigma 1}{2} \tag{4.11}$$

$$\Delta Q < \Delta 1 \tag{4.12}$$

$$S = \{ -0.[1\text{-}9]\ [0\text{-}9]^*|-1.0\ \}+ \tag{4.13}$$

$$\sigma S > \sigma 1 \tag{4.14}$$

$$\Delta S < \Delta 1 \tag{4.15}$$

The initial state q0 = {0}.
The finite set of states Q = {0, 1, 2, 3, 4, 5}.
The set of finite states F = {4,5}.
The finite set of symbols ∑ = {0,1,2,3,4,5,6,7,8,9, -,.}
The transition functions are:
δ (0, -) = 1
δ (1.0) = 2
δ (2,.) = 3
δ (3.1-9) = 4
δ (4.0-9) = 4
δ (4, ε) = 0
δ (1.1) = 5
δ (5, ε) = 0

In practice, the Q, R and S peaks are possibly separated by very short resting phases. The following regular expression describes a normalized rest phase:

$$rest = \{\{-\}?\ 0.0\ [0-9]*\}+ \tag{4.16}$$

$$\Delta rest < \frac{\Delta 1}{2} \tag{4.17}$$

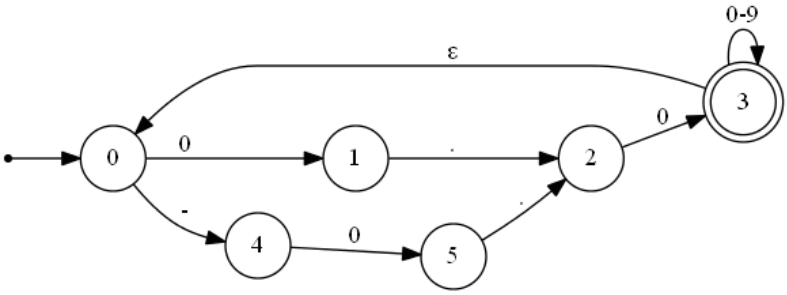

Figure 4.7: Deterministic automaton depicting standardized rest phase

The deterministic automaton above (Figure 4.7) discloses a standardized rest phase where:

The initial state q0 = {0}.
The finite set of states Q = {0, 1, 2, 3, 4, 5}.
The final state F = {3}.
The finite set of symbols ∑ = {0,1,2,3,4,5,6,7,8,9, -,.}
The transition functions are:
δ (0.0) = 1
δ (1,.) = 2
δ (2.0) = 3
δ (3.0-9) = 3
δ (3, ε) = 0
δ (0, -) = 4
δ (4.0) = 5
δ (5,.) = 2

The regular expression below and Figure 4.8 describe an entire standard QRS complex. Q is the first peak directed downwards, which is always visible on the ground. Peak R is the second; it has high amplitude and it is directed upwards. The S peak is the last; it is directed downwards.

Grammatically, the complex QRS is assimilated to a succession of positive and negative peaks which are separated optionally by a very short resting phase.

The regular expression and the deterministic PLC below (Figure 4.8 and Figure 4.9) assume that the peaks of Q and the resting phases may be absent.

$$QRS = \{Q\}? \{rest\}? \{R\} \{rest\}? \{S\} \quad (4.\ 1\ 8)$$

The initial state q0 = {0}.
The finite set of states Q = {0, 1, 2, 3-27, 28}.
The set of finite states F = {27, 28}.
The finite set of symbols ∑ = {0,1,2,3,4,5,6,7,8,9, -,.}
The transition functions are:
δ (0,.) = 1
δ (1.0) = 2
δ (2,.) = 3
δ (3.1-9) = 4
δ (4.0-9) = 4

$\delta(4, \varepsilon) = 6$
$\delta(1.1) = 5$
$\delta(4, \varepsilon) = 0$
$\delta(5, \varepsilon) = 6$
$\delta(5, \varepsilon) = 0$

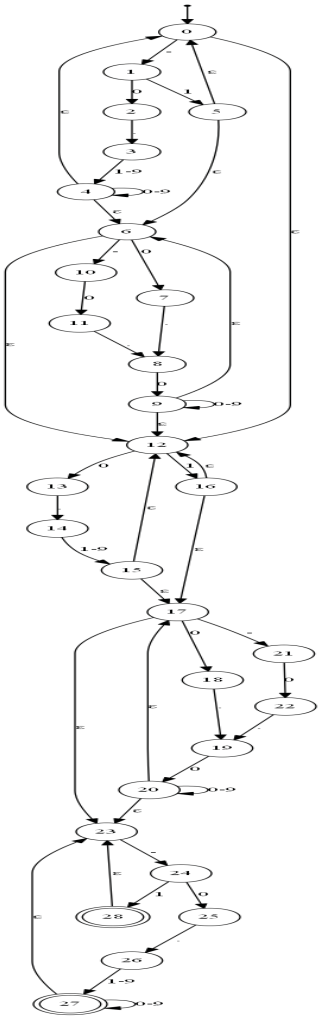

Figure 4.8: Deterministic automaton representing normalized QRS complex.

δ (6,0) = 7
δ (7,.) = 8
δ (8,0) = 9
δ (6,.) = 10
δ (10,0) = 11
δ (11,.) = 8
δ (9,0-9) = 9
δ (9, ε) = 6
δ (6, ε) = 12
δ (0, ε) = 12
δ (9, ε) = 12
δ (12.0) = 13
δ (13,.) = 14
δ (14.1-9) = 15
δ (15, ε) = 17
δ (15, ε) = 12
δ (12,1) = 16
δ (16, ε) = 12
δ (16, ε) = 17
δ (17.0) = 18
δ (18,.) = 19
δ (19.0) = 20
δ (20.0-9) = 20
δ (17,.) = 21
δ (21.0) = 22
δ (22,.) = 19
δ (20, ε) = 17
δ (17, ε) = 23
δ (20, ε) = 23
δ (23,.) = 24
δ (24,0) = 25
δ (25,.) = 26
δ (26,1-9) = 27
δ (27, ε) = 23
δ (27.0-9) = 27
δ (24.1) = 28
δ (28, ε) = 23

The QRS complex represents the ventricular depolarization curve. All these three peaks have durations between 0.06 and 0.1 seconds [Cha’09, Ayt'99, Moo'01, Ham'04, Kha'09, Sum'09, Che'06, and Su’05].

To better represent describing the controller while a QRS complex in a simpler way, the following automaton (Figure 4.9) show an entire QRS complex where we have modified and minimized the finite set of symbols, the entire finished states and the set of finite states.

The initial state q0 = {0}.
The finite set of states Q = {0, 1, 2, 3, 4, 5}.
The set of finite states F = {5}.
The finite set of symbols ∑ = {Q, R, S, Rest}
The transition functions are:
δ (0, Q) = 1
δ (0, Rest) = 2
δ (0, R) = 3
δ (1, R) = 3
δ (2, R) = 3
δ (3, Rest) = 4
δ (4, S) = 5
δ (3, S) = 5

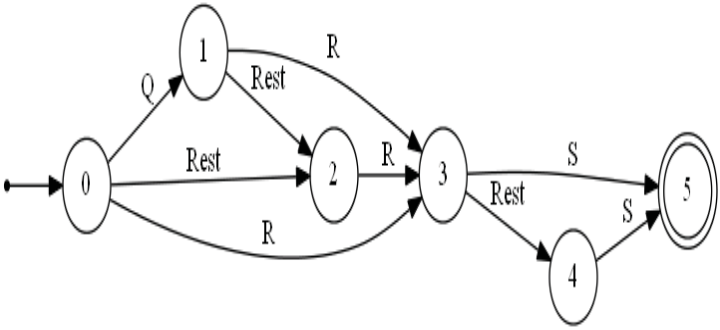

Figure 4.9: Deterministic automaton representing QRS complex.

II.3 Results

In this section, the method described above is applied on multiple real signals representing the ECG of different patients and derived from the standard database MIT-BIH arrhythmia. For all input signals, the Q, R, and S peaks, the RR distances, and the QRS complexes are detected. The RR distance is the time between two successive peaks of R. It is the most important indicator of the rate of ventricles. In addition, a comparison study with a large number of methods [Pan'85, Szu'92, Sai'12, Ben'10,

Ham'86, Cho'07, Chr'06, Gha'08, Had'10, Kyr'88, Meh'08, Gri'98, Tra'93] is applied in terms of detection of the QRS complex.

Table 4.1 shows an application on multiple real ECG signals to extract the QRS complexes. True Positive (TP), False Positive (FP), False Negative (FN), Sensitivity (Se), Positive Predictivity (+P), Fault Detection Rate (FDR), and Rate false negative (FNR) are determined where:

TP represents correctly identified QRSs,

FP represents incorrectly identified QRSs,

FN represents incorrectly rejected QRSs.

$$\text{Sensitivity}\ (\%) = \frac{\text{TP}}{\text{TP+FN}} * 100 \tag{4.19}$$

$$\text{Positive predictivity}\ (\%) = \frac{\text{TP}}{\text{TP+FP}} * 100 \tag{4.20}$$

$$\text{False detection rate}\ (\%) = \frac{\text{FP}}{\text{TP+FP}} * 100 \tag{4.21}$$

$$\text{False negative rate}\ (\%) = \frac{\text{FN}}{\text{TP+FN}} * 100 \tag{4.22}$$

Table 4.1 shows an application of the proposed method on different types of ECG signals from the MIT-BIH arrhythmia database in order to extract the QRS complex. The sampling frequency is 360Hz, the gain is 200 and the base is 1024mV.

For an input signal, several parameters are determined, such as the number of QRS, the RR distances, the QRS duration, the standard deviation of the RR distances, the standard deviation of the QRS durations, and the amplitudes of the peaks.

Practically, the average rate of the sensitivity (Se) of the proposed method is 99.74% and the mean rate of the positive predictivity (+P) is 99.86%. The mean rate of false detection (FDR) is 0.14% and the average rate of false negative (FNR) is 0.26%.

Table 4.1: Application on several actual ECG signals from standard database MIT-BIH. Extraction of QRS complexes and calculation of Sensitivity rate (Se) and positive Predictivity (+ P).

Record	Record length	Real number of QRS	TP	FN	FP	Se (%)	+ P (%)	FDR (%)	FNR (%)	$\overline{RR}$	σRR	$\overline{QRS}$	σQRS
100	1805	2273	2272	1	0	99.96	100.00	0.00	0.04	0.79	0.05	0.05	0.00
101	1805	1865	1864	1	0	99.95	100.00	0.00	0.05	0.96	0.07	0.06	0.00
102	1805	2187	2183	4	2	99.82	99.91	0.09	0.18	0.83	0.09	0.14	0.01
103	1805	2084	2082	2	2	99.90	99.90	0.10	0.10	0.86	0.05	0.05	0.00
104	1805	2230	2211	19	24	99.15	98.93	1.07	0.85	0.81	0.08	0.04	0.04
105	1805	2572	2571	1	0	99.96	100.00	0.00	0.04	0.70	0.11	0.07	0.00
106	60	67	67	0	0	100.00	100.00	0.00	0.00	0.88	0.09	0.06	0.00
107	60	70	70	0	2	100.00	97.22	2.78	0.00	0.82	0.12	0.12	0.02
108	1805	1763	1761	2	0	99.89	100.00	0.00	0.11	1.02	0.21	0.09	0.08
109	1805	2532	2526	6	2	99.76	99.92	0.08	0.24	0.71	0.05	0.09	0.00
111	60	69	69	0	0	100.00	100.00	0.00	0.00	0.89	0.15	0.05	0.01
112	1805	2539	2537	2	6	99.92	99.76	0.24	0.08	0.71	0.03	0.06	0.00
113	1805	1794	1794	0	1	100.00	99.94	0.06	0.00	1.00	0.09	0.05	0.00
114	60	54	54	0	0	100.00	100.00	0.00	0.00	1.10	0.04	0.03	0.00
115	1805	1953	1953	0	0	100.00	100.00	0.00	0.00	0.92	0.08	0.05	0.00
116	60	78	78	0	0	100.00	100.00	0.00	0.00	0.76	0.01	0.06	0.00
117	1805	1535	1534	1	1	99.93	99.93	0.07	0.07	1.17	0.05	0.06	0.00
118	1805	2275	2275	0	12	100.00	99.48	0.52	0.00	0.78	0.10	0.07	0.00
119	1805	1987	1987	0	0	100.00	100.00	0.00	0.00	0.90	0.25	0.07	0.02
121	1805	1863	1861	2	3	99.89	99.84	0.16	0.11	0.96	0.09	0.08	0.00
122	1805	2476	2475	1	2	99.96	99.92	0.08	0.04	0.72	0.04	0.07	0.00
123	1805	1518	1517	1	4	99.93	99.74	0.26	0.07	1.18	0.12	0.06	0.00

124	60	49	49	0	0	100.00	100.00	0.00	0.00	1.21	0.02	0.07	0.01
200	60	87	87	0	0	100.00	100.00	0.00	0.00	0.72	0.40	0.09	0.01
201	60	90	90	0	0	100.00	100.00	0.00	0.00	0.66	0.13	0.06	0.00
202	1805	2136	2111	25	0	98.83	100.00	0.00	1.17	0.85	0.30	0.07	0.00
203	60	97	97	0	0	100.00	100.00	0.00	0.00	0.61	0.24	0.08	0.01
205	60	89	89	0	0	100.00	100.00	0.00	0.00	0.66	0.01	0.05	0.00
207	1805	1862	1859	3	0	99.84	100.00	0.00	0.16	0.96	0.21	0.07	0.09
208	60	87	87	0	0	100.00	100.00	0.00	0.00	0.69	0.26	0.07	0.02
209	1805	3004	3002	2	7	99.93	99.77	0.23	0.07	0.59	0.08	0.05	0.00
210	1805	2647	2606	41	9	98.45	99.66	0.34	1.55	0.69	0.13	0.07	0.01
212	1805	2748	2748	0	5	100.00	99.82	0.18	0.00	0.65	0.04	0.06	0.00
213	1805	3251	3243	8	2	99.75	99.94	0.06	0.25	0.55	0.04	0.06	0.01
214	1805	2262	2229	33	0	98.54	100.00	0.00	1.46	0.81	0.22	0.07	0.00
215	1805	3363	3337	26	0	99.23	100.00	0.00	0.77	0.54	0.09	0.06	0.00
217	1805	2208	2206	2	0	99.91	100.00	0.00	0.09	0.88	0.25	0.10	0.01
219	1805	2154	2152	2	0	99.91	100.00	0.00	0.09	0.83	0.22	0.06	0.00
220	1805	2048	2047	1	4	99.95	99.80	0.20	0.05	0.88	0.09	0.05	0.00
221	1805	2427	2400	27	0	98.89	100.00	0.00	1.11	0.75	0.20	0.06	0.01
222	60	75	75	0	0	100.00	100.00	0.00	0.00	0.81	0.12	0.05	0.00
223	60	80	80	0	0	100.00	100.00	0.00	0.00	0.75	0.08	0.07	0.00
228	60	68	68	0	0	100.00	100.00	0.00	0.00	0.86	0.27	0.07	0.01
230	1805	2256	2219	37	0	98.36	100.00	0.00	1.64	0.81	0.18	0.06	0.00
231	60	63	63	0	0	100.00	100.00	0.00	0.00	0.94	0.11	0.06	0.00
232	1805	1780	1747	33	4	98.15	99.77	0.23	1.85	1.03	0.65	0.06	0.00
233	60	94	94	0	0	100.00	100.00	0.00	0.00	0.58	0.13	0.07	0.01
234	1805	2753	2752	1	0	99.96	100.00	0.00	0.04	0.65	0.03	0.06	0.00
Total	**58720**	**73562**	**73278**	**284**	**92**	**99.74**	**99.86**	**0.14**	**0.26**	**0.82**	**0.13**	**0.07**	**0.01**

In addition, the standard deviation of the distances RR denoted σRR and the standard deviation of the QRS durations denoted σQRS are calculated.

Please note that the standard deviation parameters are a sign of the relationship between the obtained values and the mean value where:

$$\sigma RR = \sqrt{\sum_{i=1}^{n} \frac{(RRi - \overline{RR})^2}{n}} \quad (4.23)$$

$$\overline{RR} = \sum_{i=1}^{n} \frac{RRi}{n} \quad (4.24)$$

$$\sigma QRS = \sqrt{\sum_{i=1}^{n+1} \frac{(QRSi - \overline{QRS})^2}{n+1}} \quad (4.25)$$

$$\overline{QRS} = \sum_{i=1}^{n+1} \frac{QRSi}{n+1} \quad (4.26)$$

Mathematically, a short standard deviation (less than 0.1) of RR distances means that all RR distances are regular. A high standard deviation (more than 0.1) means that the values of RR distances are irregular.

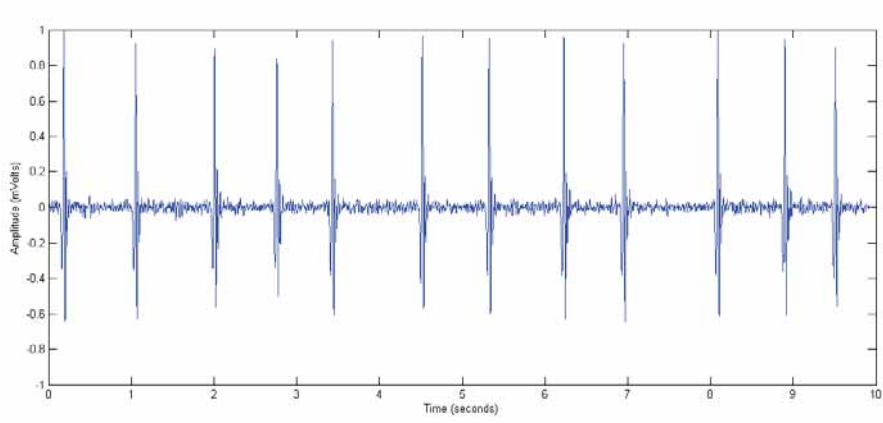

Figure 4.10: Portion of standard ECG representing rate of irregular heartbeat

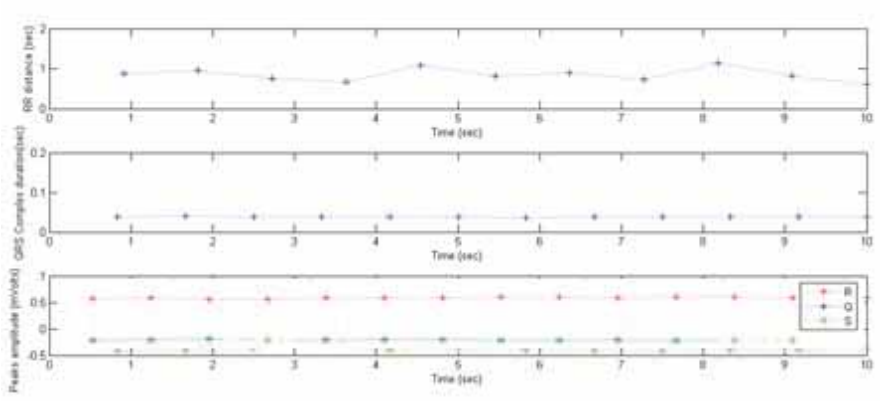

Figure 4.11: Change in RR distances, QRS duration and amplitudes of peaks; $\overline{RR}$= 0.84 sec., σRR=0.15, $\overline{QRS}$=0.03 sec., σQRS=0.01

Consistently, a short-lived standard deviation (less than 0.1) of the QRS duration means that all QRS durations are regular. However, a high standard deviation (more than 0.1) means that the obtained values of QRS durations are irregular.

Figure 4.10 and Figure 4.11 show an application on a portion of a signal ECG representing a rate of irregular heartbeat. The various indicators of the signal (RR distance, duration of the QRS; amplitudes of Q, R and S) are shown.

Primarily, the average values of the RR distances and QRS times are 0.84 seconds and 0.03 seconds, respectively. However, the RR distances are irregular. In fact, the standard deviation of the RR distances is σRR = 0.15. This plus or minus value proves that the RR distance is not stable. QRS complexes have normal durations of less than a 0.1 second. In addition, the QRS duration values are regular. Indeed, the standard deviation σQRS = 0.01. This low value demonstrates that the duration of the QRS is stable.

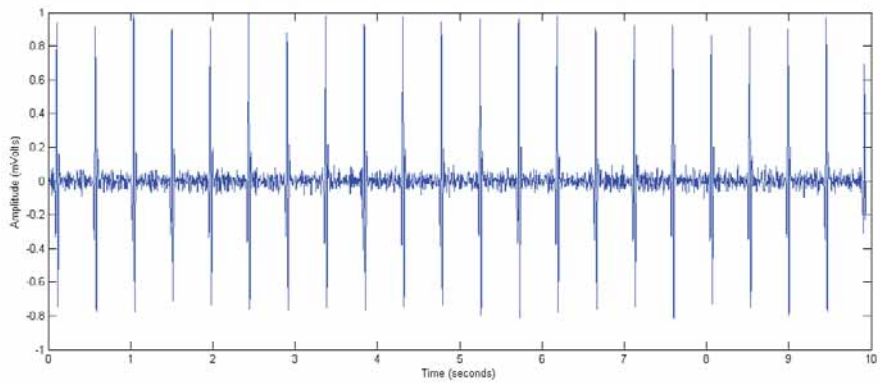

Figure 4.12: Portion of standard ECG representing steady beat

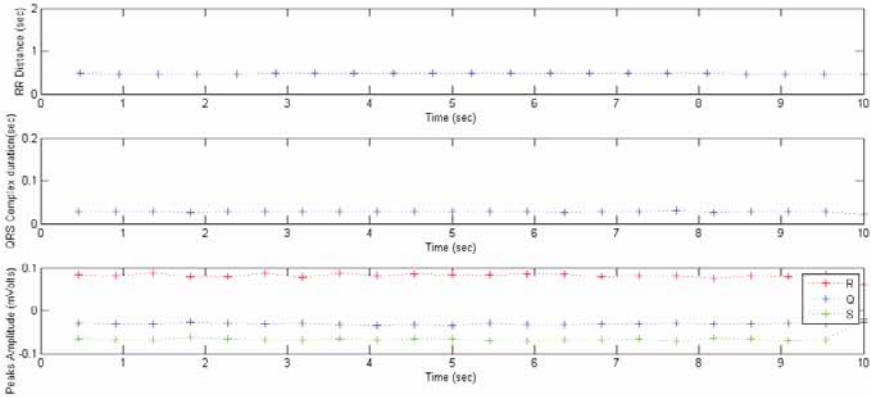

Figure 4.13: Change in RR distances, QRS duration and amplitude of peaks; $\overline{RR}$ = 0.46, σRR = 0.00, $\overline{QRS}$ = 0.02, σQRS = 0.00

Similarly, Figure 4.12 and Figure 4.13 illustrate an application on a portion of an ECG showing a tachycardia rate and a regular beat. Mainly, the mean values of the RR and the QRS are respectively 0.46 seconds and 0.02 second. Indeed, the RR distances are regular. In fact, the standard deviation of the RR distances is σRR = 0.00. This low value indicates that the RR distance is stable.

QRS complex durations have normal durations of less than a 0.1 second. In addition, the QRS durations are regular. Indeed, the standard deviation

of the QRS durations is σQRS = 0.00. This low value indicates that the duration of the QRS is stable.

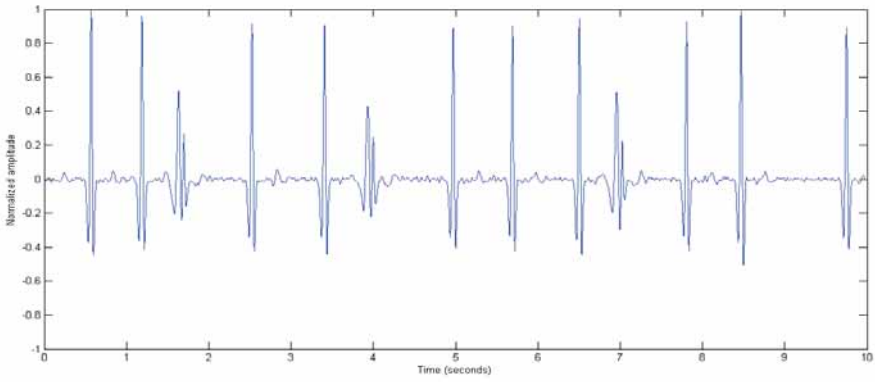

Figure 4.14: Portion of record 221 representing irregular beat

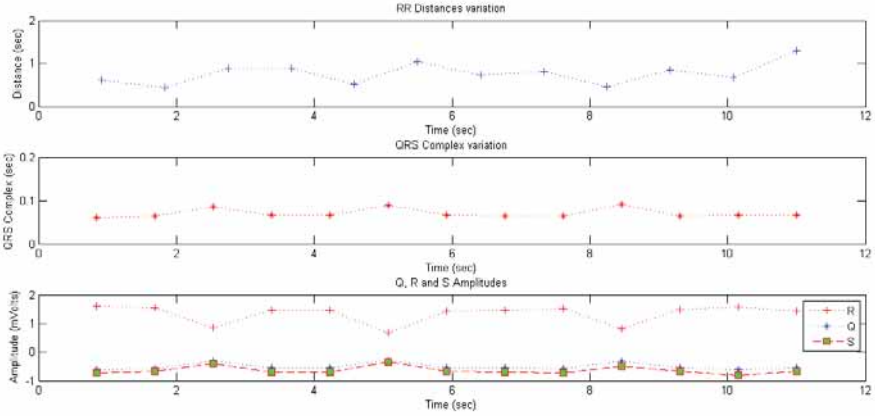

Figure 4.15: Change of RR distances, QRS durations and peak amplitudes; $\overline{RR}$= 0.76 sec., σRR=0.23, $\overline{QRS}$=0.07 sec., σQRS=0.02

Figure 4.14 and Figure 4.15 depict an application to a portion of record 221 showing an irregular beat rate. Different signals (RR distance, duration QRS amplitudes of Q, R and S) are shown. Primarily, the art value s of the average RR and QRS are 0.84 seconds and 0.03 seconds,

respectively. However, the RR distances are irregular. Indeed, σRR is 0.15. This plus or minus value proves that the RR distance is not stable. The QRS complex durations have normal durations less than a 0.1 second. In addition, the QRS durations are regular. Indeed, σQRS is equal to 0.01. This low value demonstrates that the duration of the QRS is stable.

Likewise, Figure 4.16 and Figure 4.17 illustrate an application to a portion of record 234 showing tachycardia and a steady beat rate. Primarily, the art values of the average RR and QRS are 0.46 seconds and 0.02 second, respectively. In addition, the RR distances are regular and σRR is equal to 0.00. This low value shows that the RR distance is stable. The QRS complex durations have normal durations less than a 0.1 second. In addition, the QRS durations are regular. Actually, σQRS is 0.00. This low value indicates that the QRS duration is stable.

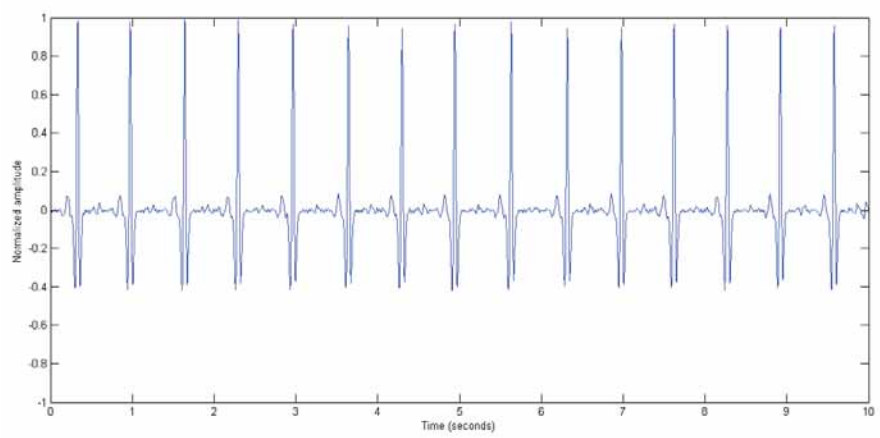

Figure 4.16: Portion of record 234 representing regular beat

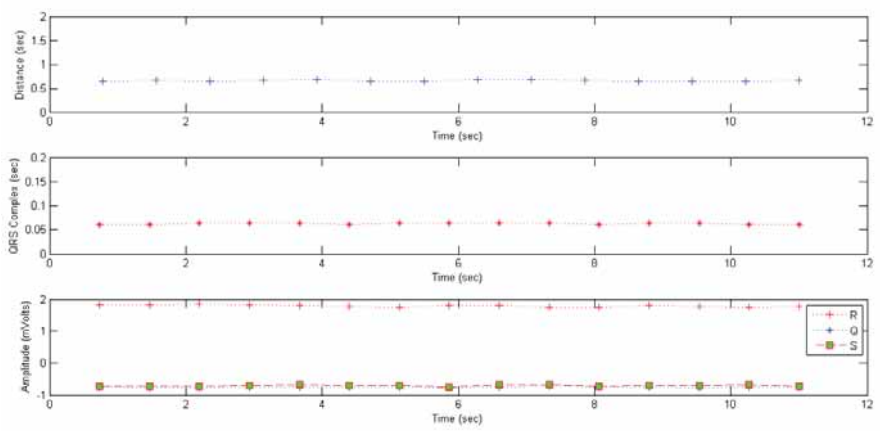

Figure 4.17: Variation of RR distances, QRS durations and peaks amplitudes; $\overline{RR}$ = 0.66, σRR = 0.01, $\overline{QRS}$ = 0.06, σQRS = 0.01

Figure 4.18 and Figure 4.19 synthesize the variation in the σRR and σQRS parameters, respectively, for several ECG signals from the base of MIT-BIH arrhythmia.

Indeed, the non-pathological signals show values of σRR and σQRS which are low and even almost zero. However, pathological signals show values of σRR and / or σQRS significant.

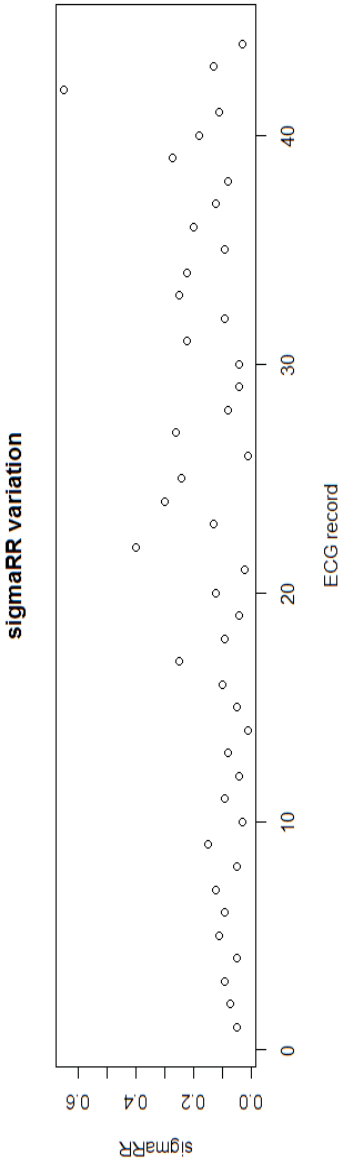

Figure 4.18: Variation in σRR parameter for different ECG signals

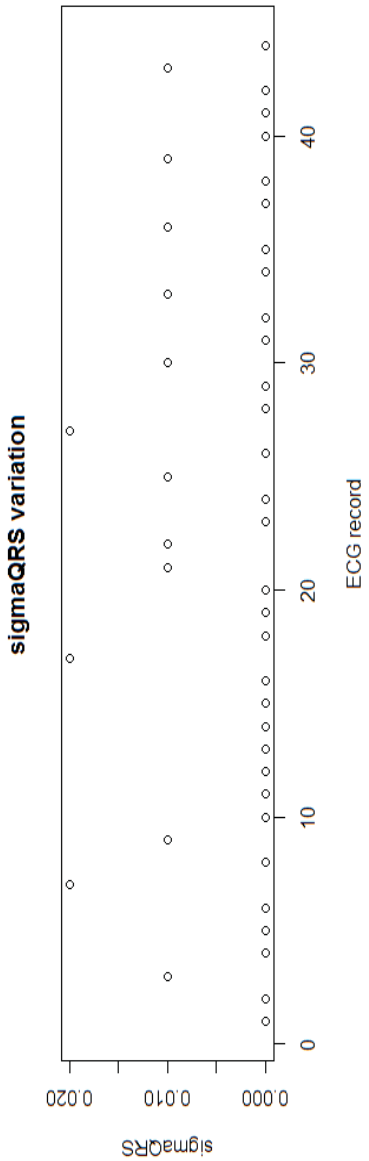

Figure 4.19: variation in σQRS parameter for different ECG signals

II.4 Noise sensitivity

Table 4.2 displays the noise sensitivity, where the method is applied on different ECG recordings. Table 4.2 shows the variation in the sensitivity rate and the positive predictivity according to the Signal to Noise Ratio (SNR).

For SNR values greater than 40dB, the method provides high sensitivity values exceeding 99%. For values of an SNR greater than 30dB, the method gives sensibility values that exceed 97%. For low SNR values that are less than 24 dB, the sensitivity value decreases by 90%.

Figure 4.20 tracks the variation rate of the SNR of sensitivity according to different ECG recordings (100, 101, 102, 103 and 105) derived from the database standard MIT-BIH. For the SNR values low and less than 20dB, the method provides sensitivity levels that are below 50%. However, the sensitivity becomes increasingly important when the SNR values are above 30dB. For values of an SNR which are greater than 30dB, the method provides sensitivity rates exceeding 97%. If the SNR is greater than 40dB, the method provides high values of sensitivity which exceed 99%.

Table 4.2: Study of noise sensitivity. Application on ECG signals with different values of SNR

Record	SNR (dB)	90	80	70	60	50	40	30	25	24	23	22	21	20
100	Se (%)	99.96	99.96	99.96	99.96	99.96	99.96	99.96	93.27	90.32	85.97	79.94	63.57	55.52
	+ P (%)	100.0	100.0	100.0	100.0	100.0	100.0	99.91	83.73	80.29	76.99	72.80	62.72	57.52
101	Se (%)	99.95	99.95	99.95	99.95	99.95	99.95	99.79	95.28	86.27	84.13	81.88	87.56	48.04
	+ P (%)	100.0	100.0	100.0	100.0	100.0	100.0	99.95	84.86	69.44	66.65	65.37	69.05	39.54
102	Se (%)	99.82	99.82	99.82	99.82	99.82	97.49	91.13	83.36	79.84	74.67	66.03	57.80	43.80
	+ P (%)	99.91	99.91	99.91	99.91	99.91	96.22	88.90	83.51	75.52	68.84	58.87	51.34	40.47
103	Se (%)	99.90	99.90	99.90	99.90	99.90	99.90	99.86	97.46	95.30	88.58	83.25	70.59	54.89
	+ P (%)	99.90	99.90	99.90	99.90	99.90	99.90	99.90	95.85	92.07	81.75	74.95	60.46	45.52
105	Se (%)	99.96	99.96	99.96	99.96	99.96	98.41	97.51	93.58	90.90	81.22	73.21	73.13	53.30
	+ P (%)	100.0	100.0	100.0	100.0	100.0	99.10	99.09	95.90	92.56	79.61	73.15	73.04	61.01
Total	Se (%)	99.92	99.92	99.92	99.92	99.92	99.14	97.65	92.59	88.53	82.91	76.86	70.53	51.11
	+ P (%)	99.97	99.97	99.97	99.97	99.97	99.20	97.95	88.12	79.89	73.42	68.42	64.28	47.27

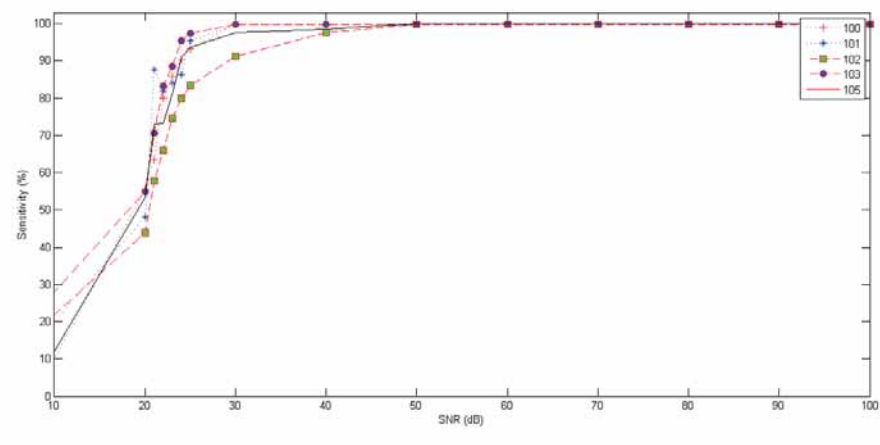

Figure 4.20: Variation in sensitivity rate according to SNR. Application on 100, 101, 102, 103 and 105 records.

II.5 R peak detection accuracy

In this part, we determine the exact time of the first two R peaks present in recordings 100 to 110. Next, we compare the exact time of each R peak to the one detected automatically and calculate the RR distance. Thus, we can determine the precision value for each peak. According to the values presented in Table 4.3, the precision values are very low and vary between 0.000 sec and 0.010 sec. Moderately, the precision value is 0.002 sec for the detection of the R peaks and 0.003 for the calculation of the RR distance. In addition, Figure 4.21 plots the variation in the precision value of the detection time of the R peaks from recordings 100, 101,…, and 110.

Table 4.3: Accuracy method proposed for detection of R peaks and calculating RR distance

ECG	R Peak order	Exact peak time R (sec)	R peak detected time (sec)	Accuracy (sec)	Exact distance from RR (sec)	RR distance detected (sec)	Accuracy (sec)
100	1	0.171	0.172	0.001	-	-	-
	2	0.985	0.986	0.001	0.814	0.814	0.000
101	1	0.189	0.186	0.003	-	-	-
	2	1,060	1,050	0.010	0.871	0.864	0.007
102	1	0.269	0.269	0.000	-	-	-
	2	1,090	1.088	0.002	0.821	0.819	0.002
103	1	0.693	0.694	0.001	-	-	-
	2	1.56	1,555	0.005	0.867	0.861	0.006
105	1	0.502	0.502	0.000	-	-	-
	2	1.230	1.230	0.000	0.728	0.728	0.000
106	1	0.933	0.933	0.000	-	-	-
	2	1,970	1,972	0.002	1.037	1,039	0.002
107	1	0.712	0.708	0.004	-	-	-
	2	1,530	1,533	0.003	0.818	0.825	0.007

108	1	0.140	0.141	0.001	-	-	-
	2	0.978	0.977	0.001	0.838	0.836	0.002
109	1	0.261	0.261	0.000	-	-	-
	2	0.906	0.905	0.001	0.645	0.644	0.001
110	1	0.507	0.507	0.000	-	-	-
	2	1.320	1.317	0.003	0.813	0.810	0.003
Average accuracy rate				**0.002**	-	-	**0.003**

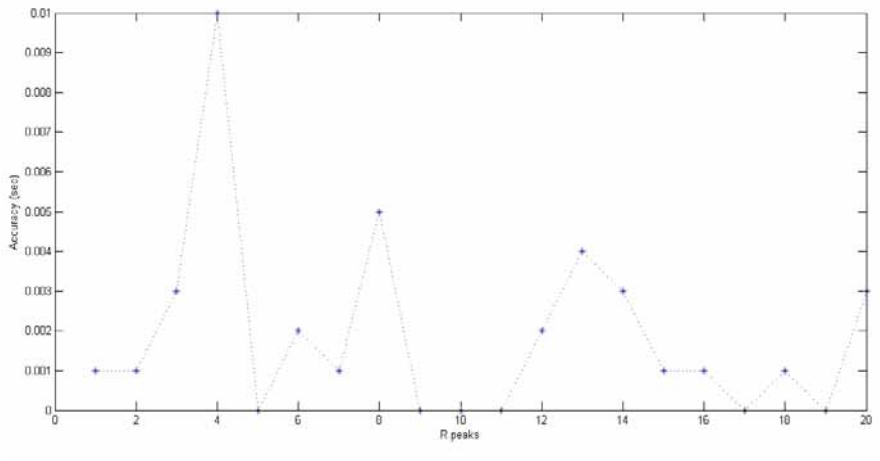

Figure 4.21: Variation in precision rate for detection of R peaks

II.6 Performance comparison

In order to place the QRS detection algorithm compared to other literature work, the quality of the detection performance is compared with several algorithms tested and validated on the MIT-BIH database. These algorithms are varied and each is based on an appropriate technique.

Table 4.4 shows a comparative study with a large number of methods applied on the same MIT-BIH database in terms of sensitivity levels. Based on the results presented in Table 4.4, all algorithms for detecting QRS complexes have a good detection capability with a sensitivity rate that exceeds 99%.

Similarly, the proposed method provides satisfactory and competitive results with sensitivity (99.74%) and can be considered a powerful tool for the detection of the QRS complex in the ECG signal.

Table 4.4: Performance comparison of several QRS detection algorithms cited in the literature.

Method	Description	Sensitivity (%)
Pan'85	Derivative approach based on filtering and slope analysis	99.30
Ham'86	Derivative approach based on filtering using optimized decision rule process	99.46
Kyr'88	Technique based on recursive temporal prediction	99.00
Szu'92	Neural network based on adaptive filtering	99.50
Tra'93	Approach based on mathematical morphology	99.38
Gha'98	Mathematical model based on continuous wavelet transform	99.91
Gri'98	Transformation based on time and energy	99.26
Chr'06	Use of adaptive thresholding	99.65
Cho'07	Multi wavelet packet decomposition	99.14
Meh'08	Support vector machine-based approach	99.75
Ben'10	Approach based on discrete wavelet decomposition and energy calculation	99.39
Had'10	Empirical modal decomposition	99.92
Sai'12	Using Euclidean metric distance with KNN algorithm	99.81
Suggested method	Approach about regular grammar and calculation of standard deviations	99.74

II.7 Discussion

In the literature, a few approaches have been based on grammatical formalism for the processing and control of ECG signals. However, researchers have not used the grammar formalism during the signal peak extraction phase. Peak recognition has been performed using other methods independent of the grammar. In our work, the proposed method confirms that the application domains of a regular grammar can be extended to be applied for the recognition of positive and negative peaks and the extraction of QRS complexes. A QRS complex is described for a deterministic finite automaton (DFA). In fact, different parameters are determined, such as the number of QRS complexes, the QRS duration, the RR distance, the standard deviations as well as the amplitudes of the peaks.

The proposed approach asserts that the use of grammar, as compared to statistical methods, can effectively represent QRS structures and therefore facilitate data retrieval through their structures. The main advantage of the proposed method is that the representation is visible. The proposed syntactic approach can powerfully represent the pattern of structures and therefore make information retrieval easy. The input ECG signal appears to be a structured scene having a hierarchical order as the grammar clearly represents hierarchical structures using deterministic automata.

In addition, the syntactic approach is able to describe a large set of ECG signals using the regular grammar. The learning of automata is exploited to recognize the phases of rest, the negative peaks and the positive peaks. The QRS complex is described for automation devices. Thus, many parameters are determined, such as the number of R peaks, the durations of the QRS complexes, the RR distances, and the values of the amplitudes of the peaks.

In addition, we add parameters such as the standard deviation of the RR distances, noted σRR, and the standard deviation of the QRS durations, noted σQRS. These standard deviation parameters are a sign of the relationship between the obtained values and the mean value. Mathematically, a low standard deviation (less than 0.1) of RR distances means that all RR distances are regular. On the other hand, a high standard deviation (more than 0.1) of the RR distances means that the values obtained for the RR distances are irregular.

Consistently, a short standard deviation of the QRS duration (less than 0.1) means that all QRS durations are regular. However, a high standard deviation (more than 0.1) means that the values obtained from the QRS times are irregular.

The proposed method is applied on the MIT-BIH arrhythmia database; the average rate of the sensitivity (Se) is 99.74% and the average rate of the positive text predictivity (+P) is 99.86%. In addition, the average false detection rate (FDR) is 0.14% and the average false negative rate (FNR) is 0.26%.

In order to study the sensitivity to noise, the method is applied on several ECG recordings for different SNR values. We study the variation in sensitivity and positive predictivity as a function of SNR. If the SNR values are greater than 40 dB, the method gives high sensitivity values that exceed 99%. If the SNR values are less than 24dB, the sensitivity value will decrease by 90%.

In addition, the results obtained are evaluated by a comparison with other algorithms in the literature. The comparison is made in terms of detection rate of QRS complexes by a sensitivity parameter. The proposed method provides satisfactory and competitive results with a sensitivity rate (99.74%) and thus can be considered as a powerful tool for ECG diagnosis of ECG signals.

The method works on a UNIX platform and is capable of generating a medical report which describes the variations in the different signal parameters by each recognized QRS complex. Figure 4.22 shows a printout of the medical report that displays the different indicators for each QRS complex detected.

At the end of the report, the program calculates the average RR distance and the average QRS duration. Then the program indicates the standard deviation of the RR distances and the standard deviation of the QRS times. Mathematically, if the value of the standard deviation is small it means that the measured values are regular and very close to the mean value. However, if the value of the standard deviation is very high it means that the measured values are irregular and are far from the mean value.

```
QRS Complex 2269:
Q Peak: Q Time (sec) = 1803.349976     Q Amplitude (mv) = -0.682177
R Peak: R Time (sec) = 1803.377808     R Amplitude (mv) = 1.550369      RR Distance (sec) = 0.702759
S Peak: S Time (sec) = 1803.405518     S Amplitude (mv) = -0.584958
QRS duration (sec) = 0.055542

QRS Complex 2270:
Q Peak: Q Time (sec) = 1804.052734     Q Amplitude (mv) = -0.757653
R Peak: R Time (sec) = 1804.080566     R Amplitude (mv) = 1.639719      RR Distance (sec) = 0.702759
S Peak: S Time (sec) = 1804.105591     S Amplitude (mv) = -0.606768
QRS duration (sec) = 0.052856

QRS Complex 2271:
Q Peak: Q Time (sec) = 1804.744385     Q Amplitude (mv) = -0.714106
R Peak: R Time (sec) = 1804.772217     R Amplitude (mv) = 1.582488      RR Distance (sec) = 0.691650
S Peak: S Time (sec) = 1804.797241     S Amplitude (mv) = -0.556352
QRS duration (sec) = 0.052856

AVG RR Distance (sec) = 0.794978
Standard-deviation of RR=0.051357
AVG QRS Duration (sec) = 0.056198
Standard-deviation of QRS=0.002923

Admin@Admin-PC ~/qrs4
$
```

Figure 4.22: Screen printout of last part of generated medical report.

A type-3 grammar and deterministic automata have been shown to be useful for the recognition of peaks and QRS complexes. The latter are described using deterministic automata and regular expressions. For an input signal, all the indicators are deduced such as QRS durations, RR distances, and amplitudes of the Q, R and S peaks. This work is intended to aid in medical diagnosis and support for clinical decision.

III. Recognition of cardiac cycles by regular grammar

III.1 General view

In this part, we will show that deterministic automata are also useful for the extraction of cardiac cycles. Automata will be used to represent a normalized cardiac cycle as a sequence of waves and negative and positive peaks based on the regular grammar. An ECG is likened to a pair of waves that meet certain adjacent criteria. This method recognizes QRS complexes as well as P and T waves.

The proposed method is applied to very long ECG signals. For an input signal, several parameters are determined, such as QRS durations, RR distances, corrected QTc intervals, amplitudes of Q, R and S peaks, and amplitudes of P and T waves. Regular grammar with an addition of constraints and deterministic automata are shown to be functional for biomedical signal processing and ECG signal diagnosis. This work is intended to aid in medical diagnosis and computer aided diagnostic systems. It is in this context that this work is inscribed. Deterministic automata are exploited to recognize rest phases, waves and negative and positive peaks. Cardiac cycles and complex QRS are described by automatons. Indeed, many parameters are determined, for example the number of peaks R, the durations of QRS complexes, the distances RR, the interval QTc and the amplitudes of the peaks and the waves.

Figure 4.23 summarizes all the steps of the method. The amplitude of the input signal is filtered, centralized and normalized. Then, the lexical analysis step recognizes lexical units including resting phases, waves, and positive and negative peaks. Then, depending on the length and the standard deviation of the lexemes, the analyzer differentiates between rests, peaks and waves in a step of refinement and recognition.

The analyzer calculates the RR distance and QRS complex durations and generates a medical report, taking into account the sample rate, the time and the amplitude values.

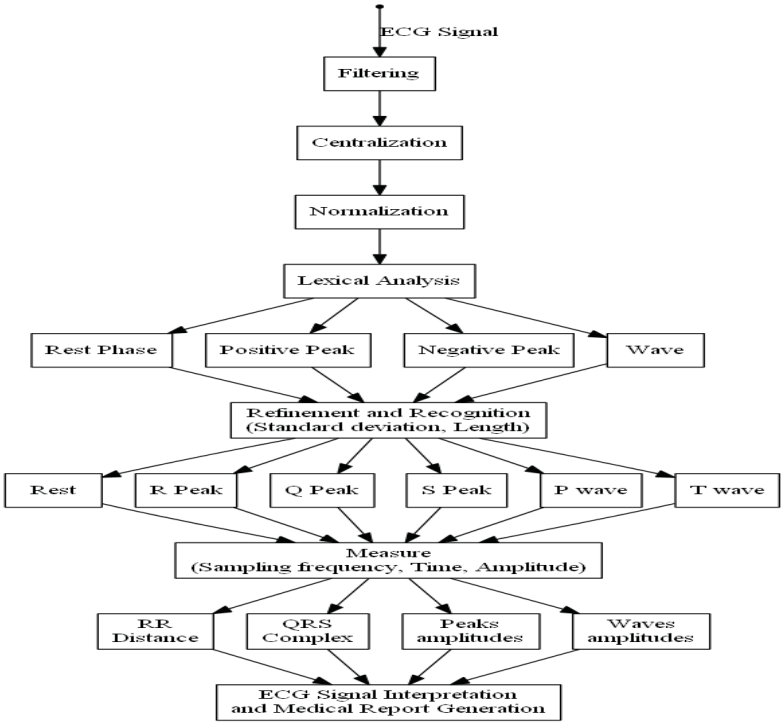

Figure 4.23: Overview of proposed method for recognition of cardiac cycles based on regular grammar

III.2 Preprocessing

In this part, the ECG signals undergo the same preprocessing phases described previously in section II.1. Figure 4.24 shows an example of an actual ECG signal before and after the filtering process. The actual ECG signal is delivered from a patient who represents a normal sinus rhythm. Figure 4.24 confirms that the filtering phase has eliminated the high frequencies and has well centered the signal.

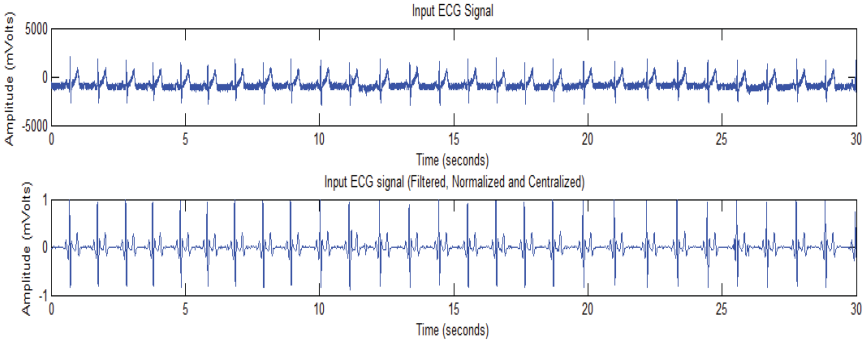

Figure 4.24: Centralized, normalized ECG signal representing normal sinus rhythm. The signal is filtered by a low pass filter and then by a high pass filter

III.3 Signal morphologies

The proposed method works on several possible signal morphologies. The technique provides, for normal signals, signals where the P wave or T wave is inverted and signals where the amplitude of the Q peak is much greater than the amplitude of the S peak.

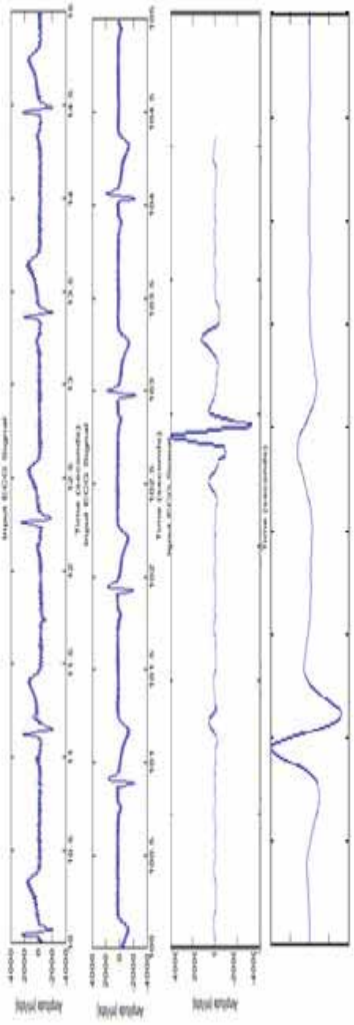

Figure 4.25: Morphologies of possible signals: a normal signal, a signal where the P wave or T wave is inverted, a signal when the amplitude of the Q peak is much larger than the amplitude of the peak S, a signal where the P-wave is absent or doubled.

III.4 Grammatical analysis of signal

Grammatically, the QRS complex is described in section II. The P wave is the first electrical phenomenon in a cardiac cycle. It is a wave that starts from the sinus node. This wave travels quickly through the atria, causing the atrial cells to contract. It represents the atrial depolarization curve. Its duration is between 0.08 and 0.1 seconds [Khe'07].

After each QRS complex, the T wave is observed on the ECG. Between this wave and the previous peak there is a brief rest called the ST segment. The study is very important for the identification of certain pathologies. It represents a ventricular repolarization curve. The duration of the T wave is between 0.20 and 0.25 seconds [Cha'09, Ayt'99, Moo'01, Ham'04, Kha'09, Sum'09, Che'06, and Su'05].

Based on the grammatical formalism presented in section II, the regular expression below and Figure 4.26 describe a normalized cardiac cycle. The deterministic automaton below predicts that the P wave and / or the rest phase may be absent. In addition, the P wave can be duplicated one or more times.

In practice, the P wave and the T wave must have duration at a threshold $\Delta 1$ and a standard deviation value less than a threshold $\sigma 1$. The values of the thresholds are predefined in section II.2.

$$P = \{0.[1\text{-}9]\ [0\text{-}9]^* \mid 1.0\ \}+ \tag{4.27}$$

$$\Delta_P = \frac{\|P\|}{Fe} \tag{4.28}$$

$$\sigma_P < \sigma 1 \tag{4.29}$$

$$\Delta_P > \Delta_1 \tag{4.30}$$

$$T = \{0.[1\text{-}9]\ [0\text{-}9]^* \mid 1.0\ \}+ \tag{4.31}$$

$$\Delta_T = \frac{\|T\|}{Fe} \tag{4.32}$$

$$\sigma_T < \sigma 1 \tag{4.33}$$

$$\Delta_T > \Delta_1 \tag{4.34}$$

$$\Delta_{rest} \geq 0 \tag{4.35}$$

CardiacCycle1=({rest}?{P}{rest}?){QRS}{rest}?{T}* (4.36)

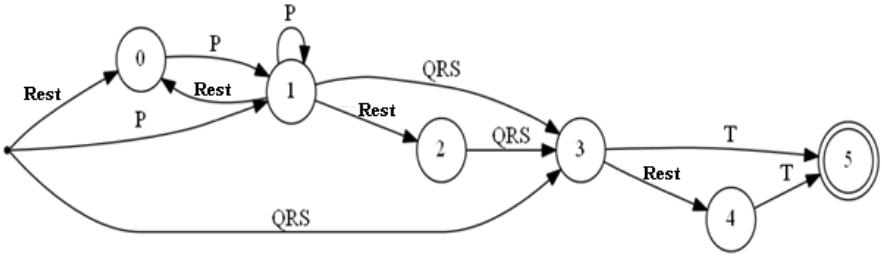

Figure 4.26: Deterministic automaton representing entire cardiac cycle

The regular expression below and Figure 4.27 describe all normalized cardiac cycles where the P wave is reversed.

Pinverted = {- 0.[1-9] [0-9] | -1.0 }+* (4.37)

$\Delta_{\text{Pinverted}} = \|Pinverted\|$ (4.38)

$|\sigma_{\text{Pinverted}}| < \sigma 1$ (4.39)

$\Delta_{\text{Pinverted}} > \Delta 1$ (4.40)

CardiacCycle2=({rest}?{Pinverted}{rest}?){QRS}{rest}?{T}* (4.41)

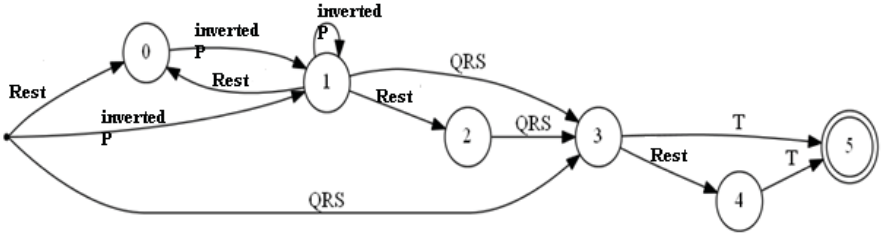

Figure 4.27: Deterministic automaton representing an entire cardiac cycle wherein P wave is reversed

The regular expression below and Figure 4.28 disclose a normalized cardiac cycle where the T wave is reversed.

$$Tinverted = \{- 0.[1\text{-}9]\ [0\text{-}9]^* \mid -1.0\ \}+ \quad (4.42)$$

$$\Delta_{\text{Tinverted}} = \|Tinverted\| \quad (4.43)$$

$$|\sigma_{\text{Tinverted}}| < \sigma 1 \quad (4.44)$$

$$\Delta_{\text{Tinverted}} > \Delta 1 \quad (4.45)$$

$$CardiacCycle3 = (\{rest\}?\{P\}\{rest\}?)^*\{QRS\}\{rest\}?\{Tinverted\} \quad (4.46)$$

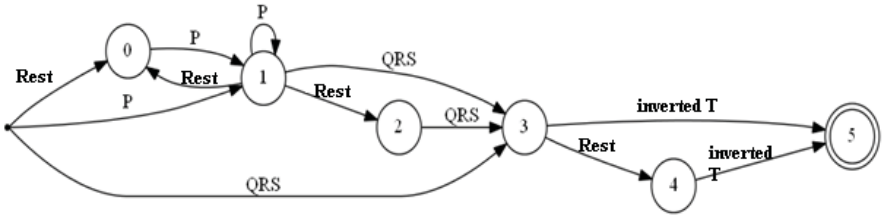

Figure 4.28: Deterministic automaton representing cardiac cycle with inverted T wave

Other waveforms, several segments and intervals characterize the electrical trace of the heart [Cha'09, Ayt'99, Moo'01, Ham'04, Kha'09, Sum'09, Che'0 6, Su'05]:

- RR distance: This is the distance between two successive peaks of R. It is the main indicator of the rate of the ventricles.
- PR interval: It represents the depolarization of the atrium and the AV node. Its duration is 0.12 to 0.2 seconds. The length of the PR interval decreases as the heart rate increases.
- The PR segment: It is the temporal distance between the end of the P wave and the start of the QRS complex and it represents the transmission time of the depolarization wave through the AV node.
- ST segment: It represents the difference between the finish of the S wave and the beginning of the T wave.

These last three intervals are variable, depending on the heart rate, and correspond to the resting phase of the cell.

- QT Interval: It is an indication of the length of the entire ventricular depolarization and repolarization. The duration varies depending on the rate of 0.3 to 0.38 seconds of heart.
- QTc interval: Practically, the normal value QTc <0.440 seconds. It represents the sum of depolarization (QRS complex) and repolarization (T) described by Bazett's formula:

$$QTc = QT/\sqrt{RR} \quad (4.47)$$

The regular expression below and Figure 4.29 describe a normalized cardiac cycle where both P and T waves are inverted.

*CardiacCycle4 = ({rest}? {P inverted } { rest }?) * {QRS } { rest }? { T inverted }* (4.48)

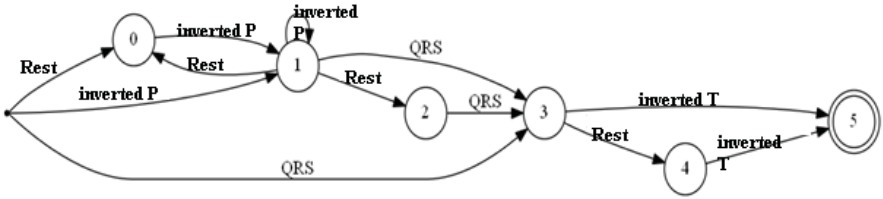

Figure 4.29: Deterministic automaton representing an entire cardiac cycle with inverted P and T waves.

Section 3 presents and discusses the results, and a comparison is made with the dyadic wavelet method [Nou'13] in terms of sensitivity and runtime. The choice of this method is justified because it is recent, known and reliable.

III.5 Results and discussion

In this section, the method described above is applied on multiple real ECG signals representative of different patients and they are issued in CHU Sahloul hospital, Tunisia. For all input signals, Q, R and S peaks, RR distances, QRS complexes, QTc intervals and P and T waves are detected. Furthermore, a comparison study with the wavelet method [Nou'13] is applied in terms of detection of R peaks.

Table 4.5 shows an application of multiple real signals ECG to extract the cardiac cycles, the QRS complex and the R peaks of patient1 representing a normal sinus rhythm.

It should be noted that:

- T P denotes the true positive and represents the correctly identified cycles;
- FP designates false positive and represents cycles that are incorrectly identified;
- FN denotes the false negative and represents incorrectly rejected cycles.

$$\text{Sensitivity (\%)} = \frac{\text{TP}}{\text{TP+FN}} \tag{4.49}$$

In practice, the average sensitivity rate of the proposed method is 99.63% and the average sensitivity rate of the wavelet method [Nou'13] is 99.05%.

In addition, the proposed method determines for each ECG signal the mean value of the QTc intervals and the absolute values of the P and T amplitudes.

Moderately, the absolute values of the P and T waves are respectively 349 and 737 mvolts. The QTc interval has a normal value of 0.334 seconds to less than 0.440 seconds. It represents the sum of depolarizations and repolarizations.

Table 4.5: Application to several real ECG signals and extraction of R peaks, QTc intervals, P and T wave amplitudes of patients 1.

ECG	Real number of cycles	TP	FP	FN	Se using wavelet (%)	Se (%)	QTc interval (sec)	P wave amplitude (mvolts)	T wave amplitude (mvolts)
ECG1	1	1	0	0	100.00	100.00	-	363	804
ECG2	5	5	0	0	100.00	100.00	0.340	372	732
ECG3	9	9	0	0	100.00	100.00	0.380	370	797
ECG4	19	19	0	0	100.00	100.00	0.366	363	785
ECG5	28	28	0	0	100.00	100.00	0.371	368	804
ECG6	37	37	0	0	100.00	100.00	0.369	372	794
ECG7	46	46	0	0	100.00	100.00	0.372	367	788
ECG8	55	55	0	0	100.00	100.00	0.372	376	810
ECG9	87	87	1	0	96.55	100.00	0.375	373	764
ECG10	116	116	1	0	99.13	100.00	0.365	361	744
ECG11	145	144	1	1	96.55	99.31	0.356	362	740
ECG12	173	171	1	2	98.26	98.84	0.349	359	754
ECG13	202	201	2	1	97.52	99.50	0.346	360	757
ECG14	231	228	0	3	98.26	98.70	0.340	320	665
ECG15	260	258	0	2	98.07	99.23	0.339	320	672
ECG16	289	287	4	2	100.00	99.31	0.324	371	809
ECG17	391	388	5	3	99.74	99.23	0.224	266	643
ECG18	488	485	5	3	98.61	99.39	0.217	286	553
ECG19	585	582	5	3	99.31	99.43	0.210	306	583
Total	**3167**	**3147**	**29**	**20**	**99.05**	**99.63**	**0.334**	**349**	**737**

Table 4.6: Application on several real ECG signals and extraction of R peaks, QTc intervals, P and T wave amplitudes of patient 2.

ECG	Signal length (sec)	Real number of cycle s	TP	FP	FN	Se (%)	S **e** using wavelet (%)	QTc interval (s ec)	P wave amplitude (mvolts)	T wave amplitude (mvolts)
ECG 20	60	111	110	0	1	99.10	100.00	0.337	568	404
ECG2 1	120	228	227	0	1	99.56	99.12	0.294	311	382
ECG 22	180	347	347	2	0	100.00	99.71	0.376	137	228
ECG 23	240	463	458	2	5	98.92	99.13	0.387	169	314
ECG 24	30 0	579	579	1	0	100.00	99.13	0.321	257	383
ECG 25	360	697	693	0	4	99.43	99.56	0.388	138	211
ECG 26	420	809	804	0	5	99.38	99.25	0.370	130	292
ECG 27	480	920	909	0	11	98.80	98.69	0.398	131	295
ECG 28	540	1029	1014	0	15	98.54	98.34	0.394	135	292
ECG 29	600	1136	1117	0	19	98.33	97.97	0.430	119	247
Total	**3276**	**6319**	**6258**	**5**	**61**	**99.21**	**99.09**	**0.370**	**210**	**305**

The table above shows an application of various actual signals to extract the ECG QRS complexes, the R peaks, the intervals QTc, and P and T of patient 2 showing a sinus tachycardia. The table indicates that for the R detection of the peaks, the average sensitivity rate of the proposed method is 99.21% and the average rate sensitivity of the method of the wavelet is 99.09%.

On average, the P wave has an absolute amplitude value of 210 mvolts and the T wave has an absolute amplitude value of 305 mvolts. Additionally, the QTc interval has a normal value of 0.370 seconds.

Table 4.7 shows a comparison between the different methods. For each method, the type of the ECG signal is determined, and the used variety and the shapes of waves to be taken into consideration or not are defined.

Table 4.7: Comparative study between proposed method and numerous references in terms of maintained account of ECG signal types

Reference	Method	R peak detection	QRS complex detection	P wave detection	T wave detection	Rest detection	P reversed detection	reversed T detection
Kokai et al. [Kok'97]	Grammar out of context	Yes	Yes	No	No	No	No	No
Panagiotis et al. [Tra'90]	Grammar out of context	Yes	Yes	Yes	Yes	Yes	No	No
Ibtihel et al. [Nou'13]	Dyadic wavelet	Yes	No	No	No	No	No	No
Salah et al. [Sal'14]	Grammar out of context	Yes	Yes	Yes	Yes	Yes	No	No
The proposed method	Regular grammar	Yes	Yes	Yes	Yes	Yes	Yes	Yes

The three following tables show several applications on very long ECG signals representative of different patients in order to extract the cardiac cycles, particularly the QRS complexes, and measure the mean values of RR distances and QRS duration. Each time, the standard deviation of the RR distances and the QRS durations is calculated.

Please note that the machine used has the following characteristics: CPU (TM) i7-2600 CPU frequency = 3.40GHz, and RAM = 4GB.

Table 4.8: Application on several real ECG signals of patient 3: Measurement of RR distances, QRS times and run times

ECG	Signal length (hour)	Detected cardiac cycles	RR distance (sec)	σRR	QRS duration (se c)	σQRS	Runtime (sec)	Runtime using wavelet (sec)
ECG 30	1	4836	0.743	0.44	0.101	0.01	11.26	14.05
ECG 31	2	9969	0.721	0.38	0.100	0.01	23.24	29.91
ECG 32	3	16465	0.655	0.35	0.104	0.02	37.28	43.14
ECG 33	4	22037	0.653	0.34	0.103	0.02	54.46	58.37
ECG 34	5	27357	0.657	0.32	0.102	0.02	72.36	74.09
ECG 35	6	33127	0.651	0.30	0.101	0.02	90.87	92.57
ECG36	7	38728	0.650	0.29	0.101	0.02	109.78	112.84
ECG37	8	45019	0.639	0.28	0.101	0.01	129.08	134.71
Total	**36**	**197538**	**0.671**	**0.33**	**0.101**	**0.01**	**528.33**	**559.68**

Table 4.9: Application on several real ECG signals of patient 4: Measurement of RR distances, QRS times and run times

ECG	Signal length (hour)	Detected cardiac cycles	RR distance (sec)	σ RR	QRS duration (sec)	σQRS	Runtime (sec)	Runtime using wavelet (sec)
ECG 38	1	5595	0.642	0.20	0.109	0.01	15.06	16.98
ECG 39	2	10677	0.673	0.3 4	0.10 9	0.01	30.43	33.52
ECG 40	3	16395	0.658	0.31	0.108	0.01	46.8	50.06
ECG 41	4	22232	0.647	0.29	0.109	0.01	63.81	66.93
ECG 42	5	27383	0.657	0.28	0.109	0.01	81.53	83.57
ECG 43	6	33028	0.653	0.28	0.109	0.01	99.73	101.15
ECG44	7	39392	0.639	0.27	0.110	0.01	118.93	122.04
ECG45	8	45410	0.634	0.26	0.109	0.01	138.58	140.86
Total	**36**	**200112**	**0.650**	**0.27**	**0.109**	**0.01**	**594.87**	**615.11**

Table 4.10: Application on several actual ECG signals of patient 5: Measurement of RR distances, QRS times and run times

ECG	Signal length (hour)	Detected cardiac cycles	RR distance (sec)	σRR	QRS duration (se c)	σQRS	Runtime (sec)	Runtime using wavelet (sec)
ECG 46	1	5986	0.601	0.43	0.133	0.03	14.79	15.63
ECG 47	2	11520	0.624	0.45	0.1 2 0	0.0 3	30.38	31.91
ECG 48	3	16190	0.666	0.59	0.126	0.03	46.5	48.37
ECG 49	4	22525	0.639	0.56	0.125	0.03	63.84	65.78
ECG 50	5	26241	0.685	0.66	0.128	0.03	81.52	83.62
ECG 51	6	30579	0.706	0.68	0.129	0.03	99.71	101.39
ECG52	7	36087	0.698	0.65	0.128	0.03	118.94	120.14
ECG53	8	43041	0.669	0.62	0.127	0.03	138.51	139.89
Total	**36**	**192169**	**0.661**	**0.58**	**0.127**	**0.03**	**594.19**	**606.73**

Mathematically, a low standard deviation means that the values obtained are very close to the mean value, and vice versa. If the value of the standard deviation is small, the measured values are regular and very close to the mean value.

However, if the value of the standard deviation is large, it means that the measured values are irregular. In addition, a comparison study with the wavelet method is applied in terms of execution time.

Figure 4.30 shows an application on a portion of the ECG signal. The various signal indicators (remote RR; complex QRS; Q, R and S amplitudes) are displayed. Primarily, the QRS durations have normal periods of a 0.1 second. Additionally, most RR distance values are less than 1 second. RR distances, QRS lines and s-wave amplitudes are stable. Similarly, Figure 4.31 and Figure 4.32 illustrate an application on ECG25 and ECG33, each having a time length. RR distances, complex QRS durations and Q, R and S amplitudes are displayed.

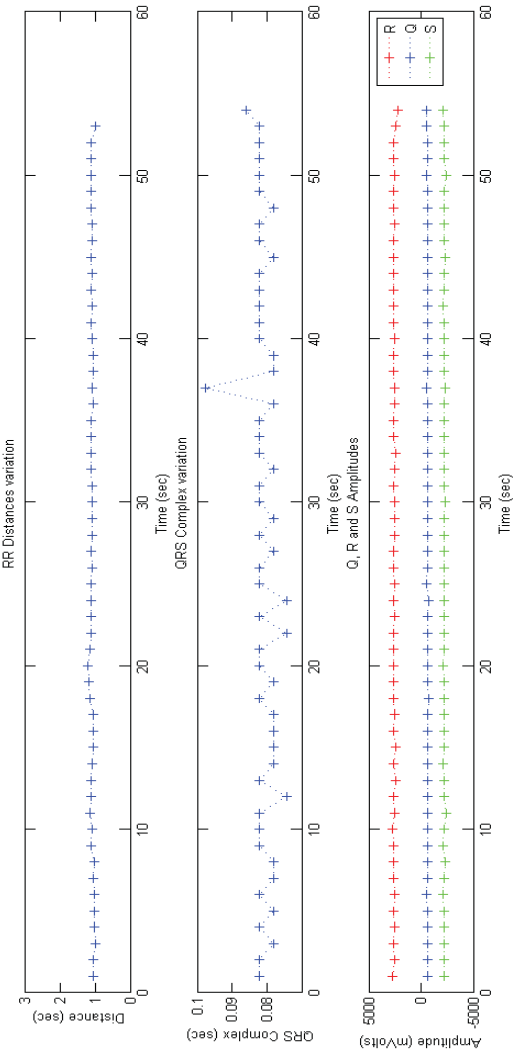

Figure 4.30: Application on portion of ECG signal and variation indifferent indicators (RR distances; QRS durations; Q, R and S amplitudes)

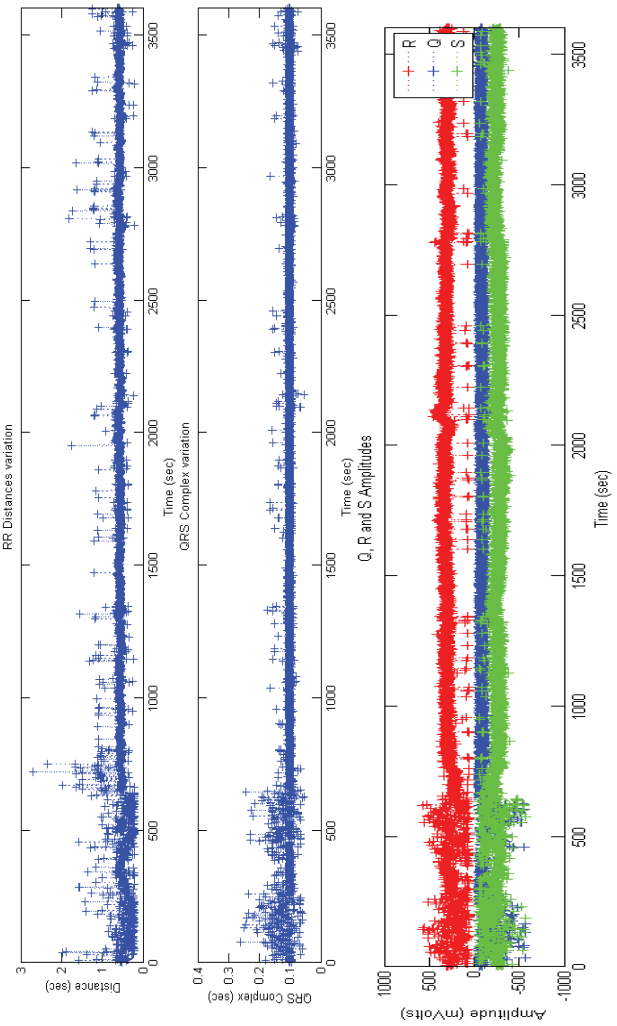

Figure 4.31: Application on ECG 17 and variation in different indicators (RR distances; QRS complex; Q, R and S amplitudes)

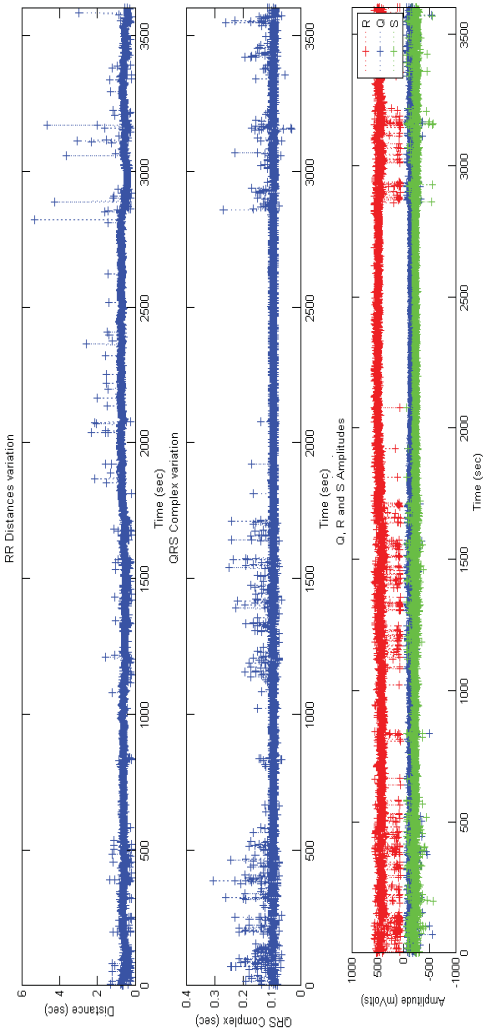

Figure 4.32: Application on ECG 36 and variation of different indicators (RR distances QRS complex; Q, R and S amplitudes)

Most of the RR distance values are less than 1 second. The durations of QRS complexity have normal durations of about a 0.1 second. A small number of spikes, half the huge amount of R peaks, are improperly disqualified. In fact, RR distances and QRS times are almost stable.

Figure 4.33 and Figure 4.34 shows the variation amplitude of P and T and associated parameters (QT interval, PR interval and segment PR), where the two waves are directed upwards. Figure 4.33 confirms that amplitude T is much greater than amplitude P. In general, amplitudes P and T are stable. This type of cardiac cycles is described by an automaton in Figure 4.26.

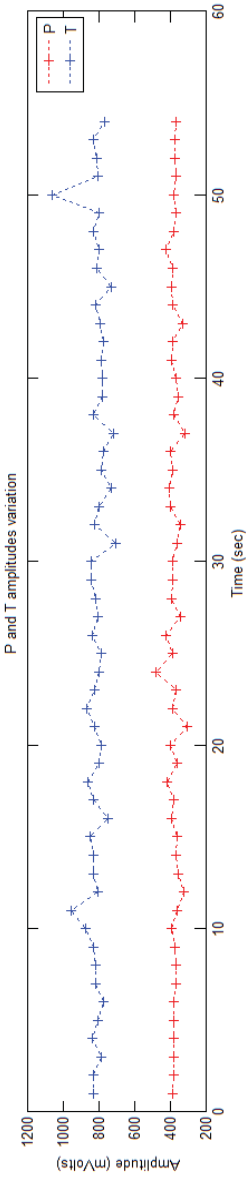

Figure 4.33: Amplitude variation in P and T waves with both waves directed upwards.

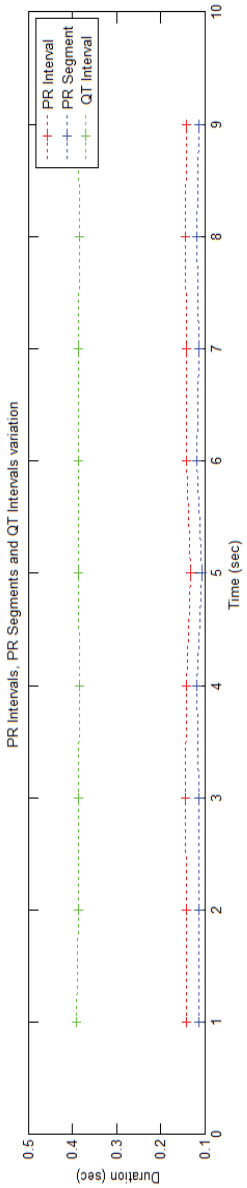

Figure 4.34: Variation in PR intervals, PR and QT interval segments.

Figure 4.35 and Figure 4.36 represent the amplitude variation the P and T waves and the associated metric (RR distance, complex QRS duration and amplitudes of the peaks Q, R and S), where a combination of rising and falling waves is detected.

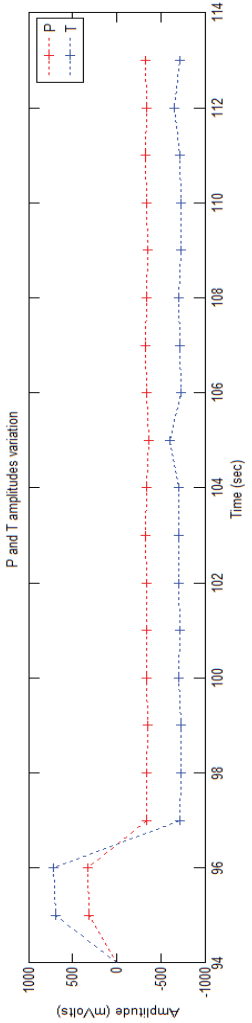

Figure 4.35: Variation in wave amplitudes. A combination of waves directed upwardly and downwardly.

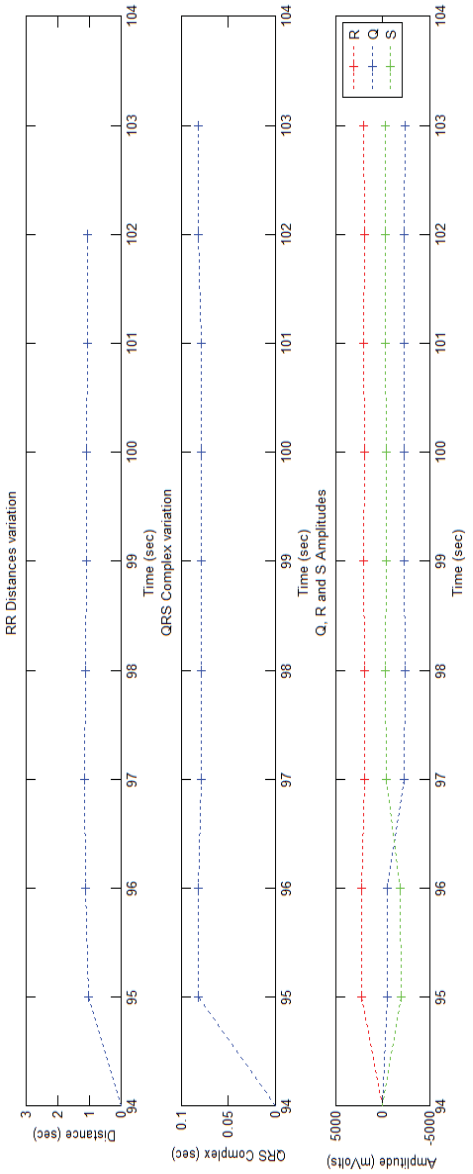

Figure 4.36: Variation in amplitudes, RR distances, QRS complexes and peaks Q, R and S.

Only the first two waves are directed upwards, then the rest of the P and T waves become inverted. Primarily, Figure 4.35 confirms that in absolute terms, the magnitude of T is much greater than the magnitude of P. In general, the amplitudes of P and T are stable. This type of cardiac cycle is described by an automaton of Figure 4.26 and Figure 4.29.

The proposed method capable of generating a medical report that displays the value of each parameter associated with the ECG signal per cardiac cycle (Figure 4.37). At the end of the report, the program calculates the average RR distance, the average QRS duration, the average QTc interval, the average P wave amplitude and the average T wave amplitude.

Then the program indicates the standard deviation of the RR distances and the standard deviation of the QRS times. Mathematically, if the value of the standard deviation is small, it means that the measured values are regular and are very close to the average value. However, if the value of the standard deviation is very important, this means that the measured values are irregular and are far from the average value.

Figure 4.37: Screen print of the generated report

IV. Recognition of cardiac cycles by out-of-context grammar

In this first part, we show the grammar outside environment that can be expanded to apply to the recognition Electrocardiogram (ECG) signals. We will describe an ECG signal as a sequence ofwaves and peaks based on a specific vocabulary and a set of grammatical rules. The QRS times, the RR distances and the QT and PR intervals will be calculated. This type of work is intended to aid in the medical diagnosis of an ECG signal.

Figure 4.38 summarizes the different stages of our grammatical method. First, the signal is normalized and then filtered by a series of low pass and high pass filters to reduce noise. Second, lexical analysis is used to specify recognized lexemes. In this case, a lexical unit corresponds to an element of the signal (wave, peak or rest). Third, parsing arranges tokens known as a grammar. The aim of this step is to determine whether a lexical unit belongs to the language generated by a grammar or not. If the lexeme sequence respects the language, the input signal is an ECG. Indeed, the QRS complex, the RR distance, and the PR and QT intervals are deduced. Finally, these indicators will clearly classify the normal or abnormal ECG signal.

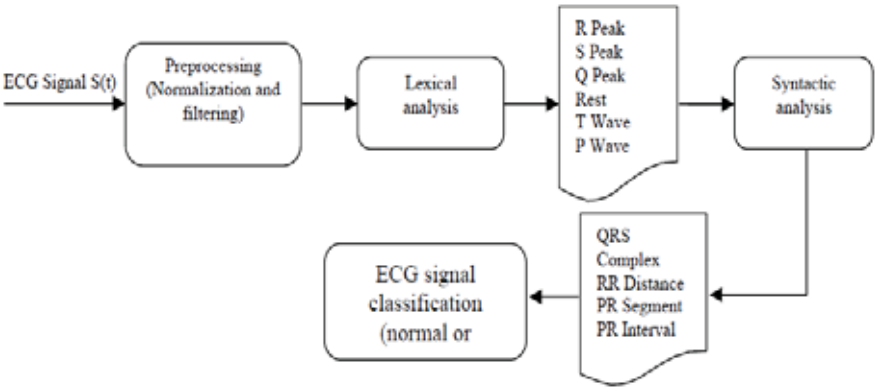

Figure 4.38: General view describing context free grammar for recognition of ECG signal

IV.1 Signal preprocessing

In this part, the art ECG signals undergo the same preprocessing steps described above in section II.1.

IV.2 Grammatical analysis of ECG signal

In this section, and after having normalized the ECG signal, we will process the values of the amplitudes that belong to the limited range [-1, 1]. Indeed, we have come to describe the signal as a sequence of almost zero amplitude, positive or negative.

We are based on a grammar G = (VT, VN, Ax, P) to describe the normal ECG signal, where VT is the terminal vocabulary of grammar, VN is the non-terminal vocabulary, Ax is the axiom and P is the set of production rules.

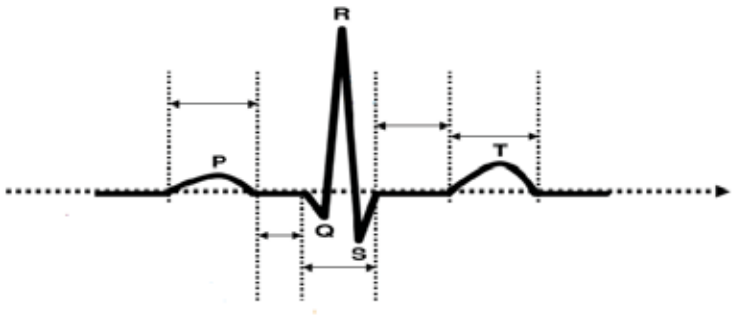

Figure 4.39: Morphology of normal ECG signal

The following grammar G can describe the ECG and automate the detection of deviations from the norm, where the character '*' means "zero or more times", the character '+' means "one or more times", the character '?'' means "zero or once", the character '|' means "or", the symbol 'ε' means an empty word of zero length and the character "." is an operator of concatenation.

G = (VT, VN, Ax, P)
VT = {P, Q, R, S, T, Rest}
VN = {ECG, Col, Landing, Coda, End}
Ax = {ECG}
P is the set of rules of next production:

ECG →Rest . P . Col | P . Col
Col →QR . Landing
Landing →S . Coda
Coda →Rest . T . End | T . End
End →ECG | ε

IV.3 Results

The proposed method has been applied to different parts of an actual ECG signal. The Flex and Bison tools [Lev'09] were also used to do lexical and syntactic analysis, respectively. Each proportion of the signal has a duration measured in seconds and represents several cardiac cycles. Each time, we apply our method to a single part in order to extract peaks and s-waveforms from it, and then measure the parameters of the signal.

Figures 4.40 and 4.41 show an application to a portion of 30 seconds. The different signal indicators such as the RR distance, the duration of the QRS complex, the PR interval and the segmented PR and QT intervals are calculated.

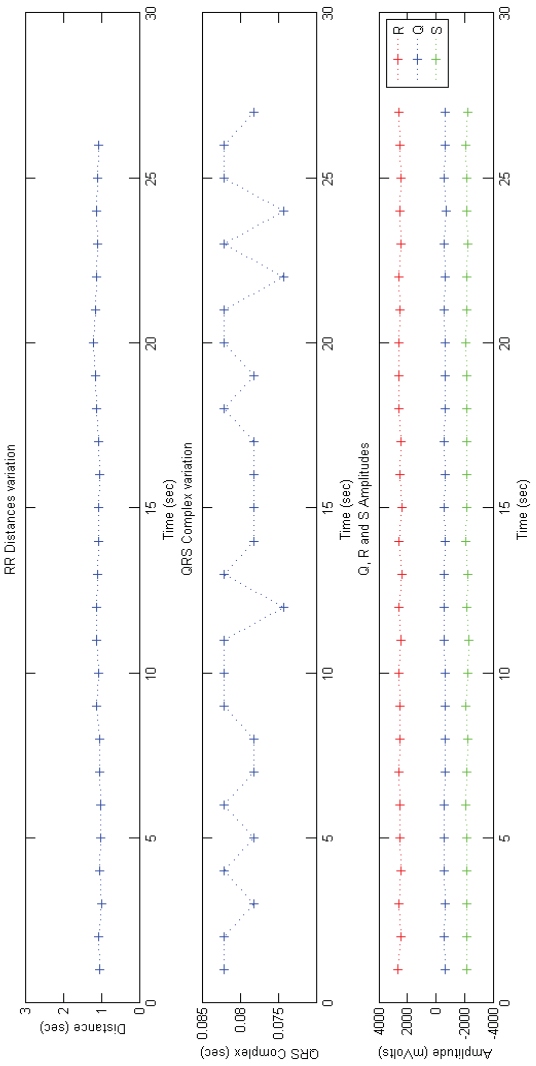

Figure 4.40: Variation in RR distance, QRS duration and amplitudes of Q, R and S peaks

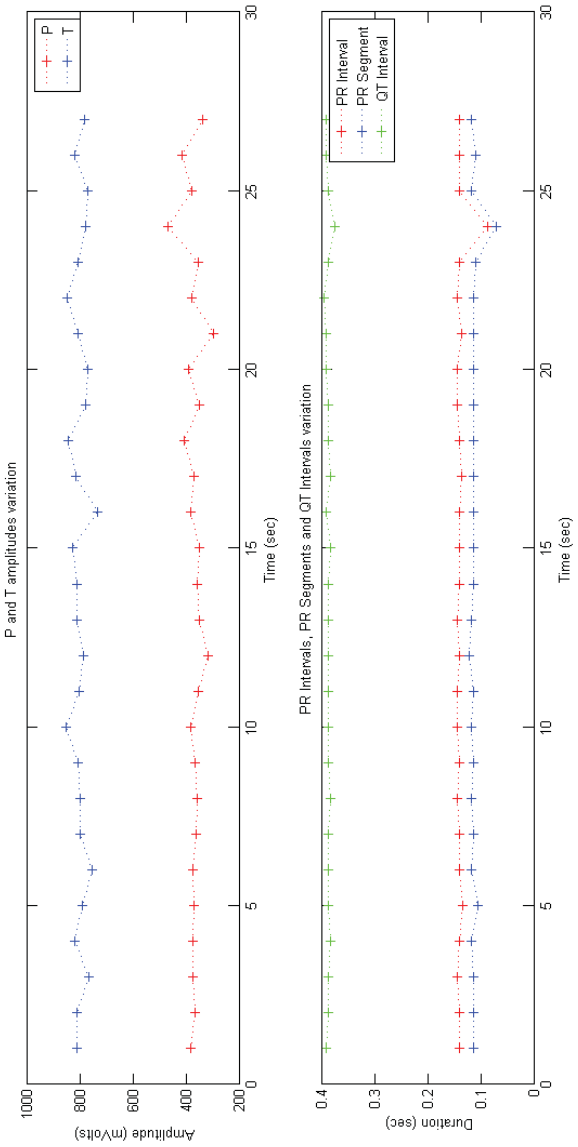

Figure 4.41: Variation in P and T wave amplitudes, PR interval, PR and QT segments

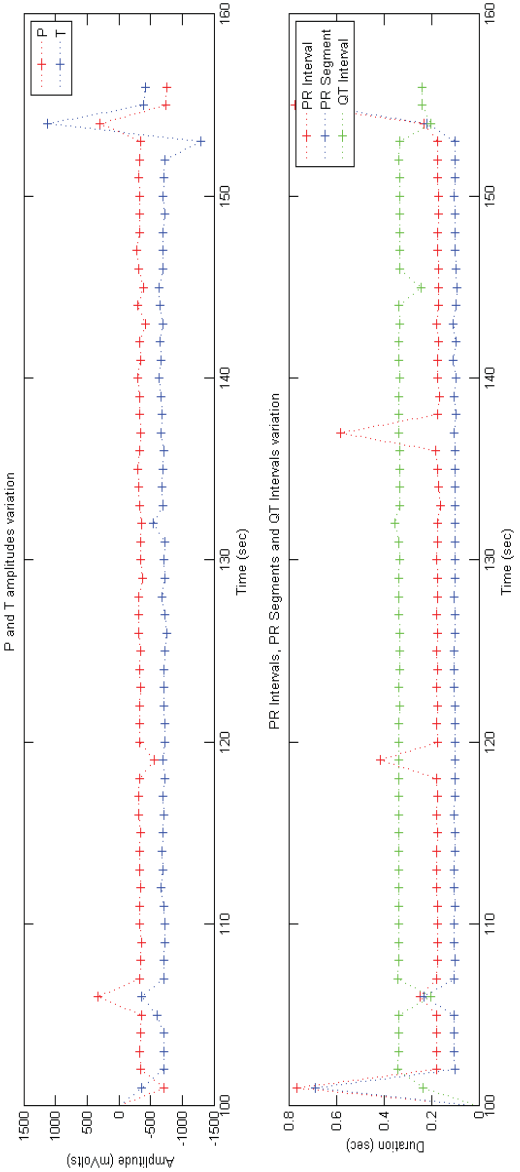

Figure 4.42: Variation in P and T wave amplitudes, PR interval, PR and QT segment with inverted P and T waves.

Similarly, Figure 4.42 shows an application to a portion of 160 seconds where P and T waves are inverted. The amplitude variation in the P and T waves are drawn, and the PR interval and the segment PR and QT interval are also calculated.

Table 4.11: Application on other portions of real ECG signal and detection of heart cycles.

ECG signal	Signal duration (sec)	Actual number of cardiac cycles	Number of cardiac cycles detected
ECG 1	0.8	0	0
ECG 2	1	1	1
ECG 3	10	9	9
ECG 4	20	19	19
ECG 5	30	27	27
ECG 6	40	37	37
ECG 7	50	46	46
ECG 8	60	54	54
ECG 9	9 0	81	81
ECG 10	120	108	108
ECG 11	150	135	135
ECG 12	180	163	163
ECG 13	210	186	186
ECG 14	240	192	192
ECG 15	270	215	215
ECG 16	290	240	240

Table 4.11 shows an application of our method based on the grammar of several portions of actual ECG signals. Each time, the number of detected cardiac cycles is measured. Table 4.11 shows that, for all parties, no parameter is crossed.

From the results shown above, the QRS complex period is less than a 0.1 seconds. In addition, the signal parameters are practically stable and the heart rate is 54 beats / min, so the input signal is a normal ECG.

We have shown that the grammar formalism can be applied for the description and classification of ECG signals. We have described an ECG as a sequence of lexemes based on specific vocabularies and grammatical rules. Thus, the QRS complex, the RR distance and thePR and QT intervals have been measured. These indicators have allowed us to clearly classify the ECG signal as normal or abnormal.

IV.4 Comparative study

In this section, we will do a comparative study with the Holsinger method [Hol'71] for R peak detection and RR distance measurement. The Holsinger method works as follows:

Calculate the threshold S which represents the maximum amplitude of the signal.

Find the first point that exceeds the threshold S which indicates the peak R.

$$s = Max(|S(t)|) * a \tag{4.50}$$

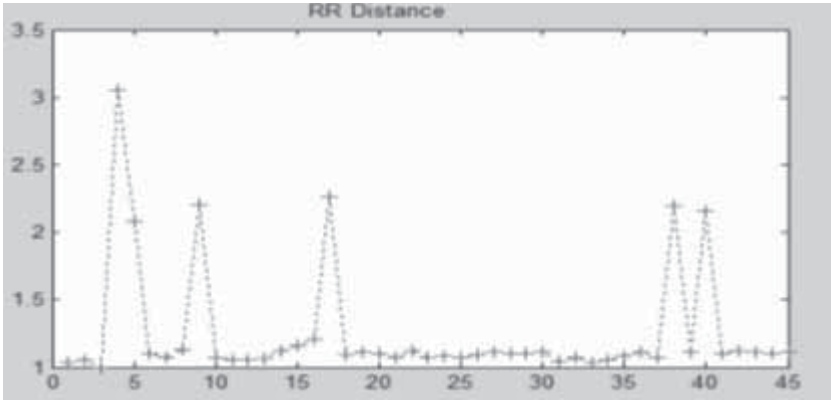

Figure 4.43: Application of the method of Holsinger

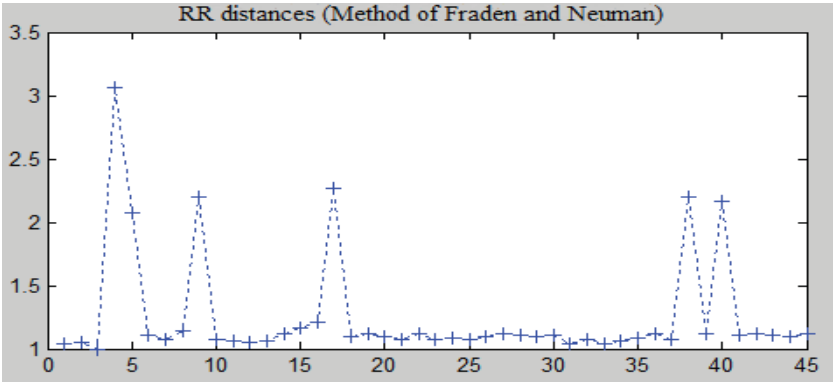

Figure 4.44: Application of Fraden and Neuman method

L represent both Figures 4.43 and 4.44, which show that the application of the technique of Holsinger [Hol'71] or Fraden and Neuman [Fra'80] has a portion 45 seconds of the actual ECG signal, where several R peaks (about 15%) are not detected. On the other hand, the application of our approach based on the grammar with no R peak is deductible and the distances of RR are stable.

The context-free grammar is proved to be useful in the recognition of standard ECG signals. The results of the experiments show that the application of our approach on several parts of an ECG signal real, where no parameter is crossed, allows us to calculate the duration of the QRS complex, the RR distances and the QT and PR intervals. In addition, a comparative study with the method of Holsinger and the method of Fraden and Neuman has been established in terms of peak detection and measurement R of RR distances.

V. Conclusion

In this chapter, a type-2 grammar, a type-3 grammar and deterministic automata have been found useful for the recognition of complex QRS and cardiac cycles and the interpretation of ECG signals. An ECG is thought of as a pair of adjacent waves and peaks that meet certain criteria for standard deviations and durations.

The context-free grammar has been found to be useful for the recognition of normal ECG signals. The results of the experiments show that the application of our approach on several parts of a real ECG signal allows us

to calculate the durations of the QRS complexes, the RR distances and the QT and PR intervals. In addition, a comparative study with the method of Holsinger and the method of Fraden and Neuman has been established in terms of R peak detection and measurement of RR distances.

However, the type-2 grammatical formalism has only been applied to normal ECGs. The context-free grammar is unable to describe any type of ECG signals. The varieties of ECG signals and the different types of wave morphologies make the use of out-of-context grammar insufficient.

Indeed, the type-3 grammar and the deterministic automata have been shown to be useful for the recognition of peaks and QRS complexes and the different morphologies of cardiac cycles. The latter have been described using deterministic automata and regular expressions. For an input signal, all indicators have been deduced such as QRS times, RR distances, QTc interval as well as peak and wave amplitudes. In addition, we have added two parameters: the standard deviation of the RR distances, noted σRR, and the standard deviation of the QRS durations, noted σQRS. These standard deviation parameters reflect the regularity of RR distances and QRS durations. This work is intended to aid in medical diagnosis and to support clinical decision-making.

CHAPTER 5

GRAMMAR-BASED MEDICAL IMAGE SEGMENTATION

I. Introduction

Segmentation is a fundamental step in many automatic image analysis systems. Its role is to delimit, in the studied image, the set of relevant zones for the interpretation or the modeling of the perceived scene. Therefore, this is a step key, and quality strongly influences the overall success of a machine vision or the computer vision. In this chapter, we will study the methods and techniques of processing images based on grammatical formalism. We mainly focus on the medical image.

II. Grammar-based image processing

Grammar and language theory (or formal language theory) began in 1950. Grammar consists of analyzing programming languages, describing natural languages, and modeling logical circuits and biological systems.

II.1 General

The following figure illustrates the number of publications (per year) for grammar-based image processing [Ped'13]. Until today, the number is becoming more and more important.

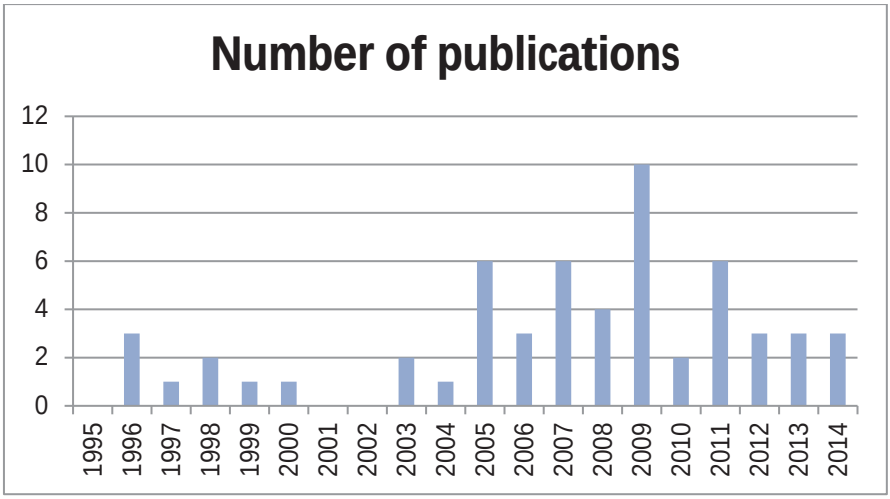

Figure 5.1: Evolution of number of publications in field of image processing by grammar, for last two decades.

The following figure illustrates the number of authors, by country, who have done grammar-based image processing [Ped'13]: image processing and medical image processing.

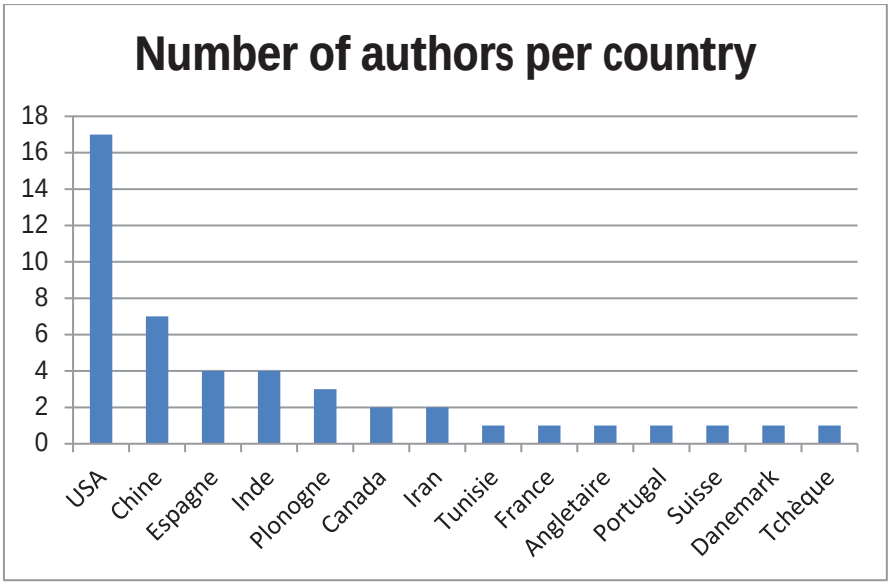

Figure 5.2: Number of authors interested in grammar for image processing.

II.2 2D image segmentation

Wu et al. (2009) presented a stochastic method for image segmentation. The proposed approach decomposed the image into visual elements and returned a hierarchical representation in the form of a graph. The problem of Bayesian inference is first formulated and a solution space is divided into a union of different sub-spaces of varying sizes. The objective is to optimize the a posteriori probability. Thereafter, a top-down approach is used to describe how objects and the region of models generate the intensity of the image. Finally, to perform the parameter estimates, the bottom-up propositions are carried out in order to guide the search in the parameter space.

II.3 Reconstruction of facades

Shape grammar has emerged as a powerful tool for describing a wide variety of architectural styles. Form grammar can be used to effectively describe complex but highly structured geometries, such as fractals, plants and buildings [Sti’72, Sti'78, Sti'80, Sti'82].

Muller et al. [Mul'07] described a semi-automatic algorithm which makes it possible to generate a 3D model of good resolution from an image of a facade at low resolution. Its objective is the reconstruction and the subdivision of the facade elements: floor, window, door, etc.

The objective of Teboul et al. [Teb'10] is to find the different regions of a facade to segment and associate each with a semantic label (wall, window…). The terminal vocabulary of basic forms is defined as follows:

IM (Image), AT (Attic), FA (Facade), GF (GroundFloor), FL (F loor), TL (Tile), Sky, Wa (Wall), Wi (Window), Sh (Shop), Do (Door), Rf (Roof) Ba (Balcony)

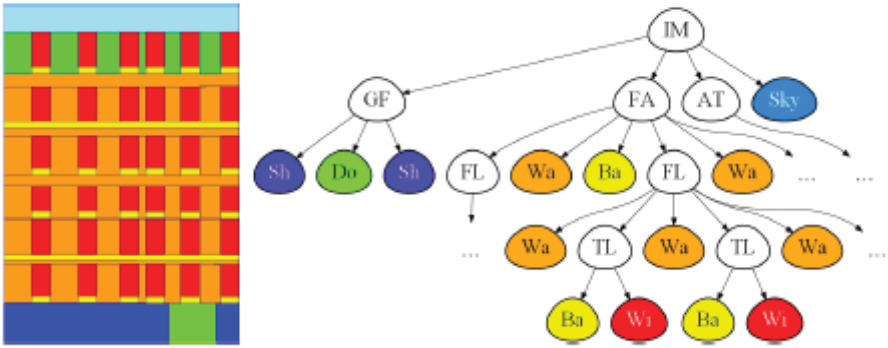

Figure 5.3: Front and associated derivation tree

However, with the same derivation tree (Figure 5. 3), a different set of parameters leads to different geometrical bodies. This is because by following the derivation process as it has been defined, we allow a large number of shapes to emerge while many of them are very unlikely to represent actual buildings. It turns out that a constraint can be applied in the calculation to deal with this problem, hence the phase of factorization of the grammar.

By applying a factorization of the grammar, we end up with a fixed grammar tree covering a more restricted space of forms. Factored grammar better expresses realistic architecture, and always covers a large area of facades.

It is possible to perform a first segmentation of the image, in which each pixel is associated with a class independently of any other pixel. The

following figure shows the probabilities obtained for each class on a single image. We build the obtained confusion matrix (Figure 5.4):

$$\begin{pmatrix} \mathbf{30} & 11 & 13 & 7 & 12 & 14 & 3 & 8 & 2 \\ 3 & \mathbf{62} & 12 & 4 & 1 & 6 & 1 & 10 & 1 \\ 11 & 9 & \mathbf{48} & 7 & 7 & 4 & 0 & 13 & 1 \\ 1 & 2 & 2 & \mathbf{81} & 0 & 0 & 0 & 14 & 0 \\ 6 & 9 & 6 & 0 & \mathbf{57} & 12 & 9 & 0 & 1 \\ 9 & 13 & 8 & 0 & 12 & \mathbf{55} & 2 & 0 & 1 \\ 1 & 0 & 0 & 0 & 4 & 6 & \mathbf{89} & 0 & 0 \\ 6 & 7 & 9 & 28 & 6 & 1 & 1 & \mathbf{40} & 2 \\ 9 & 10 & 15 & 6 & 14 & 18 & 11 & 14 & \mathbf{3} \end{pmatrix} \begin{matrix} window \\ wall \\ balcony \\ door \\ roof \\ chimney \\ sky \\ shop \\ other \end{matrix}$$

Figure 5.4: Confusion matrix

However, windows are poorly detected (30%). This is because the windows are not visually invariant; and even worse, they show the appearance of other objects in the scene by reflection or transparency.

Guowei et al. [Guo'12] used grammar rules for segmentation and 3D reconstruction of digitized facades. This is based on the definition of a set of grammar rules and a dictionary of basic shapes. The results gave precise segmentation of the facade to reconstruct a polygonal model. However, derivation trees lead to geometric instances many of which are unlikely to represent an actual facade. Thus, finding a better segmentation rests on the choice of the rules which better generate a facade.

III. Grammar for medical image processing

Grammars were to develop theories of languages. However, there was not much time to realize that this theory was essential for studies of artificial languages, computing and information technology. The grammar study has been widely used in the analysis of languages, modeling of biological systems, computer vision, and the pattern recognition and processing of images, medical.

This work is to present and discuss the results of an overview to identify the state of the art of medical images using grammars. In this context, we study documents that focus on extracting or learning the structure of

medical images. The grammar could present a flexible way to aid in the recognition and classification of diseases.

Ogiela et al. [Ogi'08] proposed a grammar-based approach for the recognition of radiograph bones and in particular bone fractures. The proposed grammar makes it possible to model several types of fractures (spiral, longitudinal, crack…) and the terminal vocabulary of the grammar used constitutes intervals of angles of different degrees.

For example, the first node *a* represents the interval [-10, 10] degree, while the second node *b* represents the interval [10, 70] degree (Figure 5.5). Indeed, the grammar recognizes the angles which separate the elements of the bone and from the values of angles one identifies the type of the fracture.

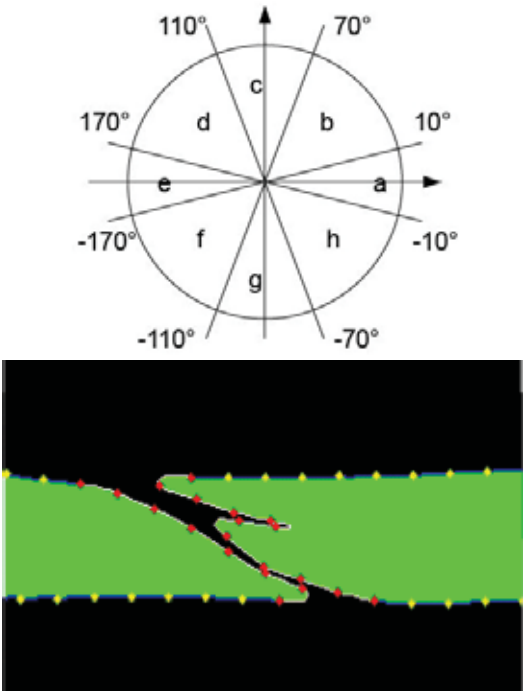

Figure 5.5: Terminal vocabulary (a, b, c, d, e, f, g, h) represents feeling intervals of angles of fractures

The grammar production rules and the lesion types are described in Table 5.1:

Table 5.1: Grammar outside context for recognition of fractures of type: cracks, spiral, longitudinal, and displaced fracture

Lesion	Production rules
Fracture Crack	FRACTURE → a CRACK a; CRACK → hb | hab
Spiral Fracture	FRACTURE → a SPIRAL a SPIRAL → MEMBERSHIP f | MEMBERSHIP gf | MEMBERSHIP fe | MEMBERSHIP fg | hf | gf | fg | f h | f MEMBERSHIP → bah | bh
Longitudinal fracture	FRACTURE → a LONGITUDINAL e LONGITUDINAL → TRANSVERSE TRANSVERSE | TRANSVERSE e TRANSVERSE | TRANSVERSE eh | he TRANSVERSE | Hey TRANSVERSE → hg | hf
Displaced fracture	FRACTURE → DISPLACED_M1 f | DISPLACED1 f | DISPLACED_M2 d | DISPLACED2 d DISPLACED_M1 → ba | bg | bh DISPLACED_M2 → hg | hf | Hey DISPLACED1 → bahg | bah | bag | bagh DISPLACED2 → hgfe | hge
Delayed union fracture	FRACTURE → a DELAYED_UNION a DELAYED_UNION → MEMBERSHIP MEMBERSHIP | MEMBERSHIP to MEMBERSHIP | MEMBERSHIP g MEMBERSHIP | MEMBERSHIP c MEMBERSHIP | MEMBERSHIP ga MEMBERSHIP | MEMBERSHIP gc MEMBERSHIP | MEMBERSHIP gac MEMBERSHIP | MEMBERSHIP ac MEMBERSHIP | MEMBERSHIP bc MEMBERSHIP MEMBERSHIP → bah | bh

Transverse fracture	FRACTURE → ahe | a TRANSVERSE e | agfe | a TRANSVERSE he TRANSVERSE → hg | hf
Membership	FRACTURE → a MEMBERSHIP e MEMBERSHIP → bah | bh

For the recognition of fractures, the context-free grammar used is G = (Σ N, Σ T, P, S), where:

- Σ N = {FRACTURE, FISSURE, TRANSVERSE, SPIRAL, ADHESION, DELAYED_UNION, DISPLACED_M1, DISPLACED_M2, DISPLACED1, DISPLACED2, LONGITUDINAL, A, B, C, D, E, F, G, H}.
- Σ T = {a, b, c, d, e, f, g, h}.
- S = FRACTURE; the axiom.
- P is the set of production rules defined in Table 5.1.

To identify the type of the fracture, the grammar recognizes the values of angles between the parts of the human bones. The proposed method achieves an accuracy level of over 90%.

Ogiela et al. [Ogi'09] presented a method to obtain a bone description of the wrist in the form of a graph. Before their analysis, the images are subjected to a pre-processing step, the purpose of which is to indicate the contours of the bone. The pretreatment operations must be completed first, and this results in the separation of the different parts of wrist structures to extract the individual bones. Thereafter, the terminal symbols of the grammar are represented by the centers of gravity of each bone of the hand (Figure 5.6). The application of the proposed techniques achieves a recognition rate of approximately 93%. The grammar is aimed at the automatic construction and semantic and topological interpretation of the bones of the wrist.

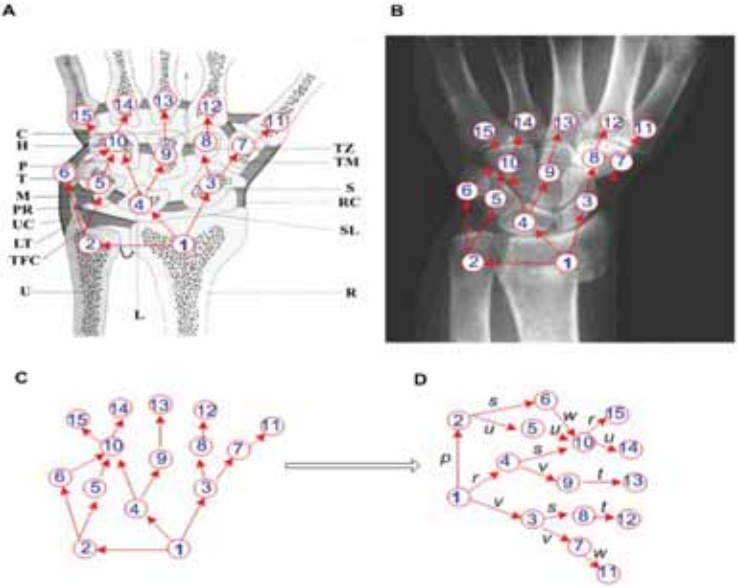

Figure 5.6: Graphic description of wrist examined by X-ray and definition of topological relations between bones

The grammar used is G = (N, Σ, Γ, P, S), where:

N = {ST, ULNA SCAPHOID, LUNATE, TRIQUETRUM, PISIFORM, TRAPEZIUM, TRAPEZOID, CAPITATE, HAMATE, M1, M2, M3, M4, M5},
∑ = {r, u, s, l, t, p, tm, tz, c, h, m1, m2, m3, m4, m5},
Γ is all labels used in the rules,
S = ST is the axiom,
P is the set of production rules presented in Table 5.2.

The proposed grammar achieves about a 93% recognition rate to analyze and interpret lesions.

Table 5.2: Grammar which can recognize many types of lesions: cyst, spiral, stenosis, dilatation, etc.

Lesion	Production rules
Cyst	LESION → CYST CYST → IP NI | GP NG | IP NG | GP NI | IS NI | GS NG | IS NG | GS NI | I NS NI | G NS NG | I NS NG | G NS NI
Stenosis	LESION → STENOSIS STENOSIS → NS S | NS G | NS PS | NS PI | NG S | NI NS I | NI S
Dilation	LESION → DILATION EXPANSION → SP NG | SG NS | S NS | G NS
Ramifications	LESION → BRANCH BRANCH → I NI | I NS | NI NN IP | I NS NI NN | G NI | GS NN | GP NN | GS NI NN | S NG | S NS NN | NG NG NI N → n | N n NN → nn | NN nn I → i | I i NI → ni | Neither nor G → g | G g NG → ng | NG ng S → s | S s NS → ns | NS ns P → p

Trzupek et al. [Trz'09, Trz'11] presented an approach for the interpretation of medical images and the recognition of heart disease (stenosis) from 3D images of coronary arteries. After a phase of skeletonization of the image, a grammatical description in the form of a graph represents the spatial relations between the arteries. This operation determines the starting point and the ending point of each branch of the arteries. Then each point is labeled to identify the type of each branch based mainly on the coordinates of the points (Figure 5.7). All of these points constitute the nodes of the generated graph which represents a semantic model for the spatial reconstruction of the coronary arteries. The coordinates of the branches

represent the terminal vocabulary of the grammar used while the non-terminal vocabulary represents the different possibilities of distribution of the arteries and thus the different types of stenosis. The proposed method shows a stenosis classification rate of 85%.

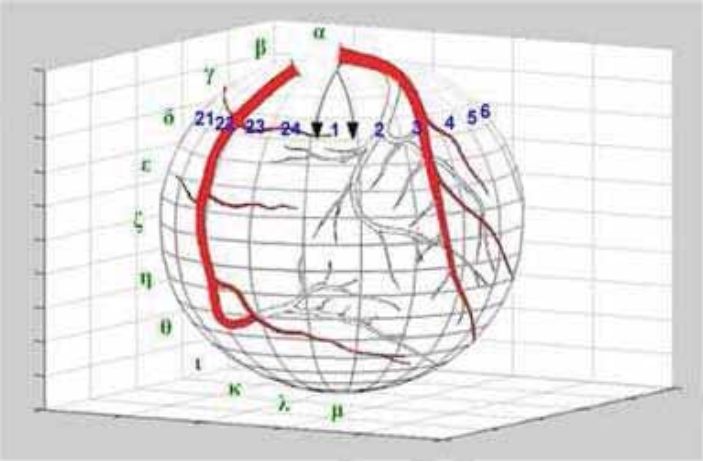

Figure 5.7: Spatial coordination of branches and coronary arteries. The coordinates constitute the terminal vocabulary of the grammar used.

The graph shows the spatial relationships between the arteries (Fig 5.8) where the elements are defined by introducing spatial relationships: horizontal defined by the set of labels {1, 2, ..., 24} and vertical defined by the set of labels { α, β, ..., μ } on a hypothetical sphere.

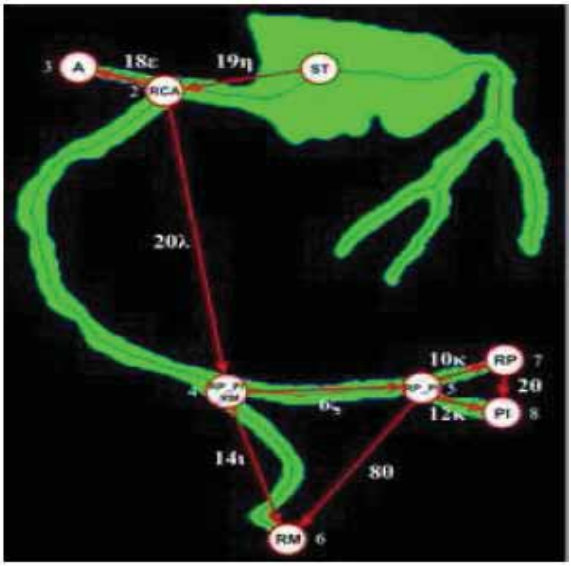

Figure 5.8: Presentation of right coronary artery

For the Right Coronary Artery (RCA) described in Figure 5.8, the grammar used is

G = (Σ, Δ, Γ, P, Z), where:
Σ = {ST, RCA, A, RP_PI_RM, RM, RP, PI, C_Right, C_Right_post_marg, C_Right_post_int},
Δ = {ST, RCA, A, RP_PI_RM, RM, RP, PI},
Γ = {19 η, 18 ∈, 20 λ, 6 ζ, 14 τ, 10 κ, 12 κ, 2 θ, 8 θ },
Z is the starting axiom.

For the left coronary artery (LCA), the grammar used is G = (Σ, Δ, Γ, P, Z), where:

Σ = {ST, LCA, CX, L_LAD, C_Left, C_Left_ant},
Δ = {ST, LCA, CX, L_LAD, L, LAD},
Γ = {2 κ, 14 τ, 23 λ, 4 λ, 16 θ, 15 δ, 12 δ},
Z is the starting axiom.

The grammar can recognize locations, amounts and types of stru<cture with an accuracy classification rate of approximately 85%.

IV. Synthesis and discussion

The medical data are perceived as a structured scene having a hierarchy because the grammars can obviously describe hierarchical structures using their non-leaf nodes and terminal. Most applications use grammars out of context. However, depending on the purpose of the application, regular, largely well-organized grammars can be used for image segmentation. In addition, another advantage of using regular grammars is the accessibility of efficient methods for grammar rules, allowing supervised learning of the models used.

Also, context-free grammars take a lot of time compared to regular grammars. This type of grammar represents more the structural patterns of computer vision applications. Thus, the context-free grammar can represent several lesions in medical images.

Once the advantages of grammars are presented, it is important to set a comparison with non-grammatical methods. Gao et al. [GAO'00] asserted that, compared to statistical methods, the use of grammars would offer greater flexibility in applications. In addition, stochastic grammars provide the probability of a given model in each considered class, but other discriminated methods such as support vector machines or neural networks only give the result classification.

Table 5.3 shows a combination of the analyzed state-of-the-art work, and the techniques and methods used for each of them. Each of the documents is analyzed individually. In fact, several types of grammars have been used and are often combined with a variety of other techniques. Although all the analyzed documents have used the grammar, different ways have been found to recognize objects, pattern recognition and image segmentation.

Table 5.3 summarizes the work related to my thesis as well as the methods and techniques used. For each job, we identify the objective, the techniques and primitives used, the field of application and the results achieved:

Table 5.3: Synthesis syntactic methods for processing 2D images

Objective	Reference	Primitive	Results
Shape recognition Brodatz images of buildings	Wang et al. [Wan'05]	Pixels and Image Regions	Rating rate is 100% for textures and 97% for building classification.
Object recognition of Building images	Wang et al. [Wan'06]	Pixels and Image Regions	Rating rate is 97%
Object recognition of facade images	Tylecek et al. [Tyl'01]	Small rectangles	Presentation of generated images
Object recognition i mages cars and houses	Siskind et al. [Sis'07]	Vector image features	Rating rate is 97%
Clothing images	Chen et al. [Che'06]	Segments and garment parts	Presentation of generated images
Object recognition of images of human faces	Reddly et al. [Red'09]	Block of pixels representing an element of the face (eyes, nose, etc.)	Rating rate is 95 %
Recognizing objects in a graphical user interface (GUI)	Parag et al. [By'12]	Characteristics of a GUI interface	Rating rate is 90% for buttons, 100% for menus, 90% for radio buttons and 67% for checkboxes
Handwritten Chinese Character Recognition	Gao et al. [Gao'00]	Traces and segments	Recognition rate is 77.4% for characters written in an article
Classification of medical arteries	Trzupek et al. [Trz'09, Trz'11]	Segments and points	Rating rate is 85%

Classification of medical images and recognition of fracture type	Ogiela et al. [Ogi'08]	Segments	Rating rate is 90%
Object recognition of images of human bones and organs	Ogiela et al. [Ogi'09]	Center of gravity of image and segments	Rating rate is 93%
Image segmentation	Wu and al. [Wu'09]	Pixels	Presentation of generated images and execution time is 10 to 20 minutes

In general, the use of grammars allows, in a more flexible way, to describe and represent images, mainly when the input data have a well-established hierarchical pattern, since it is possible to realize a direct relation between the structure data and the grammatical rules.

The methods and techniques examined provide an overview of the use of grammar in medical imaging. Most of the work has been published in the last decade. Moreover, it can be concluded that it is an extremely promising line of research, especially when studies have shown a recognition rate over 90%.

In the following section, we segment a medical image using grammatical analysis. To validate our approach, we will apply it first on scintigraphic images and tomographic 2D images.

Grammar can represent different lesions in medical images such as ultrasound, scintigraphic, coronary and bone x-ray images. The methods and techniques examined provide an overview. Most of the articles have been published in the last decade. Moreover, it can be concluded that it is an extremely promising line of research, especially when studies have shown a recognition rate over 90%.

However, we have seen in a previous section the grammatical formalism used only during a high level (level 3) for pattern recognition (Figure 5.9). Indeed, in this chapter, we will use the grammar for the extraction of forms (level 2) as well as the spatial interpretation of the forms (level 3) in Figure 5.9. We will make segmentation of scintigraphic images and tomographic CTA based on the grammar.

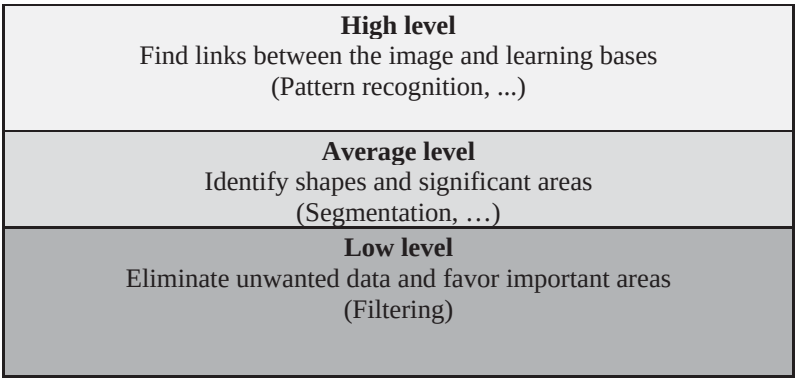

Figure 5.9: Three levels of image processing

V. Segmentation of scintigraphic images

For this type of scintigraphic image, we have chosen lexical and syntactic analyzers which rotate along a spiral path from the inside to the outside and extract the homogeneous regions according to a criterion of homogeneity set by the user. The contours of the endocardium and of the epicardium are thus detected and a quantification of the mass of the myocardial muscle is obtained.

V.1 Scintigraphy technique

Scintigraphy is a method of medical imaging that is part of nuclear medicine. The patient receives the molecules and sends out the radiation once they are received by the organ to be explored. In practice, the gamma-camera machine detects the radiation emitted by the body. Finally, the resulting image is reconstructed. The inner wall is called endocard and the outer wall is called epicardium. The two organs are separated by the epicardial muscle (Figure 5.10).

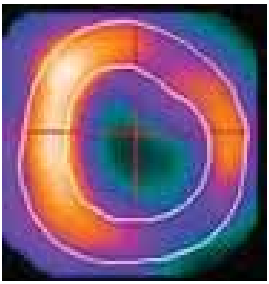

Figure 5.10: Scintigraphic image.

In the following part, a detailed step-by-step description of the method will be established with illustrative figures.

V.2 A detailed description of the method

We use vocabulary intensities VT, which are histogram-based (Figure 5.11) to segment and represent the major strengths in the image.

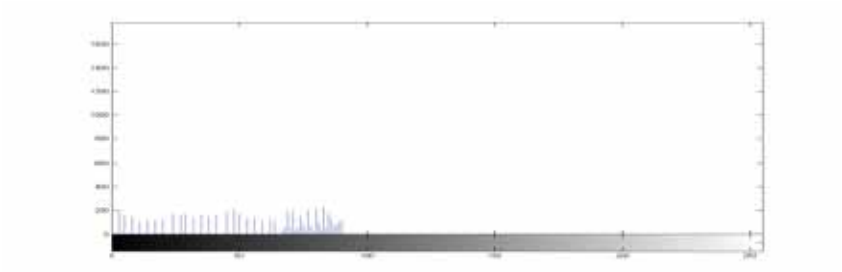

Figure 5.11: Histogram of a scintigraphic image.

Step 1:

Read the image I to segment.

Choose the first two intensities a1 and a2.

Initialize the grammar G = (VT, VN, S, P) where:

VT = {a1, a2} is the terminal vocabulary of intensities.
VN = {Image, Endocardium, Epicardium, Background, X, Y, Z, T} is the non-terminal vocabulary.

S = {Image} is the axiom of grammar.
P is the following set of rules:
Image → *Endocardium . Epicardium . Background | Epicardium . Fund*
Endocardium → *X | X . Y . X*
X → *a1 . X*
X → *ε*
Y → *a2 . Y*
Epicardium → *Z | Z . T . Z*
Z → *a2 . Z*
Z → *ε*
T → *a1 . T*

The characters '+' and '|' mean "one or more times" and "or", respectively. The symbol '.' is an operator for concatenation.

Step 2:

Initialize the center of image *O (x0, y0).*

Division of the image 8n sectors (n1) by applying the second way is described in Figure 5.12.b.

$$n = E\left(\frac{N*M}{r^2}\right) \qquad (5.1)$$

where NxM is the image dimension in pixels and r is the radius of the sectors measured in pixels.

This key step speeds up the algorithm execution time especially when the user increases the value of radius r (Figure 5.12.b and Figure 5.13)

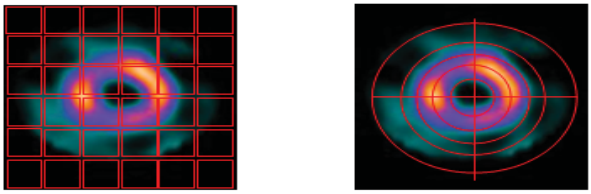

Figure 5.12: Different ways of dividing an image into blocks (a) or sectors (b).

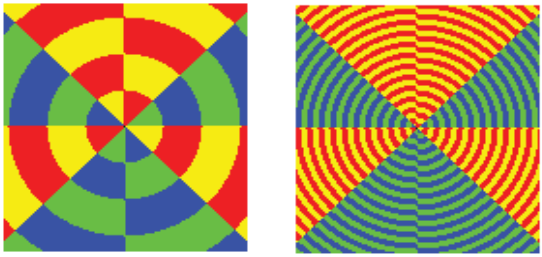

Figure 5.13: image division into sectors; (a) r = 20 pixels; (b) r = 3 pixels.

Order sectors $8k + 1;\ k \geq 0$:

$$\{P(x,y)\ where\ (x-x0)^2 + (y-y0)^2 > kr^2;\ x \in M, y \in N\} \cap \{P(x,y)\ où\ (x-x0)^2 + (y-y0)^2 \leq (k+1)r^2;\ x \in M, y \in N\} \quad (5.2)$$

$$x \geq 0 \quad (5.3)$$

$$y \geq 0 \quad (5.4)$$

$$y \leq x \quad (5.5)$$

Order sectors $8k + 2;\ k \geq 0$:

$$\{P(x,y)\ where\ (x-x0)^2 + (y-y0)^2 > kr^2;\ x \in M, y \in N\} \cap \{P(x,y)\ où\ (x-x0)^2 + (y-y0)^2 \leq (k+1)r^2;\ x \in M, y \in N\} \quad (5.6)$$

$$x \geq 0 \quad (5.7)$$

$$y \geq 0 \quad (5.8)$$

$$y > x \quad (5.9)$$

Order sectors $8k + 3;\ k \geq 0$:

$$\{P(x,y)\ where\ (x-x0)^2 + (y-y0)^2 > kr^2;\ x \in M, y \in N\} \cap \{P(x,y)\ où\ (x-x0)^2 + (y-y0)^2 \leq (k+1)r^2;\ x \in M, y \in N\} \quad (5.10)$$

$$x < 0 \quad (5.11)$$

$$y \geq 0 \tag{5.12}$$

$$y > -x \tag{5.13}$$

Order sectors $8k + 4;\ k \geq 0$:

$$\{P(x,y)\ where\ (x - x0)^2 + (y - y0)^2 > kr^2;\ x \in M, y \in N\} \cap \{P(x,y)\ o\grave{u}\ (x - x0)^2 + (y - y0)^2 \leq (k+1)r^2;\ x \in M, y \in N\} \tag{5.14}$$

$$x < 0 \tag{5.15}$$

$$y \geq 0 \tag{5.16}$$

$$y \leq -x \tag{5.17}$$

Order sectors $8k + 5;\ k \geq 0$:

$$\{P(x,y)\ where\ (x - x0)^2 + (y - y0)^2 > kr^2;\ x \in M, y \in N\} \cap \{P(x,y)\ o\grave{u}\ (x - x0)^2 + (y - y0)^2 \leq (k+1)r^2;\ x \in M, y \in N\} \tag{5.18}$$

$$x < 0 \tag{5.19}$$

$$y < 0 \tag{5.20}$$

$$y \leq x \tag{5.21}$$

Order sectors $8k + 6;\ k \geq 0$:

$$\{P(x,y)\ where\ (x - x0)^2 + (y - y0)^2 > kr^2;\ x \in M, y \in N\} \cap \{P(x,y)\ o\grave{u}\ (x - x0)^2 + (y - y0)^2 \leq (k+1)r^2;\ x \in M, y \in N\} \tag{5.22}$$

$$x < 0 \tag{5.23}$$

$$y < 0 \tag{5.24}$$

$$y > x \tag{5.25}$$

Order sectors $8k + 7;\ k \geq 0$:

$$\{P(x,y)\ where\ (x - x0)^2 + (y - y0)^2 > kr^2;\ x \in M, y \in N\} \cap \{P(x,y)\ o\grave{u}\ (x - x0)^2 + (y - y0)^2 \leq (k+1)r^2;\ x \in M, y \in N\} \tag{5.26}$$

$$x \geq 0 \tag{5.27}$$

$$y < 0 \tag{5.28}$$

$$y \leq -x \tag{5.29}$$

Order sectors $8k + 8;\ k \geq 0$:

$$\{P(x,y)\ where\ (x - x0)^2 + (y - y0)^2 > kr^2;\ x \in M, y \in N\} \cap \{P(x,y)\ o\grave{u}\ (x - x0)^2 + (y - y0)^2 \leq (k+1)r^2;\ x \in M, y \in N\} \tag{5.30}$$

$$x \geq 0 \tag{5.31}$$

$$y < 0 \tag{5.32}$$

$$y > -x \tag{5.33}$$

Step 3:

Calculate the dominant intensity of each pixel sector.

Round off each intensity value to the nearest I value belonging to VT.

Step 4:

The lexical analyzer scans the image sector by sector in a spatial spiral path and an ascending and return the lexemes, which coincides with the regular expressions described in step 1.

In other words, the lexical analyzer analyzes the intensities of the sectors which come from the following vector V:

The analyzer indicates the endocardium and the epicardium by lexical UL1 and UL2 units, respectively.

Step 5:

The syntax analyzer determines the arrangement of the lexemes according to the grammar G described in step 1.

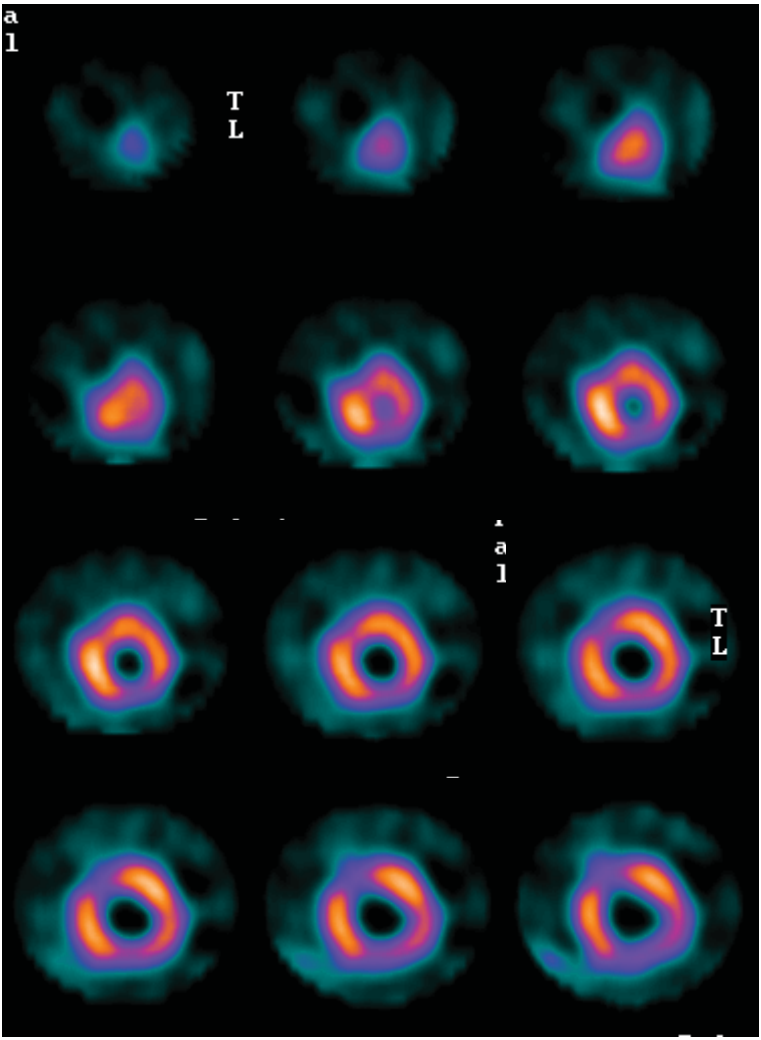

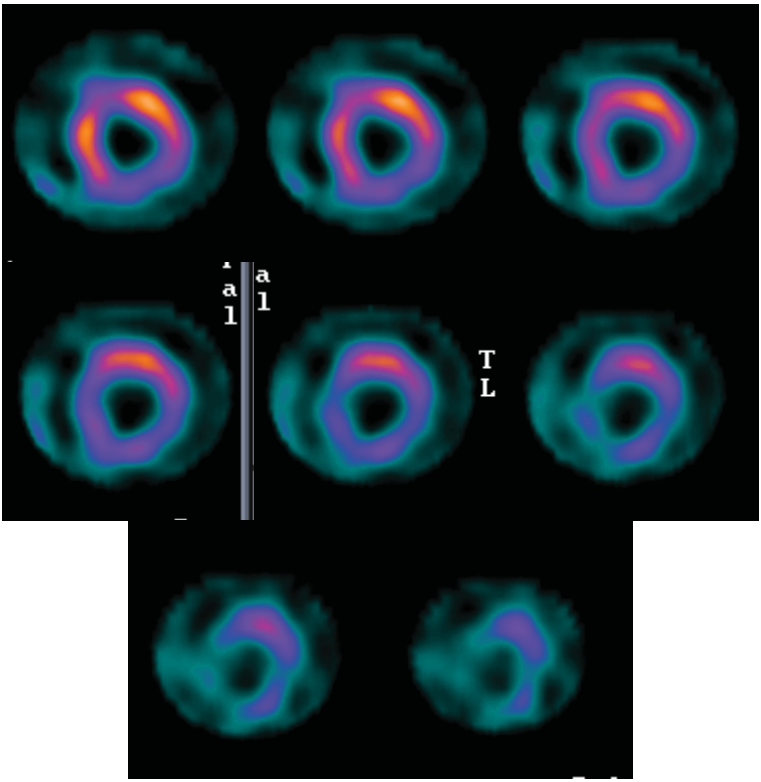

Figure 5.14: Scintigraphic issues of actual sequence images during a resting state.

Step 6:

A phase of extraction of quantitative information is added to estimate the surface of the endocardium, the diameter of the latter and the thickness of the epicardial muscle.

V.3 Results

Figure 5.14 shows a real sequence of scintigraphic pictures during the resting phase. Next, Figure 5.15 provides the segmented images based on the method described above. Each segmented image shows the inner contour representing the endocardium and the outer contour representing the epicardium.

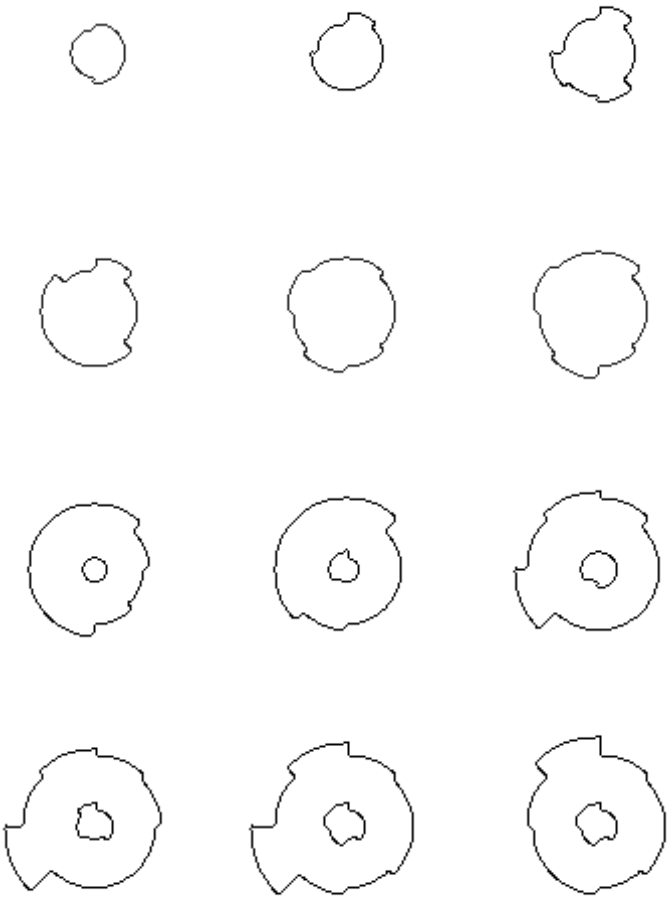

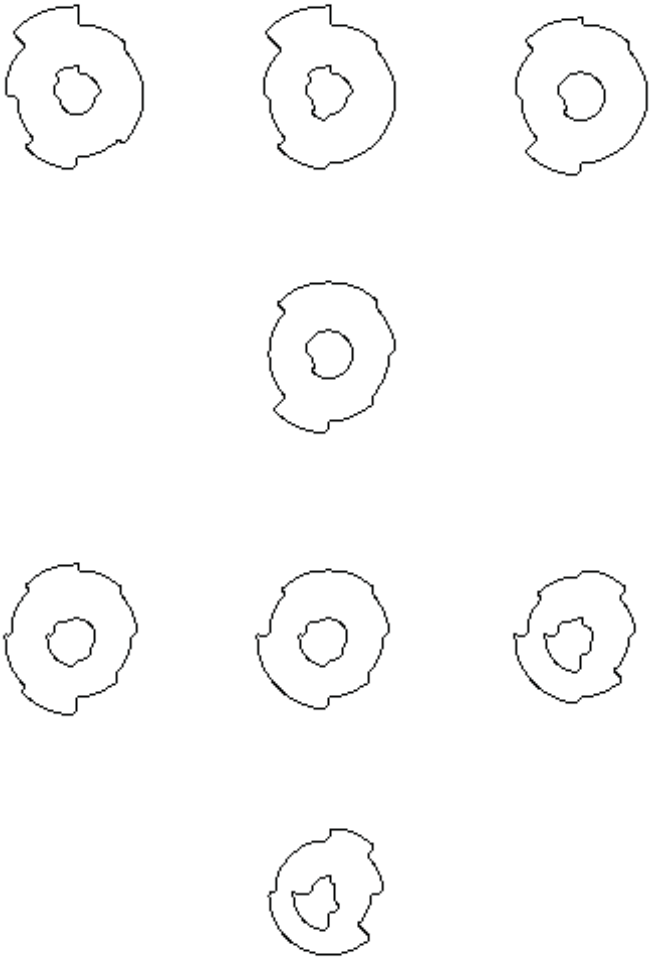

Figure 5.15: Segmented scintigraphic images during a state of rest. The inner contour represents the endocardium and the outer contour represents the epicardium.

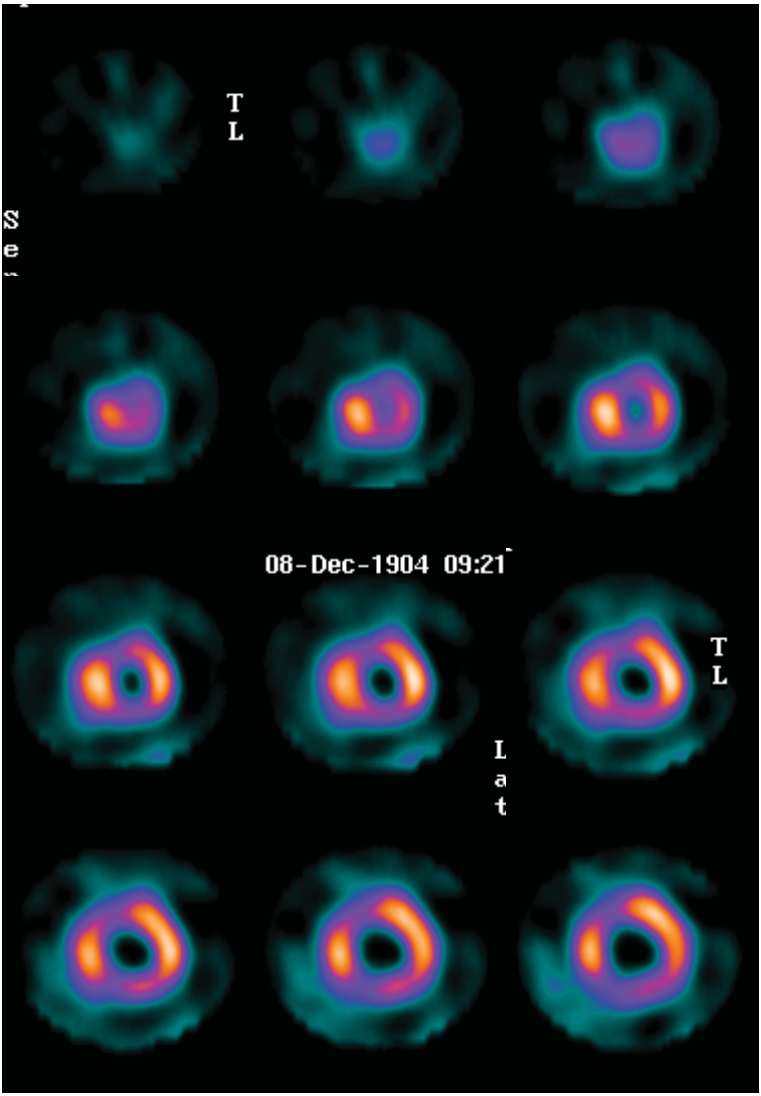

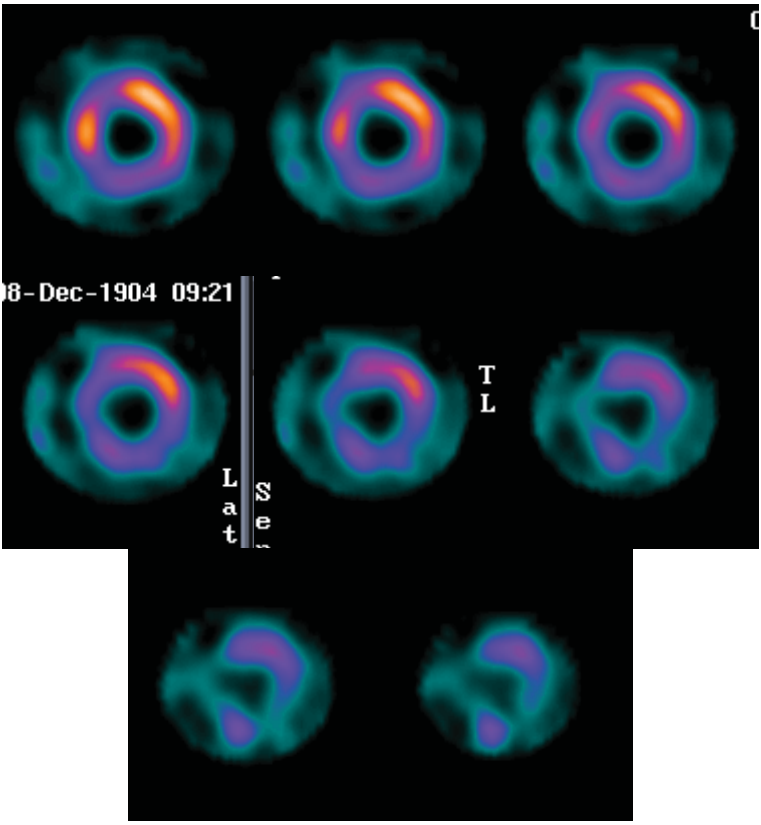

Figure 5.16: Scintigraphic actual sequence images during a state of stress.

Figure 5.16 represents a real sequence of scintigraphic pictures during a state of stress. Next, Figure 5.17 provides the segmented images based on the method described above. Each segmented image shows the inner contour representing the endocardium and the outer contour representing the epicardium. Figure 5.18 represents a sample of scintigraphic images segmented based on the algorithm of Snakes [Gun'02].

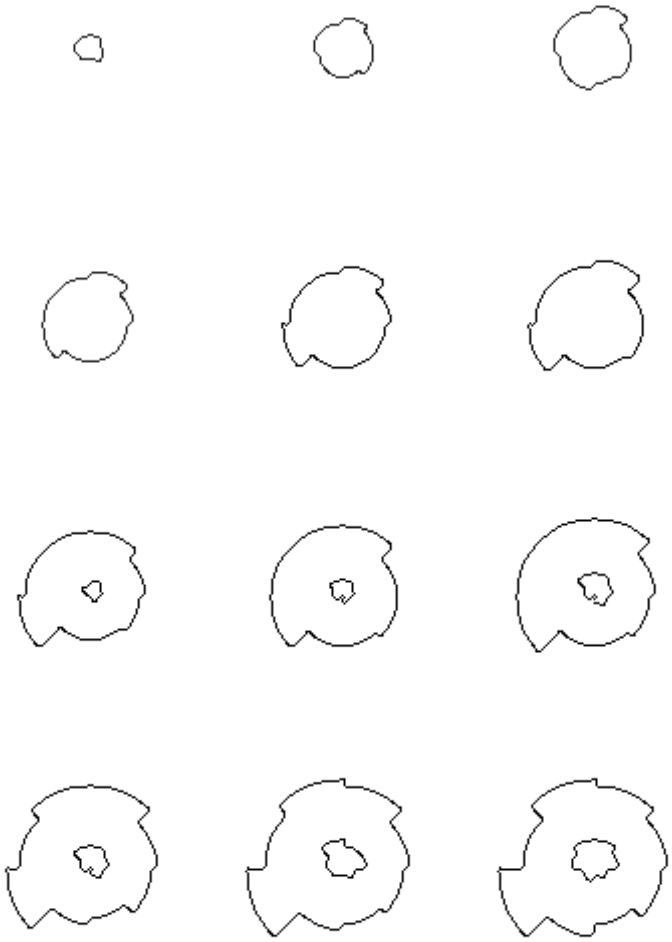

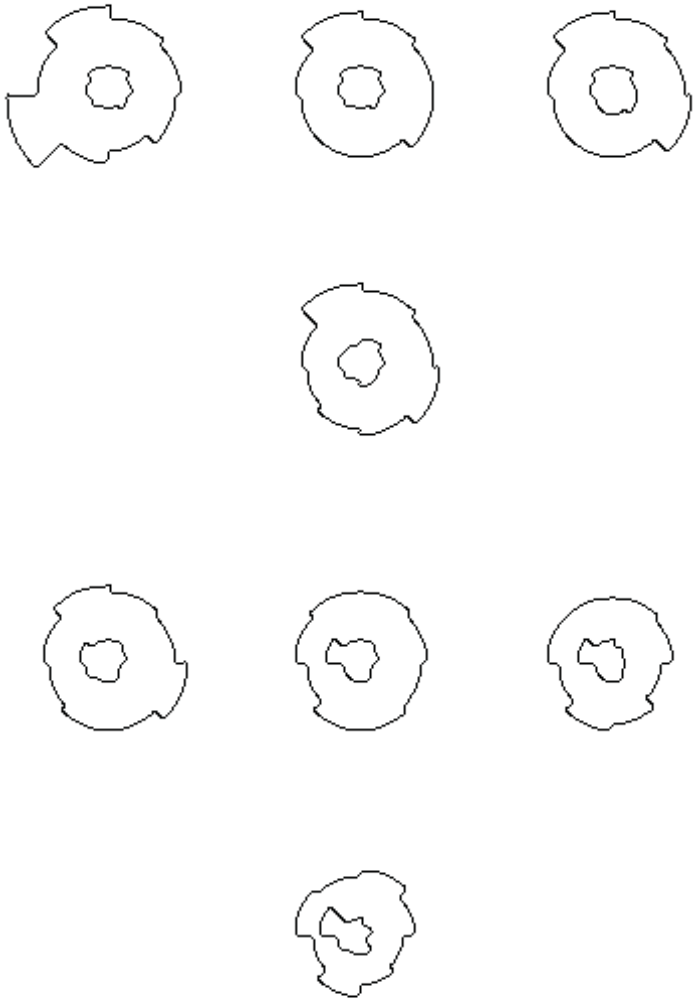

Figure 5.17: Segmented scintigraphic images during a state of stress. The inner contour represents the endocardium and the outer contour represents the epicardium.

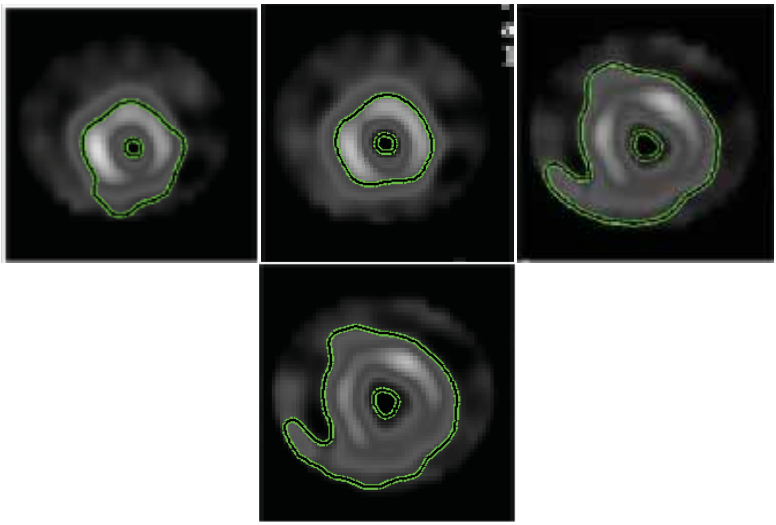

Figure 5.18: Segmented scintigraphic images based on algorithm of Snakes [Gun'02].

V.4 Endocardium area and muscle thickness estimation

In this part, note that the endocardium and the epicardium are assimilated to two superimposed circles with a common center O (xo, yo). The analyzer represents the endocardium and the epicardium by UL1 and UL2, respectively.

Indeed, the following mathematical equations allow us to estimate the surface of this the endocardium, and the area is the endocardial and muscle thickness epicardial:

$$Area_{\ endocardium}(mm^2) = \|UL1\| * r^2 * \alpha^2 \qquad (5.34)$$

where r is the radius of the sector measured in pixels during the step of dividing into sectors, and α is the dimension of a pixel measured in *mm*.

Practically $\alpha = 0.264583333\ mm$.

$$Ray_{\ endocarde} = \sqrt{surface_{\ endocarde} / \pi} \qquad (5.35)$$

$$Area_{\ epicardium\ muscle}(mm) = \|UL2\| * r^2 * \alpha^2 \qquad (5.36)$$

$$Thickness_{\ epicardium\ muscle} = \sqrt{(Area_{\ endocardium} + Area_{epicardium\ muscle})/\pi} - \sqrt{Area_{endocardium}/\pi} \quad (5.37)$$

Table 5.4 provides a numerical estimate of the surface of the endocardium in mm², the diameter of the endocardium and the muscle thickness epicardial in mm for both a patient during a load condition and during a state of rest, respectively.

During a state of stress, the method described above provides an estimate of the surface area of the endocardium with an average precision value of around 0.66 mm². For an endocardial diameter, the accuracy of the average value is in the order of 0. 04 mm and the muscle thickness epicardial is estimated with a value of 0.77 mm.

Table 5.4: Estimating the area of endocardium, diameter of endocardium and muscle thickness epicardium during state of stress.

	Area real of endocardium (mm^2)	Area of the endocardium (mm^2)	Diameter of the endocardium (mm)	Muscle thickness epicardium (mm)
Image 1	-	-	-	1.59
Image 2	-	-	-	2.10
Image 3	-	-	-	2.45
Image 4	-	-	-	2.75
Image 5	-	-	-	3.18
Image 6	-	-	-	3.18
Image 7	8.82	10.40	3.64	3.58
Image 8	8.82	10.40	3.64	4.22
Image 9	18.90	17.19	4.68	4.41
Image 1 0	20.93	21.23	5.20	5.32

Image 11	24.92	25.68	5.72	5.94
I mage 12	24.92	25.68	5.72	6.08
Image 13	24.92	35.87	5.72	6.23
Image 14	24.92	35.87	5.72	6.30
Image 15	36.26	35.87	6.76	6.30
Image 16	36.26	35.87	6.76	6.41
Image 17	43.33	44.76	7.55	6.25
Image 18	43.33	44.76	7.55	6.47
Mean value of precision	0.66 mm²		0.04 mm	0.77mm

Table 5.5: Estimation of area of endocardium, diameter of endocardium and thickness of epicardial muscle during idle state.

	real area of endocardial (mm^2)	Area of the endocardium (mm^2)	Diameter of the endocardium (mm)	Muscle thickness epicardial (mm)
Image 1	-	-	-	0.77
Image 2	-	-	-	1.72
Image 3	-	-	-	1.72
Image 4	-	-	-	2.25
Image 5	-	-	-	3.13
Image 6	-	-	-	3.13
Image 7	7.84	7.64	3.12	3.42
Image 8	11.76	10.40	3.64	3.42
Image 9	16.31	13.58	4.16	4.08
Image 1 0	18.55	17.19	4.68	4.86

Image 11	20.51	21.23	5.20	5.58
I mage 12	22.96	24.68	5.61	5.67
Image 13	32.20	30.57	6.24	5.76
Image 14	32.20	30.57	6.24	5.76
Image 15	32.20	30.57	6.24	5.76
Image 16	32.20	30.57	6.24	5.97
Image 17	37.17	39.60	7.10	6.11
Image 18	37.17	39.60	7.10	6.11
Mean value of precision	1.67 mm²		0.09 mm	0.49 mm

During a state of rest, the method described above provides an estimate of the endocardium surface area with an average precision value of around 1.6 7 mm².

For an endocardial diameter, the accuracy of average value is in the order of 0.09 mm and the epicardial muscle thickness are estimated with a value of 0.49 mm.

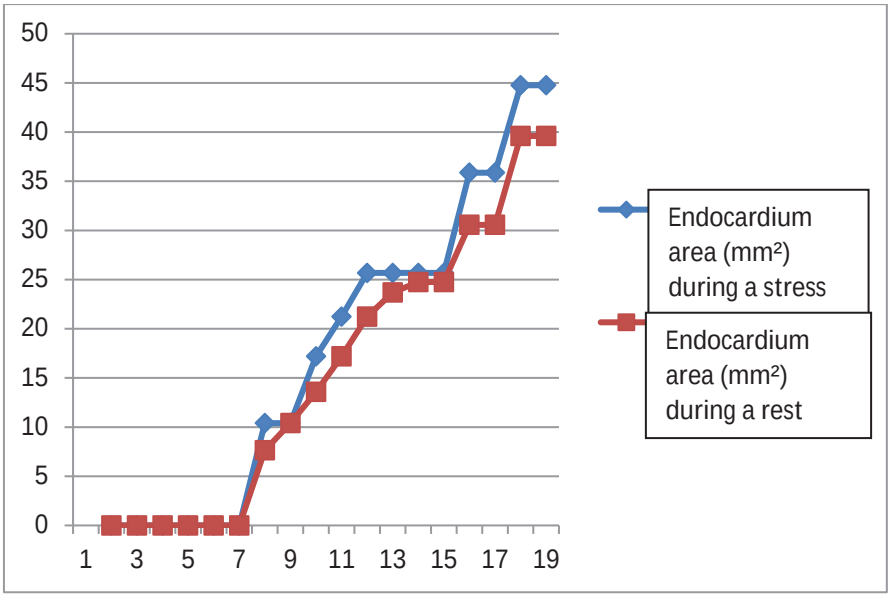

Figure 5.19: Variation in surface of endocardium (mm²) during rest state and state of stress.

Figure 5.19 shows the variation in the surface of the endocardium (mm²) during a rest state and a state of stress. Figure 5.19 confirms that the volume of the endocardium is more important to the state effort to the idle state. This indicates that during a phase of relaxation, the heart rate is much less important compared to that of a phase of effort.

V.5 3D Reconstruction of endocardium

A set of real scintigraphic images are segmented and we allow the 3D reconstruction of the endocardium during a phase of effort. Figure 5.20 represents the 3D reconstruction of the endocardium where images are

segmented respectively grammar (left) and manually (right) of a patient during a phase of effort.

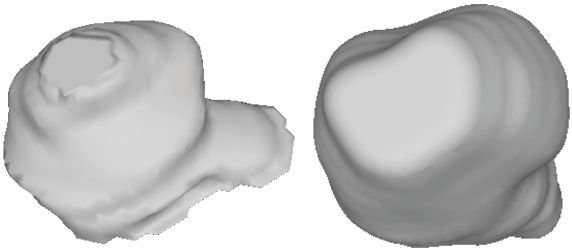

Figure 5.20: 3D reconstruction of endocardium where images are segmented respectively by grammar (left) and manually (right) during state of stress.

Figure 5.21: 3D reconstruction of endocardium where images are segmented by grammar during a resting state.

Figure 5.21 represents 3D endocardium reconstruction where images are segmented by the grammar of a patient during a resting state. One could conclude that the volume of the endocardium is greater in the state of effort than in the state of rest.

VI. Tomographic angiography (CTA) segmentation

Grammars current consider each symbol, not terminal or terminal, two attachment points: one left and one right. This part generalizes and creates an extension of existing grammars for the recognition of objects, called e grammar in two dimensions, taking into consideration that the symbols can be read according to two attachment points.

VI.1 CTA image alphabet

An image alphabet must be supported initially and must include all the elements that an image cannot contain. In this work, the proposed method is based on an alphabet of intensity noted A and generated by the histogram of the CTA image:

A = {a1, a2, ..., an}

The alphabet of the image represents the first important strengths. Here the user can manage the parameter n and select the number of elements that the alphabet A can contain.

VI.2 Operating mode

Step 1: Initialization of alphabet

Read the CTA input image and select the region of interest (ROI) to segment.

Generate the histogram of the ROI.

Select the number n of the most important intensities.

Initialize the terminal vocabulary A = {a1, a2, ..., an}.

Step 2: Quantification phase

The quantification step comprises rounding each pixel intensity value in the one closest belonging to A.

Step 3: Division into blocks

Divide the image into blocks having regular sizes, NxM pixels.

Calculate the dominant intensity of each block of pixels.

Therefore, an image corresponding to a matrix Q which contains elements belonging only to A.

$$Q = \begin{bmatrix} a1\ a1 & \cdots & a2\ a1\ a1 & \cdots & a2 \\ \vdots & \ddots & \vdots \quad \vdots & \ddots & \vdots \\ an\ an & \cdots & a1\ an\ an & \cdots & a1 \\ \cdots & \cdots & a2\ a1\ a1 & \cdots & a1 \\ \ddots & & \vdots \quad \vdots & \ddots & \vdots \\ a3\ an & \cdots & a3\ an\ an & \cdots & a1 \end{bmatrix}$$

Step 4: Lexical analysis

Perform a lexical analysis by scanning the resulting matrix Q according to a type of browse (row by row, column by column, Hilbert curve, Lebesgue curve,…) and extract the lexemes described by regular expressions.

Regular expressions rewrite every token of a language and model and its structure. Grammatically, each regular term ERi can be formulated as follows where the character "+" means "one or more times":

ERi = { a $_i$ } + where i ∈ { 1, ..., n }.

VI.2.1 Different ways of browsing the image

It must be noted that in step 4, we could apply other course manners such as those of Hilbert, Moore, Sierpinsky or Lebesgue (Figure 5.22).

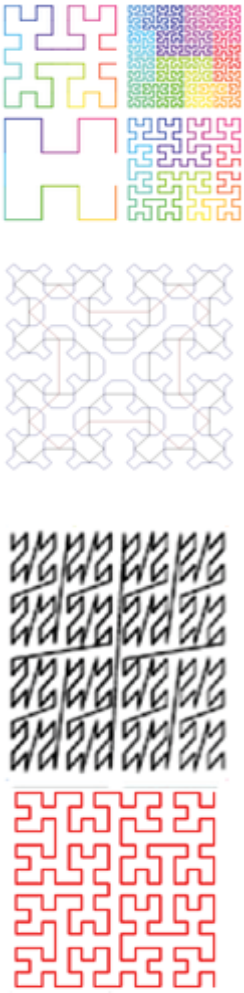

Figure 5.22: Different ways of transforming 2D to 1D. (a) Hilbert, (b) Lebesgue, (c) Sierpinsky, (d) Moore

VI.2.2 Hilbert transform

David Hilbert (1862-1943) was a German mathematician [Hil'91]. Its curve was studied in 1891.

The Cartesian parameterization of the Hilbert curve is defined by induction according to the following algorithm:

Algorithm

The Hilbert transform is described by the following algorithm:

1) Divide [0, 1] 2 into 4 equal squares.

2) Number each square so that two successive square touch at one side, starting with the lower left square, and ending with the lower right square.

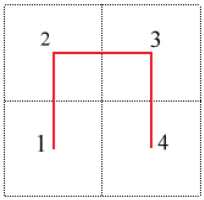

Figure 5.23: order Hilbert Matrix 1

3) Partition each of these squares into 4 equal squares.

4) Number each square so that two micro square successive touch at one side, starting with the micro-square on the bottom left, and ending with micro-square at the bottom right, the first micro-square of a small square that must have one side in common with the last micro-square of the previous small square and the last micro-square that must touch the following small square on one side.

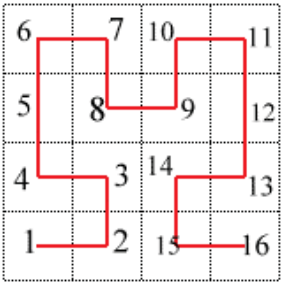

Figure 5.24: Hilbert matrix of order 2

5) Repeat this process ad infinitum.

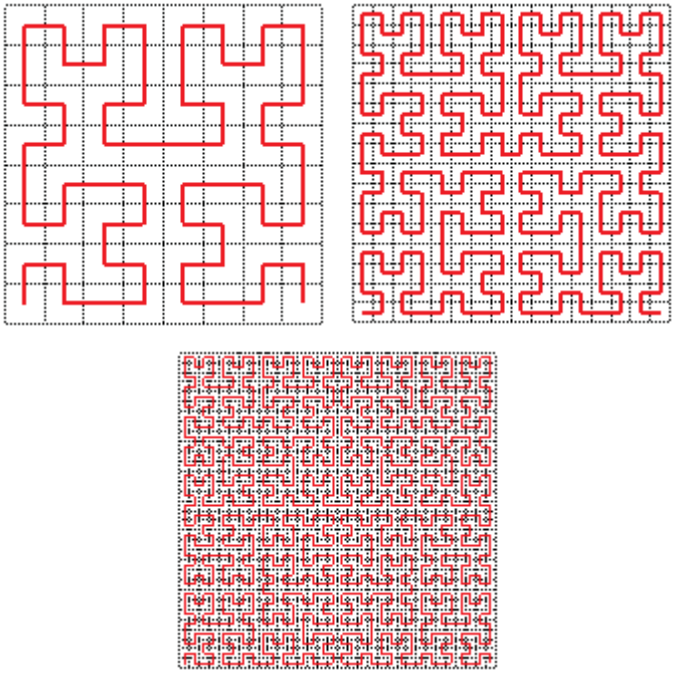

Figure 5.25: Hilbert matrices of orders 3, 4 and 5

Table 5.6 shows a comparison between different ways of scanning and the course of the matrix resulting Q. For each image, one determines the number of objects detected. Therefore, browsing row by row or column by column results in over-segmented images. Indeed, the application of the transformation of Hilbert or of Lebesgue avoids a little the phenomenon of over- segmentation, but the images are always over-segmented.

Indeed, we have thought of making a 2D course. In this case, each lexeme is a tuple (x, y, s, I) characterized by a pair (x, y) and two natural integers l and I. Couple (x, y) is space of coordinates of the first symbol, parameter l is the length of the recognized lexeme and I is the intensity. The current step is to specify the accepted lexical units from the input matrix.

The recognized entities are called tokens: $UL_{x, y, w, i.}$ The lexical analyzer is invited to analyze the resulting matrix and extract unites ed lexical recognized $UL_{x, y, w, i.}$

Table 5.6: Application on synthetic images and determination of objects detected for each way of 1D traversal.

		Image 1	Image 2	Image 3	Image 4	Image 5	Image 6	Image 7	Image 8	Image 9	Image 10
Objects	Row-by-row scan	61	34	71	106	127	209	75	71	48	105
	Column-by-column scan	34	15	60	157	132	196	84	60	59	138
	Hilbert scan	23	14	56	112	91	125	52	63	46	88
	Lebsegue scan	18	10	53	105	80	114	49	53	41	98

Step 5: Syntax analysis

The current syntax analyzer does not allow a proper analysis of this type of grammar as recognized dimensional tokens, which are distributed in a 2D space and depend on (x, y), whereas analyzers today are one-dimensional. Therefore, the fundamental contribution is manifested in the development of a two-dimensional analyzer able to verify the arrangement of the regions R i distributed in 2D space, while respecting the rules and the criterion of homogeneity *hc*:

The grammar used is *G = (VT, VN, S, P)* where:

$VT = \{ UL_{xj, yj, lj, Ij, j} > = 1\}$
$VN = \{ R_{i,} i > = 1\}$
$S = Image$
$Image \rightarrow$
$R_i \rightarrow UL_{x1, y1, l1, I1} . UL_{x2, y2, l2, I2} \ldots UL_{xj, yj, lj, Ij} \ldots UL_{xn, yn, ln, In}$
where:

$$|xj - xj - 1| \leq 1 \quad (5.38)$$

$$yj - 1 + lj - 1 \geq yj \quad (5.39)$$

$$yj + lj \geq yj - 1 \quad (5.40)$$

$$|lj - 1 - lj| \leq hc \quad (5.41)$$

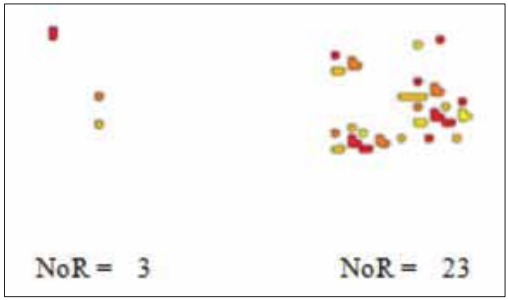

Figure 5.26: Application on synthetic images. Each time, one determines the number of detected objects.

Table 5.7: Application on synthetic images and determination of the objects detected for each way of 1D and 2D traversal.

Number of regions (NoR)		Image 1	Image 2	Image 3	Image 4	Image 5	Image 6	Image 7	Image 8	Image 9	Image 10	Image 11	Image 12
One-dimensional parser	Row by row scan	61	45	71	106	127	209	75	71	48	105	104	126
	Column by column scan	34	15	60	157	132	196	84	60	59	138	111	135
	Lebesgue transform	23	14	56	112	91	125	52	63	46	88	88	112
	Hilbert transform	18	10	53	105	80	114	49	53	41	98	68	82
Two-dimensional parser		1	1	3	1	3	23	3	2	4	4	1	1

Table 5.7 confirms that 2D scanners have enabled us to merge a maximum number of regions and better avoid the phenomenon of over-segmentation. The method has been applied to synthetic images, some of which are shown in Figure 5.26.

VI.3 Results

A set of real 80 tomographic angiographic images (CTA) are segmented. In addition, the experimental results allow the 3D reconstruction of the carotid artery.

Figure 5.2 7 shows a sample of segmented ROI using the grammar in two dimensions.

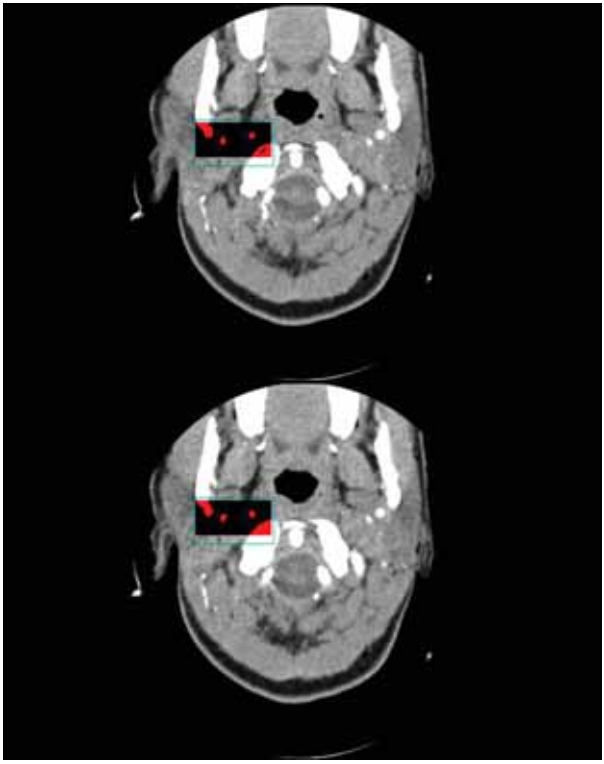

Figure 5.27: Sample of actual CTA images where regions of interest (ROI) have been segmented.

VI.4 3D reconstruction and Hausdroff distance

V I.4.1 Hausdroff distance

The Hausdorff Distance (HD) is a metric of comparison two forms. It is a topological tool that measures the distance of two subsets from an underlying metric space.

Mathematically, for two finite sets of points s M = {m1, m2, ..., mp } representing a pattern in the data set and T = {t1, t2, ..., tq } representing an image of test, the Hausdorff distance is defined as:

$$HD(M,T) = \max\left(d(M,T), d(T,M)\right) \tag{5.42}$$

where:

$$d(M,T) = max_{m_i \in M} min_{t_j \in T} \left\| m_i - t_j \right\| \tag{5.43}$$

For a certain number of points P in M, we denote the HD as:

$$d(M,T) = \frac{1}{P} \sum_{m_i \in M} \; min_{t_j \in T} \left\| m_i - t_j \right\| \tag{5.44}$$

Figure 4 2 8 shows a comparison between the 3D reconstruction of the carotid artery where the ROIs are segmented by the grammar (left) and the segmentation process to hand (to right).

Practically, the Hausdroff distance shown in Figure 5.27 is 0.010430.

VI.4.2 Quality Mapper

With the colors of mapmaker quality (Quality Mapper), it is possible to see where there are large differences in the distance in a very simple manner.

The distances have a color tending towards red, while the peaks which are very close are blue, intermediate values are defined by a color gamut (Figure 5.29). Major distances have a color that tends towards red; while the distances which are very close are colorful blue.

The color quality levels are constructed from a transfer function and color vertices of the mesh. The minimum values of quality, average and maximum can be defined by the user to get a personalized quality range for cartographer.

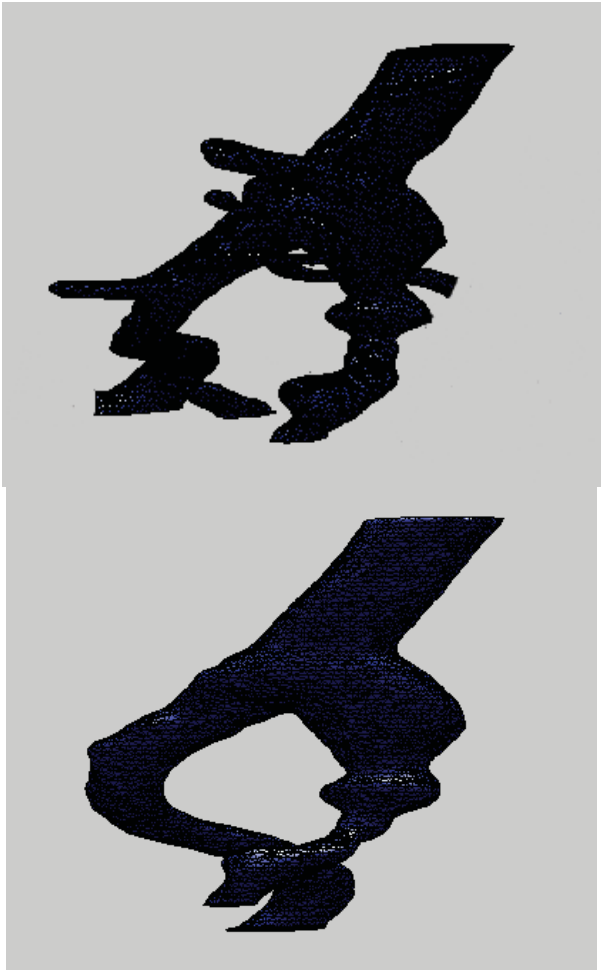

Figure 5.28: 3D reconstruction of carotid artery with images segmented by grammar (left) and manually (right), respectively. Hausdroff distance = 0.010430.

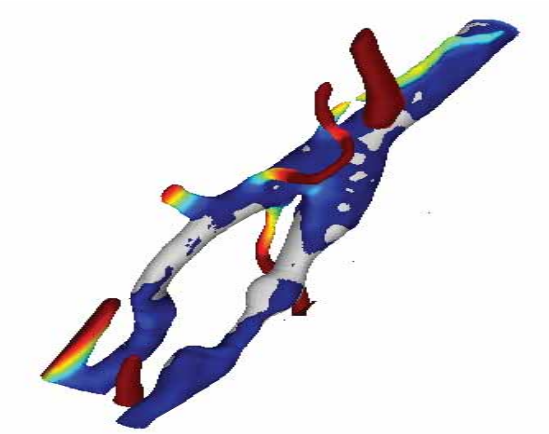

Figure 5.29: Cartographer quality color (Quality Mapper). The major differences have a color that tends towards red, while differences that are very close are colored in blue.

VII. Conclusions

In this chapter, we have studied different methods of segmentation of 2D medical images based on grammatical formalism. The grammar has been widely used for pattern recognition in medical images. The context-free grammar and graphs AND-OR have been used by more than a few research groups. Most applications focus on object recognition and the image segmentation. The first advantage concerns the more concise representation that grammars can provide. In addition, the syntactic approach can powerfully represent pattern structures and thus facilitate the search for medical images by means of their structures.

This chapter is a comprehensive overview of the art grammatical methods for the processing of medical images. This is a very current area of research, since most of the studies found have been published in the last decade. In addition, we can note that this line of research is very promising, since most of the articles studied have shown a recognition rate of over 90%.

In a first part, we have presented an overview on the use of syntactic methods for pattern recognition in the medical image. For this, we have used a systematic process; the art methods and the techniques used have

been extracted from each study, the primitives used and the results obtained using grammars for learning the rules of grammar.

In a second part, we have applied a new method of segmentation of scintigraphic and angiographic images. We could conclude that during the application of our technique, the contours are known and well defined.

In a third part, we have applied a new method of segmentation of 2D CTA images based on grammar and using lexical and syntactic analyzers which are able to recognize lexemes distributed in 2D space and to verify their arrangement in the 2D space.

The advantage of the grammatical method concerns more concise representation that the grammars can provide. The approach can powerfully represent the pattern structures and thus facilitate the search for medical images through their structures. The input medical image is perceived as a structured scene with a hierarchy because the grammars can obviously describe hierarchical structures using their non-leaf nodes and terminals. In addition, Gao et al. [Gao'00] asserted that, compared to statistical methods, the use of grammar offers more flexibility in applications.

CHAPTER 6

CONCLUSION

The analysis of 1D and 2D medical data is a very active subject and several approaches have been proposed. In the 1D case, the electrocardiogram signal ECG is a test widely used in the field of cardiology. This signal represents the electrical activity of the heart and is of great clinical added value for diagnosing one of the different types of arrhythmias. Generally, cardiac pathologies are indicated by disturbances in the electrical activities of the heart.

In this thesis work, we approached the problem of automatic processing of medical signals and images through the grammatical formalism of type 3 and type 2. This thesis includes two fundamental modules: a 1D module which applies to the signal ECG for the extraction of QRS complexes and recognition of cardiac cycles. A second 2D medical image segmentation module is applied to scintigraphic images and tomographic images.

In the 1D module for extracting ECG characteristics, an algorithm for detecting QRS complexes from the ECG signal by an approach based on regular grammar has been developed. It makes it possible to extract representative parameters of each heartbeat.

We have extended the database of ECG signals to apply the method on the standard MIT-BIH base as well as signals from the CHU Sahloul university hospital to have a balanced number between the types of signals, to include other types and varieties of signals and to increase the quality of learning.

Also, in the cardiac cycles characterization module, we have improved the capacity of the algorithm for detecting QRS complexes and delimiting P and T waves for the measurement of different segments and intervals such as RR distance, interval QT, the corrected QTc interval, the PQ interval and the ST segment. Thus, these parameters allow a representative characterization, relevant and closer to the medical language of heart beats to improve the quality of the diagnosis. The characterization of ECG signals by relevant indicators forms an essential step to have a better

classification of normal and pathological cases. In addition, we have added two parameters: σRR and σQRS. These standard deviation parameters reflect the regularity of RR distances and QRS durations.

The evaluation of the algorithms implemented allowed us to appreciate good detection rates of QRS complexes and P and T waves for normal and pathological cases affected by different types of noise. The results obtained showed that the proposed method can be considered as an effective tool for the detection of cardiac arrhythmias with a very tolerable precision of more than 99.74%.

In the 2D module of segmentation of scintigraphic images, we have chosen lexical and syntactic analyzers which rotate along a spiral path from the interior to the exterior and extract the homogeneous regions according to a criterion of homogeneity set by the user. The contours of the endocardium and epicardium are thus detected and a quantification of the mass of the myocardial muscle is obtained.

We have defined a scintigraphic image as a set of lexemes based on a vocabulary of intensities and a set of grammatical rules. The results obtained showed that the proposed method can be considered as an effective tool for the delineation of the endocardium and epicardium. In addition, some of the quantitative information allowed us to estimate the area of the endocardium, the thickness of the epicardial wall.

For the Agiographic Tomographic Image Segmentation (CTA) module, the lexical analysis step consists of specifying the accepted lexical units from the input image. The recognized entities are called lexemes. In the 2D case, each lexeme is a quadruplet. The lexical analyzer is invited to analyze the obtained matrix and extract the recognized lexical units. Therefore, the fundamental contribution is manifested in the development of a two-dimensional analyzer to verify the arrangement of lexemes distributed in 2D space which respect the rules and the criterion of homogeneity. Virtually a set of 80 real CTA images were segmented on the basis of grammar. The experimental results allow rendering the 3D reconstruction of the carotid artery.

Compared to statistical methods, the use of grammars offers more flexibility in applications. Grammatical rigor has been extended to include other areas of application such as signaling and medical imaging. The main advantage of these methods concerns the representation that it can

make available. Syntactic approaches can powerfully represent object structures and therefore make it easy to retrieve information.

Finally, grammatical formalism has proven its effectiveness in the processing and interpretation of 1D and 2D medical data. This type of work is intended for aid in medical diagnosis.

REFERENCES

A

[Afo'99] Afonso V., Tompkins W., Nguyen T., Shen, L., ECG beat detection using filter banks, IEEE Transactions on Biomedical Engineering, 46 (2), pp 192-202, 1999.

[Arz'06] Arzeno N.M., Poon C. S., Deng, Z. D., Quantitative analysis of QRS detection algorithms based on first derivative of the ECG, IEEE EMBS annual international conference, 18, pp. 1788–1791, 2006.

[Ayt'99] Aytemir K., Maarouf N., Gallagher M. M., Yap Y. G., Waktare J. E.P., Malik M., Comparison of Formula for Heart Rate Correction of QT Interval in Exercise Electrocardiograms, Pacing and Clinical Electrophysiology, 22 (9), pp 1397-401, 1999.

B

[Bal'09] Balasubramaniam D., Nedumaran D., Implementation of ECG Signal Processing and Analysis Techniques in Digital Signal Processor based System, IEEE International Workshop on Medical Measurements and Applications, 2009.

[Bar'98] Barro S., Fernandez M., Classifying multi-channel ECG patterns with adaptive neural network, IEEE Engineering in Medicine and Biology Magazine., 17 (1), pp 45–55, 1998.

[Ben'01] Benitez, D., Gaydecki, P. A., Zaidi, A., Fitzpatrick, A. P., The use of Hilbert transform in ECG signal analysis, Computers in Biology and Medicine, 31 (5), pp 399–406, 2001.

[Ben'03] Benzid R., Marir F., Boussaad A., Benyoucef M., Arar D., Fixed percentage of wavelet coefficients to be zeroed for ECG compression, IEEE Electronics Letters, 39 (11), pp 830-831, 2003.

[Ben'09] Benali R., Chikh M.A., Neuro fuzzy classifier for cardiac arrythmias recognition, Journal of Theorrtical Applied Information & Technology, 5 (5), pp 577-583., 2009

[Ben'10] Benali R., Dib N., Reguig B. F., Cardiac Arrhythmia Diagnosis Using a Neuro-Fuzzy Approach, Journal of Mechanics In Medicine and Biology, 10 (3), pp 417–429, 2010.

[Ben'12] Benali R., Reguig B. F., Hadj Slimane, Z., Automatic Classification of Heartbeats Using Wavelet Neural Network, Journal of Medical Systems, 36 (2), pp 883-892, 2012.

[Ber'08] Bernd J.P., Hans F. W., Martin S.J., Latest advances in molecular imaging instrumentation, Journal of Nuclear Medicine, 49 (2), pp 5-23, 2008.

[Bor'96] Giovanni B., Christian B., Sergio F., Possibilities of Using Neural Networks for ECG Classification, Journal of Electrocardiology, 29 (1), pp 10-16, 1996.

[Bor'05] Borries R. F., Pierluissi H. J., Nazeran H., Wavelet Transform Based ECG Baseline Drift Removal for Body Surface Potential Mapping, Annual Conference on Engineering in Medicine and Biology, 27, pp 3891–3894, 2005

[Bro'98] Brohet C., Electrocardiogramme 12 dérivations, Edition Masson, Paris, 1998.

[Bul'02] Bultheel A., Wavelets with applications in signal and image processing, Edition Citeseerx, 2006.

C

[Coa'90] Coast D.A., Stern R.M., Cano G.G., Briller S.A., An approach to cardiac arrhythmia analysis using hidden Markov models, IEEE Transactions on Biomedical Engineering, 37 (9), 826–836, 1990.

[Cab'08] Cabasson A., Meste O., Time Delay Estimation: A New Insight Into the Woody's Method, IEEE Signal Processing Letters, 15 (1), pp 573-576, 2008.

[Cey'07] Ceylan R., Ozbay Y., Comparison of FCM, PCA and WT techniques for classification ECG arrhythmias using artificial neural network, Expert Systems with Applications, 33 (2), 286–295, 2007.

[Cha'04] Chazal P., Maraia O. D., Richard B.R., Automatic Classification of Heartbeats Using ECG Morphology and Heartbeat Interval Features,

IEEE Transactions on Biomedical Engineering, 51 (7), pp 1196-1206, 2004.

[Cha'09] Chalabi Z., Boudjzmaoui A., Saadia L., Berrached N., Détection et Classification Automatiques d'Arythmies Cardiaques, Sciences of Electronic, Technologies of Information and Telecommunications, 5, 2009.

[Che'01] Chevalier P., Rodriguez C., Bontemps L., Miquel M., Kirkorian G., Rousson R., Potet F., Schott J. J., Baro I., Touboul P., Non-invasive testing of acquired long QT syndrome: evidence for multiple arrhythmogenic substrates, Cardiovasc. Res., 50 (2), 386–398, 2001.

[Che'01] Cherkassky V., Kilts S., Myopentential Denoising of ECG Signals Using Wavelet Thresholding Methods, Neural Network, 14 (8), 2001.

[Che'06] Chen S. W., Chen C. H., Chan H. L., A real-time QRS detection method based on moving-averaging incorporating with wavelet denoising, Computer Methods and Programs in Biomedicine, 82 (3), pp 187–195, 2006.

[Chi'06a] Chia-Hung L., Classification Enhancible Grey Relational Analysis for Cardiac Arrhythmias Discrimination, Medical & Biological Engineering & Computing, 44 (4), pp 311-320, 2006.

[Chi'06b] Chia-Hung L., Chia-Hao W., Adaptive Wavelet Networks for Power Quality Detection and Discrimination in a Power System, IEEE Transactions on Power Delivery, 21 (3), pp 1106- 1113, 2006.

[Chi'08] Chia-Hung L., Yi-Chun D., Tainsong C., Adaptive Wavelet Network for Multiple Cardiac Arrhythmias Recognition, Expert Systems with Applications, 34 (4), pp 2601-2611, 2008.

[Cho'07] Chouhan S., Mehta S. S., Total Removal of Baseline Drift from ECG Signal, presented at Computing: Theory and Applications, International Conference on Computer Theory and Application, 7, 2007.

[Cho'12] Chouakri S.A., Bereksi-Reguig F., Taleb-Ahmed A., QRS complex detection based on multiwavelet packet decomposition, Applied Mathematics and Computation, 217 (23), pp 9508–9525, 2011.

[Chr'04] Christov I., Real time electrocardiogram QRS detection using combined Adaptive Threshold, BioMedical Engineering Online, 3 (28), 2004.

[Chr'06] Christov, I., Herrero, G. G., Krasteva, V., Jekova, I., Gotchev, A., & Egiazarian, K., Comparative study of morphological and timefrequency ECG descriptors for heartbeat classification, Medical Engineering and Physics, 28 (9), pp 876–887, 2006.

[Chr'96] Christensen H. I., Matas J., Kittler J., Using Grammars for Scene Interpretation, IEEE Transactions on Image Processing, 3 (1), pp 793-796, 1996.

[Chu'89] Chu C. H. H., Delp E. J., Impulsive noise suppression and background normalization of electrocardiogram signals using morphological operators, IEEE Transactions on Biomedical Engineering, 36 (2), pp 262-273, 1989.

[Chu'06] Chuang K. S., Tzeng H. L., Wu S. Chen, J., T.J., Fuzzy c-means clustering with spatial information for image segmentation, Computerized Medical Imaging and Graphics, 30 (1), pp 9–15, 2006.

[Com'05] Comas L., Modéles et algorithmes pour la scintigraphie cardiaque, Thése de l'Université de Sciences et de Techniques de Franche-Comté, Décembre 2005.

D

[Dal'07] Dale D., Lecture accélérée de l'ECG, MALOINE, 2007.

[Das'99] Daskalov, I., Christov, I., Electrocardiogram signal preprocessing for automatic detection of QRS boundaries, Medical Engineering & Physics, 21 (1), pp 37-44, 1999.

[Deb97] DeBakey M. E., Le coeur en action, Edition Sanofi-Synthelabo, 1997.

[Dib'09] Dib N., Bereksi R. F., Analyse du signal ECG en vue des ondes P, QRS, T, le segment ST et intervalle QT, Thèse, université de Tlemcen, 2009.

[Dib'11] Dib N., Benali R., Hadj S. Z., Bereksi R. F., Delineation of the complex QRS and the t-end using wavelet transform and surface indicator,

IEEE International Workshop on Systems, Signal Processing and their Applications (WOSSPA), 7, pp 83-86, 2011.

[Din'02] Dinh A. N., Kumar D. K., Burton P., Wavelet for QRS detection, IEEE Engineering in medicine and Biology society, 23, pp 7803–7211, 2002.

[Don'95] Donoho D., De-noising by sof-thresholding, IEEE Transactions on Information Theory, 41 (3), pp 613 – 627, 1995.

[Dub'04] Dubois R., Application des nouvelles méthodes d'apprentissage à la détection précoce d'anomalies en électrocardiographie, Thèse de doctorat en électronique, soutenue à l'université Paris 6, le 27 Janvier 2004.

[Duv'02] Duverney D., Gaspoz J.M., Pichot V., Roche F., Brion R., Antoniadis A., Barthelemy J. C., High accuracy of automatic detection of atrial fibrillation using wavelet transform of heart rate intervals PACE, 25 (4), pp 457–462, 2002.

E

[Ein'88] Einthoven W., Ershler I., The man. The string galvanometer electrocardiograph, Arch. Intern. Med., 148 (2), 453-455, 1988.

[Eng'04] Engin M., ECG beat classification using neuro-fuzzy network, Pattern Recognition Letters, 25 (15), pp 1715–1722, 2004.

F

[Fis'02] Fischbach M., Guide pratique du cardiaque : prévention et suivi, Edition Frison-Roche, 2002.

[Fla'10] Flasinski M., Jureket J., Myśliński S., Parallel Computing Scheme for Graph Grammar-Based Syntactic Pattern Recognition, Conference on Parallel Processing and Applied Mathematics, 8, pp 156-165, 2010.

[Fra'80] Fraden J., Neumann M.R., QRS wave detection, Medical and Biological Engineering and Computing, 18 (2), pp 125–132, 1980.

[Fur'83] Furno G. S., Tompkins W. J., A learning filter for removing noise interference, IEEE Transactions on Biomedical Engineering, 30 (4), pp 234-235, 1983.

G

[Gao'00] Gao J., Ding X., Zheng J., Image pattern recognition based on examples—A combined statistical and structural-syntactic approach, Lecture Notes in Computer Science, 1876, pp 57–66, 2000.

[Gha'08] Ghaffari A., Golbayani H., Ghasemi M., A new mathematical based QRS detector using continuous wavelet transform, Computers & Electrical Engineering, 34 (2), pp 81–91, 2008.

[Gho'09] Ghoggali N., Melgani F., Bazi Y., A multiobjective genetic SVM approach for classification problems with limited training samples, IEEE Transactions on Geoscience and Remote Sensing, 47 (6), pp 1707–1718, 2009.

[Gol'42] Goldberger E., A simple, indifferent, electrocardiographic electrode of zero potential and a technique of obtaining augmented, unipolar, extremity leads, American Herat Journal, 23 (4), pp 483-92, 1942.

[Gra'00] Gramatikov B., Brinker J., Yi-chun S., Thakor N. V., Wavelet analysis and time-frequency distributions of the body surface ECG before and after angioplasty Computer Methods and Program in Biomedicine, 62 (2), pp 87–98, 2000.

[Gri'98] Gritzali F., Towards a generalized scheme for QRS detection in ECG waveforms, Signal Process; 15 (2), pp 183–192, 1998.

[Gun'02] Gunn S. R., Nixon M. S., A robust snake implementation; a dual active contour, IEEE Transactions on Pattern Analysis and Machine Intelligence, 19 (1), pp 63-68, 2002.

[Guo'12] Guowei W., Andrei S., Grammar-based 3D facade segmentation and reconstruction, Computers & Graphics, 36 (4), pp 216-223, 2012.

H

[Had'10] Hadj S. Z., Nait A. A., QRS complex detection using Empirical Mode Decomposition, Elsevier J. Digital Signal Processing, 20 (4), pp 1221–1228, 2010.

[Ham'86] Hamilton P. S., Tompkin W.J., Quantitative investigation of QRS detection rules using MIT/BIH Arrhythmia database, IEEE Transactions on Biomedical Engineering, 33 (12), pp 1157–1165, 1986.

[Ham'04] Hampton J. R., L'ECG Facile, Sixième édition, EDISEM, Maloine, 2004.

[Han'15] Hanieh L.M., Fardin A.M., Abdolhossein F., A Novel Grammar-Based Approach to Atrial Fibrillation Arrhythmia Detection for Pervasive Healthcare Environments, Journal of Computing and Security, 2015, 2, pp 155-163.

[Har'96] Hartmut D., Hartmut H., Classifying Biosignals with Wavelet Networks-A Method for Noninvasive Diagnosis, IEEE Engineering in Medicine and Biology, 15 (5), pp 103-111, 1996.

[Has'06] Hassanpour H., Parsaei A., Fetal ECG Extraction Using Wavelet Transform, IEEE Computational Intelligence for Modelling, Control and Automation , pp 179-179, 2006.

[Her'05] Herman D., Théorie des Langages et Compilation, Livre, Version 1.0, Université de Rennes, 2005.

[Hil'91] Hilbert D., Über die stetige Abbildung einer Linie auf ein Flächenstück, Math. Ann., 38, pp 459-460, 1891.

[Hol'71] Holsinger W.P., Kempner K.M., Miller M.H., A QRS preprocessor based on digital differentiation, IEEE Transactions on Biomedical Engineering, 18 (3), 212-217, 1971.

I

[Ino'98] Inoue H., Miyazaki A., A noise reduction method for ECG signals using the dyadic wavelet transform, Institute of Information and Communication Engineers, 81 (6), pp 1001–1007, 1998

[Inc'09] Ince T., Kiranyaz S., Gabbouj M., A generic and robust system for automated patient-specific classification of ECG signals, IEEE Transactions on Biomedical Engineering, 56 (5), pp 1415–1426, 2009.

J

[Joh'15] John R.H., François J., L'ECG Facile, ELSEVIER / MASSON, 2ème edition, 2015.

K

[Kad'99] Kadambe, S., Murray, R. Boudreaux-Bartels, F., Wavelet transformbased QRS complex detector. IEEE Transactions on Biomedical Engineering, 47(7), pp 838-848, 1999.

[Kam'09] Kampouraki A., Manis G., Nikou C., Heartbeat time series classification with support vector machines, IEEE Transactions on Information Technology in Biomedicine, 13 (4), pp 512-518, 2009.

[Kha'09] Khandoker A. H., Palaniswami M., Karmakar C.K., Support vector machines for automated recognition of obstructive sleep apnea syndrome from ECG recordings, IEEE Transactions on Information Technology in Biomedicine, 13 (1), pp 37–48, 2009.

[Khe'07] Khelil B., Kachouri A., Ben Messaoud M., Ghariani H., P Wave Analysis in ECG Signals using Correlation for Arrhytmias Detection, International Multi Conference on Systems, Signals and Devices, 3, 2007.

[Kie'99] Kieffer J. C., Yang E. H., Grammar based codes: A new class of universal lossless source codes, IEEE Transactions on Information Theory, 46 (3), pp 737-754 1999.

[Kie'00] Kieffer J. C., Yang E. H., Efficient Universal Lossless Data Compression Algorithms Based on a Greedy Sequential Grammar Transform, IEEE Transactions on Information Theory, 49 (11), pp 2874 – 2894, 2003.

[Kir'09] Kiranyaz T, Gabbouj S. M., A generic and robust system for automated patient-specific classification of ECG signals, IEEE Transactions on Biomedical Engineering, 56 (5), pp 1415-1426, 2009.

[Koh'02] Kohler, B. U., Hennig, C. Orglmeister, R., The principles of software QRS detection, IEEE Engineering in Medicine and Biology Magazine, 21(1), pp 42-57, 2002.

[Kok'97] Kókai G. , Csirik J. , Gyimóthy T., Learning the syntax and semantic rules of an ECG grammar, Lecture Notes in Computer Science, 1321, pp 171-182, 1997.

[Kyr'88] Kyrkos A., Giakoumakis E. A., Carayannis G., QRS detection through time recursive prediction technique, Signal Processing, 15 (4), pp 429–36, 1988.

L

[Lag'92] Laguna P., Jane R., Caminal P., Adaptive Filtering of ECG Baseline Wander, IEEE Engineering in Medicine and Biology Society, 2 (1), pp 508-509, 1992.

[Lag'00] Lagerholm, M., Peterson, C., Braccini, G., Edenbrandt, L., Sörnmo, L., Clustering ECG complexes using Hermite functions and self organizing maps, IEEE Transactions on Biomedical Engineering, 47(7), pp 838–848, 2000.

[Lag'04] Pablo J. M., Almeida R., Olmos S.S, Rocha AP, Laguna P., A wavelet-based ECG delineator: evaluation on standard database, IEEE Transactions on Biomedical Engineering, 51, (4), pp 570–580, 2004.

[Lev'09] Levine J., Flex & Bison, Livre, Edition O'REILLY, 2009.

[Li'95] Li C., Zheng, C. Tai, C., Detection of ECG characterictic points using wavelet transforms, IEEE Transactions on Biomedical Engineering, 42 (1), pp 21-28, 1995.

[Li'00] Li G., Ye W., Ling L., An artificial intelligence approach to ECG analysis, IEEE Engineering in Medicine and Biology Magazine, 19 (2), pp 95–100, 2000.

[Lim'09] Lim J.S., Finding features for real time premature ventricular contraction detection using a fuzzy neural network system, IEEE Transactions on Neural Networks, 20 (3), pp 522–527, 2009.

[Lin'01] Link A., Endt P., Oeff M., Trahms L., Variability of the QRS in high resolution electrocardiograms and magnetocardiograms, IEEE Transactions on Biomedical Engineering, 48 (2), pp 133–142, 2001.

[Lin'03] Linh, T. H., Osowski, S., and Stodolski, M., On-line heart beat recognition using Hermite polynomials and neuro-fuzzy network, IEEE Transactions on Instrumentation and Measurement 52 (4), pp 1224–1231, 2003.

[Lu'00] Lu Z., Kim D. Y., Pearlman W. A., Wavelet compression of ECG signals by the set artitioning in hierarchical trees algorithm, IEEE Transactions on Biomedical Engineering, 47 (7), pp 849-856, 2000.

M

[Mal'89] Mallat S. G., A Theory for Multiresolution Signal Decomposition: The Wavelet Representation, IEEE Transactions on Pattern Analysis and Machine Intelligence, 11 (7), pp 674 – 693, 1989.

[Mar'00] Mark W. G., William D. E., Spect in the year 2000: basic principles, Journal of Nuclear Medicine Technology, 28 (4), pp 233-244, 2000.

[Mar'04] Martinez J. P., Aleida R., Olmos S., Rocha A. P., Laguna P., A wavelet-based ECG delineator: evaluation on standard databases, IEEE Transactions on Biomedical Engineering, 51 (4), pp570-581, 2004.

[Meh'08] Mehta S. S., Lingayat N. S., Development of SVM based classification techniques for the Delineation of wave components in 12-lead electrocardiogram, Biomedical Signal Processing and Control, 3 (4), pp 341–9, 2008.

[Mel'08] Melgani F., Bazi Y., Classification of electrocardiogram signals with support vector machines and particle swarm optimization, IEEE Transactions on Information Technology in Biomedicine, 12 (5), pp 667–677, 2008.

[Min'99] Minami K., Hiroshi N., Takesshi T., Real-Time Discrimination of Ventricular Tachyarrhythmia with Fourier-Transform Neural network, IEEE Transactions on Biomedical Engineering, 46 (2), pp. 179-185, 1999.

[Moj'00] Mojsilovic A., Matching and retrieval based on vocabulary and grammar of color patterns, IEEE Transactions on Image Processing, 9 (1), pp 38-54, 2000.

[Moo'01] Moody G. B., Mark R. G., The Impact of the MIT-BIH Arrhythmia Database, IEEE Engineering in Medicine and Biology Magazine, 20 (3), pp 45-50, 2001.

[Mul'07] Muller P., Zeng P., Wonka G.P., Gool L.V., Image-based procedural modeling of facades, ACM Transactions on Graphics, 26 (3), pp 1-9, 2007.

N

[Nag'01] Nagin V., Selishchev S., Implementation of algorithms for identification of QRS-complexes in real time ECG systems, Biomedical Engineering, 35 (6), pp 304-309, 2001.

[Nik'00] Nikolaev N., Nikolov Z., Gotchev A., Egiazarian K., Wavelet domain Wiener filtering for ECG denoising using improved signal estimate, IEEE Acoustics, Speech, and Signal Processing, 6 (1), pp 3578-3581, 2000.

[Nik'01] Nikoliaev N., Gotchev A., Egiazarian K., Nikolov Z., Suppression of electromyogram interference on the electrocardiogram by transform domain denoising Medical & Biological Engineering & Computing, 39 (6), pp 649–655, 2001.

[Nou'13] Nouira I., Ben Abdallah A.B., Bedoui M.H., Dogui M., A Robust R Peak Detection Algorithm Using Wavelet Transform for Heart Rate Variability Studies, International Journal on Electrical Engineering and Informatics, 5 (3), pp 270-284, 2013.

O

[Obr'68] Obraska P., Perlemuter L., Quevauvilliers J., Médecine, appareille cardiovasculaire, Edition Masson Tome II, 1968.

[Ogi'08] Ogiela L., Tadeusiewicz R., Ogiela M. R., Cognitive modeling in medical pattern semantic understanding, International Conference on Multimedia and Ubiquitous Engineering, 8, pp 15–18, 2008.

[Ogi'09] Ogiela L., Ogiela M. R., Tadeusiewicz R., Mathematical linguistics in cognitive medical image interpretation systems, Journal of Mathematical Imaging and Vision, 34 (3), pp 328–340, 2009.

[Olm'97] T. Olmez, Classification of ECG waveforms using RCE neural network and genetic algorithm, Electronics Letters, 33 (18), pp 1561–1562, 1997

[Oso'01] Osowski, S., and Linh, T. H., ECG beat recognition using fuzzy hybrid neural network, IEEE Transactions on Biomedical Engineering, 48 (11), pp 1265–1271, 2001.

P

[Pal'10] Pal S., Mitra M., Detection of ECG characteristic points using Multiresolution Wavelet Analysis based Selective Coefficient Method, journal of Measurement, 43 (2), pp 255–261, 2010.

[Pan'85] Pan J., Tompkins W. J., A real-time QRS detection algorithm, IEEE Transactions on Biomedical Engineering, 32(3), pp 230-236, 1985.

[Par'98] Park K. L., Lee K. J., Yoon H. R., Application of a wavelet adaptive filter to minimise distortion of the ST-segment, Medical and Biological Engineering and Computing, 36 (5), pp 581–586, 1998.

[Par'01] Park K. L., Khil M. J., Lee B. C., Jeong K. S., Lee K. J., Yoon H. R., Design of a wavelet interpolation filter for enhancement of the ST-segment, Medical and Biological Engineering and Computing, 39 (3), pp 1–6, 2001.

[Par'12] Parag, T., Bahlmann, C., Shet, V., Singh, M., A grammar for hierarchical object descriptions in logic programs, IEEE Computer Society Conference on Computer Vision and Pattern Recognition Workshops, pp 33–38, 2012.

[Ped'13] Pedro R. W. D., Nunes F. L. S., Lima A. M., Using Grammars for Pattern Recognition in Images: A Systematic Review, ACM Computing Surveys, 46 (2), pp 1-34, 2013.

[Pet'09] Petersohn C., Temporal video structuring for preservation and annotation of video content, IEEE International Conference on Image Processing (ICIP), 16, pp 93 – 96, 2009.

[Pol'95] Poli R., Cagnoni S., Valli G., Genetic design of optimum linear and nonlinear QRS detectors, IEEE Transactions on Biomedical Engineering, 42 (11), pp 1137-1141, 1995.

Q

[Qin'03] Shuren Qin, Zhong Ji, and Hongjun Zhu, The ECG Recording Analysis Instrumentation Based on Virtual Instrument Technology and Continuous Wavelet Transform, International Conference of the IEEE EMBS Engineering in Medicine and Biology Society, 17-21, pp. 3176-3179, 2003.

R

[Red'09] Reddy, H. T., Karibasappa, K., And Damodaram, A., Probabilistic parser for face detection, International Conference on Methods and Models in Computer Science, pp 1–7, 2009.

[Rod'07] Rodney T. H. G., LumK M., Mok V. H., Performance Evaluation of Coifman Wavelet for ECG Signal Denoising, International Federation for Medical and Biological Engineering, 15 (1), pp 419-422, 2007.

[Ros'98] Rosaria S., Carlo M., Artificial neural networks for automatic ECG analysis, IEEE Transactions on Signal Processing, 46 (5), pp 1417–1425, 1998.

[Ruc'10] Ruchita G., Sharma A. K., Detection of QRS complexs of ECG recording based on wavelet transform using Matlab, International Journal of Engineering and Innovative Technology, 2(7), pp 3038–3034, 2010.

S

[Sah'97a] Sahambi J. S., Tandon S. M., Bhatt R. K. P., Using wavelet transforms for ECG characterization: an on-line digital signal processing system, IEEE Engineering in Medicine and Biology Magazine, 16 (1), pp 77–83, 1997.

[Sah'97b] Sahambi J. S., Tandon S. M., Bhatt R. K. P., Quantitative analysis of errors due to power-line interference and base-line drift in detection of onsets and offsets in ECG using wavelets, Medical and Biological Engineering and Computing, 35 (6), pp 747–751, 1997.

[Sah'98] Sahambi J. S, Tandon S. M., Bhatt R. K. P., Wavelet base ST-segment analysis, Medical and Biological Engineering and Computing, 36 (5), pp 568–572, 1998.

[Sai'12] Saini I., Singhb D., Khoslaa A., QRS detection using K-Nearest Neighbor algorithm (KNN) and evaluation on standard ECG databases, Journal of Advanced Research, 4(4), pp 331-344, 2012.

[Sax'02] Saxena S.C., Vinod K., Hamde S.T., QRS detection using new wavelets, Journal of Medical Engineering & Technology, 26 (1), pp 7–15, 2002.

[Sen'95] Senhadji, L., Carrault, G., Bellanger J. J., Passariello, G., Comparing wavelet transforms for recognizing cardiac patterns, IEEE Engineering in Medicine and Biology, 14 (2), pp 167-173, 1995.

[Shu'00] Shusterman, V., Shah, S. I., Beigel, A., Anderson, K. P., Enhancing the precision of ecg baseline correction : selective filtering and removal of residual error, Computers and Biomedical Research, 33(2), pp 144–60, 2000.

[Shu'12] Shuning W., Yaonan W., Yi Z., Wavelet neural networks robust control of farm transmission line deicing robot manipulators Computer Standards & Interfaces, 34 (3), pp 327–333, 2012.

[Shy'04] Shyu L.Y., Wu Y.H., Hu W., Using wavelet transform and fuzzy neural network for VPC detection form the Holter ECG, IEEE Transactions on Biomedical Engineering, 51 (7), pp 1269–1273, 2004.

[Sil'98] Silipo R., Artificial Neural Networks for Automatic ECG Analysis, IEEE Transactions on Signal Processing, 46 (5), pp 1417-1425, 1998.

[Sis'07] Siskind J. M., Sherman J., Polak I., Harper M. P., Bouman, C. A., Spatial random tree grammars for modeling hierarchical structure in images with regions of arbitrary shape, IEEE Transactions on Pattern Analysis and Machine Intelligence, 29 (9), pp 1504–1519, 2007.

[Sor'06] Sornmo L., Laguna P., Electrocardiogram ECG signal processing, Wiley Encyclopedia of Biomedical Engineering, Online, 2006.

[Ste'02] Sternickel K., Automatic pattern recognition in ECG time series, Computer Methods and Programs in Biomedicine, 68 (2), pp 109–115, 2002.

[Sti'72] Stiny G., Gips J., Shape Grammars and the Generative Specification of Painting and Sculpture, International Federation for Information Processing Congress, pp 1460–1465, 1972.

[Sti'78] Stiny G., Mitchell W. J., The Palladian grammar, Environment and Planning B: Planning and Design, 5 (1), pp 5–18, 1978.

[Sti'80] Stiny G., Introduction to shape and shape grammars, Environment and Planning B: Planning and Design, 7 (3), pp 343–351, 1980.

[Sti'82] Stiny G., Spatial Relations and Grammars, Environment and Planning B: Planning and Design, 9 (1), pp 113–114, 1982.

[Su'05] Su L., Zhao G., De-Noising of ECG Signal Using Translation-Invariant Wavelet DeNoising Method with Improved Thresholding, IEEE Engineering in Medicine and Biology, 6 (1), pp 5946-5949, 2005.

[Sum'09] Sumathi S., Sanavullah M.Y., Comparative Study of QRS Complex Detection in ECG Based on Discrete Wavelet, International Journal of Recent Trends in Engineering, 2 (5), pp 273-277, 2009.

[Szu'92] Szu, H. H., Neural network adaptive wavelets for signal representation and classification, Optical Engineering, 31(9), pp 1907–1916, 1992.

T

[Tao'10] Taouli S. A, Bereksi-Reguig F., Noise and baseline wandering suppression of ECG signals by morphological filter, Journal of Medical Engineering & Technology, 34 (2), pp 87-96, 2010.

[Teb'10] Teboul O., Simon L., Koutsourakis P., Paragios N., Segmentation of building facades using procedural shape priors, IEEE Conference on Computer Vision and Pattern Recognition,23, pp 3105–3112, 2010.

[Tig'03] Tighiouart B., Rubel P., Bedda M., Improvement of QRS boundary recognition by means of unsupervised learning, IEEE Computers in Cardiology, pp 49-52, 2003.

[Tik'99] Tikkanen P.E., Nonlinear wavelet and wavelet packet denoising of electrocardiogram signal, Biological Cybernetics, 80 (4), pp 259–267, 1999.

[Tra'93] Trahanias P., An approach to QRS-complex detection using mathematical morphology, IEEE Transactions on Biomedical Engineering, 40 (2), pp 201–205, 1993.

[Tra'90] Trahanias P., Skordalakis E., Syntactic Pattern Recognition of the ECG, IEEE Transactions on Pattern Analysis and Machine Intelligence, 12 (7), pp 648-657, 1990.

[Trz'09] Trzupek M., Ogiela M.R., Tadeusiewicz R., Image content analysis for cardiac 3D visualizations, Lecture Notes in Computer Science, 5711, pp 192–199, 2009.

[Trz'11] Trzupek M., Ogiela M.R., Tadeusiewicz R., Intelligent image content description and analysis for 3D visualizations of coronary vessels, Lecture Notes in Computer Science, 6592, pp 193–202, 2011.

U

[Ube'05] Güler, I., Übeyli, E. D., ECG beat classifier designed by combined neural network model, Pattern Recognition, 38(2), pp 199–208, 2005.

[Ube'08] Ubeyli, and Elif Derya, Feature extraction for analysis of ECG signals, IEEE EMBS Engineering in Medicine and Biology Society, pp 1080-1083, 2008.

[Ube'09] Ubeyli, E. D., Adaptive neuro-fuzzy inference system for classification of ECG signals using Lyapunov exponents, Computer Methods and Programs in Biomedicine, 93 (3), pp 313–321, 2009.

V

W

[Wal'87] Waller A. D., A demonstration on man of electromotive changes accompanying the heartbeat, The Journal of Physiology, 8 (5), pp 229-234, 1887.

[Wan'05] Wang W., Pollak I., Bouman C. A., Harper, M. P., Classification of images using spatial random trees, IEEE Workshop on Statistical Signal Processing, 13, pp 449–452, 2005.

[Wan'06] Wang W., Pollak I., Wong T. S., Bouman C. A., Harper M. P., Siskind J. M., Hierarchical stochastic image grammars for classification and segmentation, IEEE Transactions on Image Processing, 15 (10), pp 3033–3052, 2006.

[Wat'95] Watrous R., Towell, G., A patient-adaptive neural network ECG patient monitoring algorithm, Computers in Cardiology, pp 229-232, 1995.

[Wen'09] Cheng W., Classification of ECG complexes using self-organizing CMAC, Measurement, 42 (3), pp 399–407, 2009.

[Wil'87] Williams J. L., Lesaffre E., Comparison of multi-group logistic and linear discriminant ECG and VCG classification, Journal of Electrocardiology, 20 (2), pp 83–92, 1987.

[Wie'99] Wieben O., Afonso V., Tompkins W., Classification of premature ventricular complexes using filter bank features, induction of decision trees and a fuzzy rule-based system, Medical & Biological Engineering & Computing, 37(5), pp 560-565, 1999.

[Wei'10] Wei H. L., Billings S.A., Zhao Y. F., Guo L. Z., An adaptive wavelet neural network for spatio-temporal system identification Neural Networks, 23 (10), pp 1286–1299, 2010.

[Wu'09] Wu Y., Bian H., Image segmentation integrating generative and discriminative methods, International Conference on Web Information Systems and Mining, pp 769–774, 2009.

X

Y

[Yin, 1992] Ying S., Suppappola S., Wrubleski T. A., Microcontroller-Based Real-Time QRS Detection, Biomedical Instrumentation & Technology, pp.477-484, 1992.

Z

[Zhe'95] Zheng C. X., Li C. W., Detection of ECG characteristics points using the wavelet transforms, IEEE Transactions on Biomedical, 42 (1), pp 21-28, 1995.